

Nuclear fusion in dense plasmas

Setsuo Ichimaru

Department of Physics, University of Tokyo, Bunkyo, Tokyo 113, Japan

The review begins by grouping the fundamental nuclear reactions into two classifications, namely, the usual binary processes and few-particle processes. In the few-particle processes, the possibility of electron-screened cold fusion is remarked. The special features of dense plasmas rest in the enhancement of reaction rates over these fundamental processes due to *internuclear many-particle processes*. The many-particle processes arise from a modification of the short-range correlations between reacting nuclei and are the effects related closely to differences between Coulombic chemical potentials before and after the nuclear reactions. Quantum statistical-mechanical formulation of the enhancement factors is presented. Thermodynamic functions for various realizations of dense plasmas, pertinent directly to the reaction-rate theories through the screening properties and free energies, are summarized. Those analyses are then applied to the estimation of nuclear reaction rates in specific examples of dense astrophysical plasmas, namely, the Sun, brown dwarfs, giant planets, white-dwarf progenitors of supernovae, and helium burning on the degenerate stars, as well as in those dense laboratory plasmas that are found in the inertial confinement fusion experiments, in metal hydrides such as PdD and TiD₂, in cluster-impact fusion experiments, and in ultrahigh-pressure liquid metals. The essential similarity between the nuclear fusion reactions in supernovae and those projected in the ultrahigh-pressure liquid metals is particularly emphasized.

CONTENTS

I. Introduction	255	C. White-dwarf progenitors of supernovae	282
A. Scope of the review	255	1. Dense C-O mixtures	282
B. Astrophysical condensed plasmas	256	2. Screening by relativistic electrons	282
C. Dense laboratory plasmas	258	D. Helium burning—Triple α reactions	283
D. Basic parameters of dense plasmas	259	E. Metal hydrides—PdD and TiD ₂	284
II. Elements of Nuclear Reactions	260	F. Cluster-impact fusion	285
A. Contact probabilities	260	G. Ultrahigh-pressure liquid metals	285
B. Binary processes—The Gamow reaction rates	261	VI. Epilogue	286
C. Few-particle processes—Screened cold fusion	262	Acknowledgments	287
III. Enhancement by Many-Particle Processes	264	Appendix A: Thermodynamic Functions for Dense Plasmas	287
A. Historic remarks	264	1. Relativistic electron gases in the ground state	287
B. Quantum-mechanical correlation functions	265	2. Electron liquids at finite temperatures	288
1. General approach	265	3. Dense semiclassical one-component-plasma fluids of ions	290
2. Enhancement factors	266	4. Classical binary-ionic-mixture fluids	291
C. Chemical potentials	266	5. Quantum-mechanical one-component-plasma solids of ions	292
IV. Correlation Functions and Enhancement Factors	267	6. Screening by relativistic electrons	293
A. Classical one-component-plasma	267	7. Dense electron-ion two-component plasma: The incipient-Rydberg-state model	293
1. Monte Carlo screening potentials	267	Appendix B: Derivation of Equation (2.1)	296
2. Bridge functions	269	References	296
3. Improved hypernetted-chain schemes	270		
4. Enhancement factors	270		
B. Classical binary-ionic-mixture fluids	271		
1. Monte Carlo screening potentials	271	I. INTRODUCTION	
2. Ion-sphere scaling	271		
3. Enhancement factors	272		
C. Electron-screened one-component-plasma and binary-ionic-mixture fluids	272	A. Scope of the review	
1. Screening potentials	272		
2. Enhancement factors	273		
D. Crystalline solids	274		
1. Monte Carlo lattice potentials	274		
2. Pycnonuclear reaction rates in C-O solids	274		
3. Pycnonuclear reaction rates in binary-ionic-mixture solids	276		
E. Hydrogen in metal hydrides	276		
1. Monte Carlo simulations in metallic lattices	277		
2. Enhancement factors	277		
V. Rates of Nuclear Fusion Reactions	280		
A. Solar interior and inertial confinement fusion plasmas	280		
B. Interiors of Jovian planets and brown dwarfs	281		

The rate of fusion reactions between nuclear species i and j is proportional to $g_{ij}(r_N)$, the value of joint probability density $g_{ij}(r)$ for reacting pairs at a nuclear reaction radius r_N ; it is a function averaged over the motion of their center of mass and the remainder of the coordinates characterizing the surrounding medium. Either in vacuum or in a dense plasma, such a contact probability is given generally as the square of the wave functions describing the events of scattering between the reacting pairs. Being a correlation function, albeit at short distances, the contact probabilities may depend quite sensi-

tively on the changes in the microscopic, macroscopic, and thermodynamic states of the environment in case it consists of condensed matter. The rates of nuclear reactions in dense plasmas can thus differ drastically from those expected in vacuum, due to strong, many-body correlation effects, or the statistical-mechanical effects, inherent in such a condensed-matter system.

This article therefore intends to elucidate the present stages of understanding with regard to those effects of enhancement in the rates of nuclear reactions, expected from the correlation and thermodynamic effects, in various realizations of the condensed plasmas both in the astrophysical and laboratory settings. Consequently, the contexts of the review are concerned rather with the aspects of statistical condensed-matter physics than with those of nuclear reaction physics *per se*. This review is here viewed as a forum in which the interplay between nuclear physics and statistical physics may be studied usefully through the concept of correlation functions.

The review thus begins with the classification of the fundamental nuclear reactions in two elements according to process, namely, *binary* processes and *few-particle* processes. The binary processes are those that are expected without the effects of the environment, and include the celebrated Gamow rates (Gamow, 1928; Gurney and Condon, 1929) of thermonuclear reactions. In the few-particle processes, one includes possible effects of screening, or modification of internuclear forces, by light particles such as electrons; the possibility of electron-screened cold fusion is remarked.

The nuclear reaction rates are related to the short-range behavior of the pair-correlation functions, where the quantum-mechanical effects are essential. The special features of nuclear fusion in dense plasmas rest in the *enhancement of the reaction rates over those fundamental processes due to internuclear many-particle processes*. The many-particle processes arise from modification of the short-range correlations between reacting nuclei and are the effects related closely to differences between Coulombic chemical potentials before and after the nuclear reactions. In these connections, we describe recent developments in the Monte Carlo (MC) simulation study as well as those in statistical theories of the short-range correlations in various realizations of dense plasmas.

At high densities such as those in the interior of degenerate stars, the plasma may undergo a freezing transition into a solid state (e.g., Ichimaru, 1982). The nuclei in such a dense plasma then form a quantum solid in its ground state, and they perform zero-point vibrations about their equilibrium sites. The reaction rates, proportional to the square of the ground-state wave function or the contact probability between a nearest-neighbor pair, thus depend very sensitively on the density via the nearest-neighbor separation, but are independent of the temperature (Cameron, 1959; Salpeter and Van Horn, 1969). Rates of such pycnonuclear reactions in binary-ionic mixtures (BIMs)—plasmas consisting of two different types of ions immersed in a neutralizing electron

background—are analyzed through a combination of compositional scaling arguments and examinations of MC simulation results for the interparticle separations (Ogata, Iyetomi, and Ichimaru, 1991; Ichimaru, Ogata, and Van Horn, 1992).

As the aforementioned effects of correlations and freezing transitions may have illustrated, the nuclear reaction rates in dense plasmas are intimately related to the thermodynamic functions through the screening properties and the Coulombic chemical potentials. The thermodynamic properties of various plasmas are thus summarized in Appendix A.

Those analyses are then applied to the estimation of the nuclear reaction rates and enhancement factors in specific examples of dense astrophysical and laboratory plasmas: Astrophysical condensed plasmas (Van Horn, 1991) under present consideration include the solar interior (SI), the interior of a brown dwarf (BD), the interior of a giant planet (GP), a white-dwarf (WD) progenitor of a supernova, and surfaces of accreting white dwarfs and neutron stars. Examples of the condensed plasmas in laboratories are those found in the inertial confinement fusion (ICF) experiments, in metal hydrides (MH) such as PdD and TiD₂, in cluster-impact fusion experiments, and in ultrahigh-pressure liquid metals (PM). In many cases, the computed results presented in Sec. V have been newly obtained for this review and therefore replace some of the existing calculations. The essential similarity between the nuclear reactions in supernovae and those projected in the ultrahigh-pressure liquid metals will be particularly emphasized.

B. Astrophysical condensed plasmas

Interiors of main-sequence stars such as the Sun are dense plasmas constituted mostly of hydrogen. The Sun has radius $R_S \approx 6.96 \times 10^{10}$ cm and mass $M_S \approx 1.99 \times 10^{33}$ g; its mass density is 1.41 g/cm^3 on average (e.g., Allen, 1973). The total luminosity is $L_S \approx 3.85 \times 10^{26}$ W and the average luminosity per mass is $L_S/M_S \approx 1.93 \times 10^{-7}$ W/g. The central part of the Sun has a mass density of approximately $1.56 \times 10^2 \text{ g/cm}^3$, a temperature of approximately 1.5×10^7 K, and a pressure of approximately 3.4×10^5 Mbar. The mass fractions of hydrogen are 0.36 near the center and 0.73 near the surface. Rates of nuclear reactions, photon transport and opacities, conductivities, atomic states, and their miscibilities are all essential elements in setting a model for the Sun (Bahcall *et al.*, 1982). These solar luminosities are to be accounted for, in particular, by the rates of proton-proton reactions (Salpeter, 1952a).

Very low-mass stars ($0.08M_S < M < 0.3M_S$) dominate the solar neighborhood (< 10 pc)¹ and constitute the most numerous stellar component of the Galaxy (Kumar, 1963; Liebert and Probst, 1987; Burrows, Hubbard, and

¹1 pc (Parsec) = 3.26 light per year = 3.08×10^{18} cm.

Lumine, 1989). Brown dwarfs (D'Antona and Mazzitelli, 1985; Kafatos, Harrington, and Maran, 1986; Lumine, Hubbard, and Marley, 1986; D'Antona, 1987; Burrows, Hubbard, and Lumine, 1989; Stevenson, 1991) may be defined as those astrophysical objects having masses insufficient for achieving thermal equilibrium through hydrogen burning ($M < 0.08M_S$), but with masses sufficiently large to be supported primarily by thermal or electron degeneracy pressure ($M > 0.01M_S$; Nelson, Rapaport, and Joss, 1986). Because of the absence of hydrogen burning, expected surface temperatures of the brown dwarfs are low ($T < 2000$ K), so that these would possibly be observed in infrared. Although the observational evidence for their existence still remains to be confirmed (e.g., Forrest, Skrutskie, and Shure, 1988; Fienberg, 1990), the issues of brown dwarfs carry astrophysical consequences of considerable interest: A possibility has been suggested that these objects may make up a significant fraction of the local missing mass in the Galactic disk (Kafatos, Harrington, and Maran, 1986; Stevenson, 1991). An observation of a brown dwarf would provide useful clues as to the formation of planetary systems. Central temperatures and mass density of a brown dwarf may range $(2-3) \times 10^6$ K and 10^2-10^3 g/cm³, respectively. Equations of state, opacities, and rates of nuclear reactions are essential elements in theoretical prediction for the critical masses, structures, and evolution of brown dwarfs (Stevenson, 1991).

The materials inside Jovian planets (Jupiter, Saturn, Uranus, Neptune) offer important objects of study in the dense-plasma physics (e.g., Hubbard, 1980, 1984; Stevenson, 1982). Typically, Jupiter has a radius $R_J = 0.103R_S = 7.14 \times 10^9$ cm and a mass $M_J = 0.95 \times 10^{-3}M_S = 1.90 \times 10^{30}$ g. The mass density, temperature, and pressure of its interior (outside the central "rock"), consisting of hydrogen plasmas with a few percent (in molar fraction) admixture of helium, are estimated to range 2–5 g/cm³, 5000–20 000 K, and 3–30 Mbar, respectively.

Jupiter has been known to emit radiation energy in the infrared range at an effective temperature of approximately 130 K, approximately 2.7 times as intense as the total amount of radiation that it receives from the Sun (Hubbard, 1980). By observation through terrestrial atmospheric transmission windows at 8–14 μm (Menzel, Coblenz, and Lampland, 1926) and 17.5–25 μm (Low, 1966), Jupiter was known to be an unexpectedly bright infrared radiator. This feature has been accurately reconfirmed quantitatively by a telescope airborne at an altitude of 15 km (Armstrong, Harper, and Low, 1972) and through flyby measurements with Pioneers 10 and 11 (Ingersoll *et al.*, 1976). For Jupiter, the effective surface temperature determined from integrated infrared power over 8–300 μm was 129 ± 4 K, while the surface temperature calculated from equilibration with absorbed solar radiation was 109.4 K (Hubbard, 1980); the balance needs to be accounted for by internal power generation.

To account for the source of such an excess infrared

luminosity, theoretical models such as "adiabatic cooling" (Hubbard, 1968; Grabske *et al.*, 1975; Stevenson and Salpeter, 1977), "gravitational unmixing" (Smoluchowski, 1967; Stevenson and Salpeter, 1977), and "latent heat due to metallization" (Saumon *et al.*, 1992) have been considered. Theoretical predictions on evolution, internal structures, and gravitational harmonics (Hubbard and Marley, 1989) for such giant planets depend to a great extent on thermodynamic, transport, and optical properties of dense plasma materials. It is essential in these connections to explore possible nuclear reactions of deuterons, which may remain in a Jovian planet at an atomic abundance of approximately 0.003% (Anders and Grevesse, 1989).

The white dwarf (e.g., Schatzman, 1958; Van Horn, 1971; Liebert, 1980; Shapiro and Teukolsky, 1983) represents a final stage of stellar evolution, corresponding to a star of about 1 solar mass compressed to a characteristic radius of 5000 km and an average density of 10^6 g/cm³. Its interior consists of a multi-ionic condensed matter composed of C and O as the main elements and Ne, Mg, ..., Fe as trace elements. Condensed-matter problems in white dwarfs include the assessment of the possibilities of chemical separation, or the phase diagrams, associated with the freezing transitions of the multi-ionic plasmas (Stevenson, 1980; Barrat, Hansen, and Mochkovitch, 1988; Ichimaru, Iyetomi, and Ogata, 1988; Van Horn, 1990; Ogata *et al.*, 1993). These are related to internal structure, cooling rate, and evolution of a white dwarf (Clayton, 1968; Mochkovitch, 1983; Winget *et al.*, 1987), as well as the rates of nuclear reactions (Salpeter and Van Horn, 1969; Ogata, Iyetomi, and Ichimaru, 1991) and detailed mechanisms of the supernova explosion and of possible formation of neutron stars (Canal and Schatzman, 1976; Canal, Isern, and Labay, 1982; Bethe, 1990; Nomoto and Kondo, 1991).

As a progenitor of a type-I supernova, a white dwarf with an interior consisting of a carbon-oxygen mixture can be considered a kind of binary-ionic mixture with a central mass density of 10^7-10^{10} g/cm³ and a temperature of 10^7-10^9 (Starrfield *et al.*, 1972; Whelen and Iben, 1973; Canal and Schatzman, 1976). Thermonuclear runaway leading to supernova explosion is expected to take place when the thermal output due to nuclear reactions exceeds the rate of energy loss. Assuming that neutrino losses are the major effects in the latter, one estimates (e.g., Arnett and Truran, 1969; Nomoto, 1982a; Itoh *et al.*, 1989) that a nuclear runaway should take place when the nuclear power generated exceeds $10^{-9}-10^{-8}$ W/g. These values give approximate measures against which the rates of nuclear reactions in white dwarfs are to be compared.

Helium burning is one of the major reaction processes in stellar evolution (Salpeter, 1952b) and in accreting white dwarfs and neutron stars in close binary systems (Nomoto, Thielemann, and Miyaji, 1985). In the latter cases, helium burning is so explosive as to give rise to remarkable astronomical phenomena, such as x-ray bursts

in neutron stars (Lewin and Joss, 1983) and type-I supernovae in white dwarfs (Nomoto, 1982a, 1982b).

The neutron star (e.g., Baym and Pethick, 1975; Shapiro and Teukolsky, 1983), another of the final stages in stellar evolution, is a highly degenerate star corresponding approximately to a compression of a solar mass into a radius of ~ 10 km. According to theoretical model calculations, it has an outer crust, consisting mostly of iron, with a thickness of several hundred meters and a mass density in the range of 10^4 – 10^7 g/cm³. When the mass density ρ_m exceeds a critical value near 10⁷ g/cm³ for electron captures, neutron-rich “inflated” nuclei begin to emerge. At $\rho_m \approx 4 \times 10^{11}$ g/cm³, the neutron-drip density, the estimated atomic and mass numbers for such nuclei are $Z = 36$ and $A = 118$; at $\rho_m \approx 2 \times 10^{14}$ g/cm³, which defines the inner edge of an inner crust, one calculates $Z = 201$ and $A = 2500$ (Baym, Pethick, and Sutherland, 1971).

Over the bulk of the crustal parts, the nuclei are considered to form a Coulomb solid. A neutron star may be appropriately looked upon as a “three-component star” consisting of an ultradense interior of neutron fluids, a crust of Coulomb solids, and a thin surface layer of “ocean” fluids. Nuclear reactions are expected in these surface layers on accreting neutron stars in close binary systems (Lewin and Joss, 1983; Day and Tawara, 1990).

C. Dense laboratory plasmas

The states of those plasmas at the focus of inertial confinement fusion research (e.g., Motz, 1979; Hora, 1991) are similar to those in the solar interior already mentioned. The projected temperatures in the ICF plasmas need to be on the order of 10⁷–10⁸ K. Those materials that drive implosion of the fuel consist of high- Z elements, such as C, Al, Fe, Au, Pb, . . . , which after ionization form plasmas with charge numbers substantially greater than unity. The atomic physics of those high- Z elements is influenced strongly by the correlated behaviors of charged particles in dense plasmas.

Laboratory realization of condensed plasmas includes, in addition, those produced by shock compression (e.g., Fortov, 1982; Fortov *et al.*, 1990), in pinch discharges (e.g., Pereira, Davis, and Rostoker, 1989), and through metal vaporization (Mostovych *et al.*, 1991). Ultrahigh-pressure-metal physics studied in shock-compression experiments (Nellis *et al.*, 1988) aims at detection of changes in the equation of state through transitions between electronic states in the compressed metals (Al, Cu, and Pb). Another scheme of ultrahigh-pressure experiments utilizing the diamond-anvil cells (Mao, Hemley, and Hanfland, 1990) strives for the ultimate realization of *metallic hydrogen* through insulator-to-metal transitions (Wigner and Huntington, 1935) by compression to multimegabar pressures (Hemley and Mao, 1991).

Metals and alloys (solid, amorphous, liquid, and compressed) are the most typical examples of condensed laboratory plasmas (e.g., Mott and Jones, 1936; Ashcroft

and Stroud, 1978; Endo, 1990). Conduction electrons in metals form *quantum plasmas*, where the wave nature of the electrons as fermions plays an essential part (e.g., Pines and Nozières, 1966). At room temperatures, their number densities range from 10²² to 10²³ cm⁻³ for most of the simple metals such as Al, Li, and Na. In these density regimes, effects arising from exchange and Coulomb coupling between electrons become significant; thus conduction electrons in metals are referred to as *strongly coupled* (e.g., Ichimaru, 1982, 1990) quantum plasmas. Owing to the presence of the core electrons, the ion-ion and electron-ion interactions are described by the pseudopotentials, deviating away from the pure Coulombic form. The strong-coupling effect between the conduction electrons has a strong influence on the determination of those pseudopotentials (e.g., Singwi and Tosi, 1981; Hafner, 1987).

Certain metals such as palladium, titanium, and vanadium possess a remarkable ability for absorbing sizable amounts of hydrogen (Alefeld and Völkl, 1978). Nuclear reactions between hydrogen isotopes trapped in a metal hydride, such as palladium deuteride (PdD) and titanium deuteride (TiD₂), offer a unique opportunity for studying reaction processes in microscopically inhomogeneous metallic environments of regular or irregular (e.g., due to defects) lattice fields produced by the metal atoms. Experiments are usually carried out in nonequilibrium situations such as electrolysis and absorption-desorption processes; no fusion yields have been confirmed as yet. (For examples of earlier experiments, see Gai *et al.*, 1989; Jones *et al.*, 1989; and Zielger *et al.*, 1989).

The flurry of interest produced by the announcement of cold fusion rapidly polarized the scientific community into two groups: diehard enthusiasts and extreme skeptics. The initial experimental reports on power production through cold fusion have now been dismissed by almost everyone. However, it is important not to go to the extreme of rejecting all possibilities uncritically. Here we assess the fusion rates in metal hydrides in order to help provide an objective assessment of these possibilities (Leggett and Baym, 1989; Ichimaru, Ogata, and Nakano, 1990).

In a context somewhat similar to that of the aforementioned fusion in metal hydrides experiments on cluster-impact fusion were performed recently (Beuhler, Friedlander, and Friedman, 1989): deuteron-deuteron fusion, detected via the 3-MeV protons produced, was shown to occur when singly charged clusters of from 25 to 1300 D₂O molecules, accelerated to 200 to 325 keV, impinged on TiD targets, with high fusion rates observed at approximately 1–10 s⁻¹/D-D; experimental confirmation followed (Bae, Lorents, and Young, 1991; Beuhler *et al.*, 1991). A theoretical account for the high fusion yields was proposed on the basis of a “thermonuclear” model (Carraro *et al.*, 1990) at an elevated effective density (Echenique, Manson, and Ritchie, 1990) or temperature (Kim *et al.*, 1992) of deuterons. An experiment was then reported (Vandenbosch *et al.*, 1991) which showed that

the enhanced fusion rates fell off rapidly with cluster size. Very recently, the possibility appeared to be confirmed that traces of high-velocity beam contaminants (artifacts) could account for the experimental results [Beuhler, Friedlander, and Friedman, 1992(E)].

Pressurized liquid metals offer another interesting environment in which to study nuclear reactions (Ichimaru, 1991). It will be shown that $d(p,\gamma)^3\text{He}$ and $^7\text{Li}(p,\alpha)^4\text{He}$ reactions can take place at a power-producing level on the order of a few kW/cm³, if such a material is brought to a liquid metallic state under an ultrahigh pressure on the order of 10^2 – 10^3 Mbar at a mass density of 10 – 10^2 g/cm³ and a temperature of $(1$ – $2)\times 10^3$ K, slightly above the estimated melting conditions for hydrogen. Such a range of physical conditions may be accessible through extension of those ultrahigh-pressure-metal technologies (e.g., Nellis *et al.*, 1988; Mao, Hemley, and Hanfland, 1990; Ruoff *et al.*, 1990; Hemley and Mao, 1991).

D. Basic parameters of dense plasmas

The contact probabilities between reacting nuclei depend crucially on the states of dense plasmas, which may be characterized by a number of physical parameters. In this section, we summarize such fundamental quantities for plasmas. In Appendix A, thermodynamic functions for various dense plasmas are described in terms of those basic parameters.

We begin by modeling a plasma as consisting of atomic nuclei (which will be called *ions*) with electric charge $Z e$ and rest mass $M (= A m_N)$, and of electrons with electric charge $-e$ and rest mass m . Physical quantities associated with these separate constituents are distinguished by the suffixes *i* and *e*. The atomic mass number is denoted by A and m_N represents the average mass per nucleon.

In some cases, salient features of plasma can be understood through investigation of the properties of a one-component plasma (OCP). A OCP is a model consisting of a single species of charged particle embedded in a uniform background of neutralizing charges. Conduction electrons in the jellium model of metals (e.g., Pines and Nozières, 1966) offer an example of such an electron OCP, where all effects of lattice periodicity in the space-charge distribution of the ions are ignored. Another example is an outer-crustal matter of a neutron star, where one neglects polarizability of the dense, relativistic electrons and treats the Fe^{26+} nuclei approximately as forming an ion OCP.

Modeling for a dense plasma under different circumstances may call for consideration of cases containing multiple species of ions, or multi-ionic plasmas, the constituents of which will be distinguished by such subscripts as *i* and *j*; the BIM is an example of such a multi-ionic plasma. Thus, for the macroscopic neutrality of electric charges, the number densities n_i and n_e are assumed to satisfy

$$\sum_i Z_i n_i = n_e \quad (1.1)$$

A dimensionless parameter characterizing a system of electrons is (e.g., Pines and Nozières, 1966; Ichimaru, 1982)

$$r_s = \left[\frac{3}{4\pi n_e} \right]^{1/3} \frac{me^2}{\hbar^2} \approx \left[\frac{n_e}{1.6 \times 10^{24} \text{ cm}^{-3}} \right]^{-1/3}. \quad (1.2)$$

It is the Wigner-Seitz radius of the electrons

$$a_e = \left[\frac{3}{4\pi n_e} \right]^{1/3}, \quad (1.3)$$

in units of the Bohr radius,

$$r_B = \frac{\hbar^2}{me^2} = 0.5292 \times 10^{-8} \text{ cm}, \quad (1.4)$$

and depends only on the electron density.

The Fermi wave number of the electrons in a paramagnetic state, with an equal number of electrons in the two spin states, is given by

$$k_F = (3\pi^2 n_e)^{1/3} = \frac{3.63 \times 10^8 \text{ cm}^{-1}}{r_s}. \quad (1.5)$$

A parameter characterizing relativistic effects is defined by the ratio

$$x_F = \frac{\hbar k_F}{mc} = 1.40 \times 10^{-2} r_s^{-1}. \quad (1.6)$$

Fermi energy of the electrons is then given by

$$E_F = mc^2 (\sqrt{1+x_F^2} - 1) \\ = mc^2 (\sqrt{1+1.96 \times 10^{-4} r_s^{-2}} - 1), \quad (1.7)$$

with inclusion of the relativistic effect. Relativistic effects are significant in the high-density regime such that $r_s < 0.1$.

Degrees of Fermi degeneracy for electrons at temperature T are measured by the ratio

$$\Theta = \frac{k_B T}{E_F}, \quad (1.8)$$

with k_B denoting the Boltzmann constant. When $\Theta < 0.1$, the electrons are in a state of complete Fermi degeneracy; thermal effects are small. $0.1 \leq \Theta \leq 10$ corresponds to a state of intermediate degeneracy; quantum and thermal effects coexist. When $\Theta > 10$, we may regard the system of electrons being in a nondegenerate, classical state; quantum-mechanical interference effects are negligible, except in short-range collisions.

Relativistic effects are negligible in most of the electron gases at finite temperatures, that is, those with $\Theta \geq 0.1$. The thermodynamic functions for such a nonrelativistic electron gas can then be expressed in terms of the Coulomb coupling parameter for the electrons,

$$\Gamma_e = \frac{e^2}{a_e k_B T}, \quad (1.9)$$

and the degeneracy parameter Θ . A useful relation is

$$\Gamma_e = 2 \left[\frac{4}{9\pi} \right]^{2/3} \frac{r_s}{\Theta}. \quad (1.10)$$

Let us consider several parameters characterizing dense semiclassical multi-ionic systems. The Wigner-Seitz radius for an ion of the i species,

$$a_i = \left[\frac{3Z_i}{4\pi n_e} \right]^{1/3}, \quad (1.11a)$$

is called an *ion-sphere* radius. An ion-sphere radius between i and j is then given by

$$a_{ij} = \frac{a_i + a_j}{2}. \quad (1.11b)$$

In dense plasmas where the density of electrons may be assumed constant, Eq. (1.11b) offers an appropriate scaling for the internuclear spacings. Such will be referred to as the *constant electron-density, ion-sphere scaling*.

The ratio between a thermal de Broglie wavelength and the ionic spacing,

$$\Lambda_{ij} = \frac{\hbar\sqrt{2\pi}}{a_{ij}\sqrt{2\mu_{ij}k_B T}}, \quad (1.12a)$$

measures the degrees to which wave-mechanical effects enter a description of the ion fluids. For a OCP, Eq. (1.12a) may be expressed numerically as

$$\Lambda \approx 0.21 \left[\frac{A}{12} \right]^{-5/6} \left[\frac{\rho_m}{10^6 \text{ g/cm}^3} \right]^{1/3} \left[\frac{T}{10^7 \text{ K}} \right]^{-1/2}, \quad (1.12b)$$

where ρ_m designates the mass density. As Eq. (1.12b) illustrates for a WD material, $\Lambda_{ij} < 1$, a condition for a classical fluid, is satisfied in most of the cases treated here.

In an ion fluid with $\Lambda_{ij} \ll 1$, the wave-mechanical effects are negligible; the Coulomb coupling parameter for such a classical plasma is given by

$$\Gamma_{ij} \equiv \frac{Z_i Z_j e^2}{a_{ij} k_B T}. \quad (1.13a)$$

For a OCP, we compute Eq. (1.13a) as

$$\Gamma \approx 36 \left[\frac{Z}{6} \right]^2 \left[\frac{A}{12} \right]^{-1/3} \left[\frac{\rho_m}{10^6 \text{ g/cm}^3} \right]^{1/3} \left[\frac{T}{10^7 \text{ K}} \right]^{-1}. \quad (1.13b)$$

A weakly coupled plasma corresponds to the cases with $\Gamma_{ij} \ll 1$, where the Coulomb interaction can be treated perturbation-theoretically. A strongly coupled plasma refers to the cases with $\Gamma_{ij} \geq 1$, where a perturbation theory is no longer valid and the system begins to exhibit features of microscopic correlations characteristic of liquids.

At still higher densities and lower temperatures, a OCP undergoes a freezing transition into a bcc crystal-

line state (Wigner, 1934, 1938; Brush, Sahlin, and Teller, 1966). It has been shown by a Monte Carlo simulation method (Slattery, Doolen, and DeWitt, 1980, 1982; Ogata and Ichimaru, 1987, 1989; Ogata, 1992) that a dense classical OCP freezes into a crystalline solid as the Coulomb coupling parameter exceeds a critical value, $\Gamma_m \approx 180$. Here it is necessary, in general, to deal with a quantum-mechanical Coulomb solid (Wigner, 1934, 1938; Carr, 1961; Coldwell-Horsfall, and Fein, 1961; Iyetomi, Ogata, and Ichimaru, 1993); the quantum effects are measured through an Einstein frequency ω_0 of the Wigner-Seitz model (e.g., Pines, 1963) in its dimensionless form,

$$Y = \frac{\hbar\omega_0}{k_B T} = \frac{\hbar}{k_B T} \left[\frac{4\pi n_i (Ze)^2}{3M} \right]^{1/2}. \quad (1.14)$$

Thus far we have considered the basic parameters characterizing the individual constituents, electrons, and ions of a plasma. In an ultradense plasma with $r_s \leq 0.01$, the Fermi energy of electrons is relativistically high [cf. Eq. (1.7)], so that their coupling with ions is indeed weak. The kinematic effects of relativistic degenerate electrons (e.g., Landau and Lifshitz, 1969) soften the electrons against compression and thus act to enhance their polarizations (Ichimaru and Utsumi, 1983) to an extent qualitatively different from those in nonrelativistic predictions.

In nonrelativistic plasmas near the boundaries of metal-insulator transitions, effects of strong coupling between electrons and ions become pronounced, giving rise to interesting facets in plasma-physics problems interlinking with atomic and molecular physics. Noteworthy among these is an emergence of *incipient Rydberg states* (IRS) for the short-range, electron-ion correlations in the metallic (plasma) phase (Tanaka, Yan, and Ichimaru, 1990), accounting for their mutual scattering beyond the Born approximation. The IRS acts to modify the short-range interionic potentials as well, and may influence the nuclear reaction rates in dense plasmas through such a modification.

II. ELEMENTS OF NUCLEAR REACTIONS

A. Contact probabilities

The reaction rate (in units of reactions/cm³/s) between nuclei of i and j species at number densities n_i and n_j with a relative kinetic energy E is calculated as

$$R_{ij}(E) = \frac{2S_{ij}(E)r_{ij}^*n_i n_j}{\pi(1+\delta_{ij})\hbar} |\Psi_{ij}(r_N)|^2. \quad (2.1)$$

Here $\Psi_{ij}(r_N)$ refers to the wave function of scattering at the nuclear reaction radius r_N , and

$$r_{ij}^* = \frac{\hbar^2}{2\mu_{ij}Z_i Z_j e^2} \quad (2.2)$$

corresponds to the nuclear Bohr radius, with μ_{ij} denoting

the reduced mass between i and j . Kronecker's delta δ_{ij} enters Eq. (2.1) to account for the cases with $i=j$. The wave function in Eq. (2.1) is normalized so that

$$\int_{\Omega} dr 4\pi r^2 |\Psi_{ij}(r)|^2 = \Omega \quad (2.3)$$

over a spherical volume Ω with a radius $2a_{ij}$, an average nearest-neighbor distance between i and j . Equation (2.1) differs from the rate cited in Salpeter and Van Horn (1969) and in Ogata, Iyetomi, and Ichimaru (1991) by a factor of 4π ; its derivation, as well as the origin of this discord, is explained in Appendix B.

The nuclear cross-section factor $S_{ij}(E)$ is related to the cross section of nuclear reactions via

$$\sigma_{ij}(E) = \frac{S_{ij}(E)}{E} \exp[-\pi(E_G/E)^{1/2}], \quad (2.4)$$

where

$$E_G = \frac{Z_i Z_j e^2}{r_{ij}^*} \quad (2.5a)$$

$$= 50(Z_i Z_j)^2 \frac{2\mu_{ij}}{m_N} \text{ (keV)} \quad (2.5b)$$

is the Gamow energy.

The controlling factor in the analysis of the scattering event is the effective potential between the nuclei in the short-range domain, where the potential may be regarded as isotropic. The calculation of reaction rates [Eq. (2.1)] is then facilitated by the observation that the major contributions to $|\Psi_{ij}(r_N)|^2$ arise from the s -wave scattering acts between the reacting nuclei. The observation stems from the fact that the wave function of scattering in a spherically symmetric potential with the azimuthal quantum number l is proportional to r^l in short ranges (e.g., Schiff, 1968). Since one can generally assume that

$$r_N < r_{ij}^* \ll a_{ij}, \quad (2.6)$$

the s -wave scattering gives the major contribution to the reaction rate, and $r_N \approx 0$ may be taken as far as the calculations of the contact probabilities are concerned.

The s -wave scattering with relative kinetic energy E is described by the Schrödinger equation

$$\left[-\frac{\hbar^2}{2\mu_{ij}} \frac{d^2}{dr^2} + W_{ij}(r) - E \right] r \Psi_{ij}(r) = 0, \quad (2.7)$$

where $W_{ij}(r)$ is the effective potential of scattering.

In analyzing the nuclear reactions in dense plasmas, we single out "reacting (R)" nuclei i and j and name all others as "spectator (S)" nuclei. In addition to those " R " and " S " nuclei, the system contains electrons (and/or muons). The contact probabilities $|\Psi_{ij}(0)|^2$ averaged over the motion of the center of mass for the reacting pairs and over the states of " S " nuclei coincide with the joint probability densities $g_{ij}(0)$. The reaction rates at temperature T are finally obtained through an average:

$$R_{ij}(T) = \langle R_{ij}(E) \rangle_R \quad (2.8)$$

over the states of " R " nuclei.

The central quantity in the theory of nuclear fusion in dense plasmas is therefore $g_{ij}(0)$, the joint probability density at zero separation. It is an *equal-time*, two-particle distribution function evaluated in an equilibrium ensemble; the reaction rates depend on the *static* correlations. In the usual statistical treatment (e.g., Ichimaru, 1992), such a correlation function is expressed in terms of the static and dynamic structure factors, $S(\mathbf{k})$ and $S(\mathbf{k}, \omega)$, via the sum-rule integrations as

$$g(0) = 1 + \frac{1}{n} \int \frac{d\mathbf{k}}{(2\pi)^3} [S(\mathbf{k}) - 1] \\ = 1 + \frac{1}{n} \int \frac{d\mathbf{k}}{(2\pi)^3} \left[\frac{1}{n} \int_{-\infty}^{\infty} d\omega S(\mathbf{k}, \omega) - 1 \right].$$

Since the dynamic structure factor represents the power spectrum of the density-fluctuation excitations in the frequency and wave-vector space, all the dynamical processes are duly taken into account through the sum-rule integrations in the calculation of such a static correlation. In most cases it is therefore incorrect to evoke an additional account of "dynamical" or "nonequilibrium" processes (Salpeter and Van Horn, 1969; Itoh, Totsuji, and Ichimaru, 1977; Mitler, 1977; Carraro, Schäfer, and Koonin, 1988; Schramm and Koonin, 1990) in a calculation of the reaction rates. The reason favoring an equilibrium calculation may be traced to the fact that nuclear reactions are extremely rare events as compared with other scattering and relaxation processes. All the dynamical effects have been incorporated in a correct evaluation of the joint probability density via the sum rule.

B. Binary processes—The Gamow reaction rates

In a tenuous plasma, the effects of the " S " particles and of the electrons are negligible in the thermonuclear reactions of the " R " pairs; the reacting pair may be assumed to interact via the bare Coulomb potential,

$$W_{ij}(r) = W_0(r) = \frac{Z_i Z_j e^2}{r}. \quad (2.9)$$

Equation (2.7) is solved with the "cusp" relation,

$$\lim_{r \rightarrow 0} \frac{d \ln \Psi_{ij}(r)}{dr} = \frac{1}{2r_{ij}^*}, \quad (2.10)$$

which sets a rigorous boundary condition for the wave function in the short-range limit. The contact probabilities are then obtained as (e.g., Schiff, 1968; Ogata, Iyetomi, and Ichimaru, 1991)

$$|\Psi_{ij}(0)|^2 = \frac{\pi \sqrt{E_G/E}}{\exp(\pi \sqrt{E_G/E}) - 1} \quad (2.11a)$$

$$\approx \pi \left[\frac{E_G}{E} \right]^{1/2} \exp \left[-\pi \left[\frac{E_G}{E} \right]^{1/2} \right] \\ (E_G \gg E). \quad (2.11b)$$

The Gamow rate R_G of thermonuclear reactions for an i nucleus is thus calculated by substituting Eq. (2.11b) in Eq. (2.1) and by carrying out the average in Eq. (2.8) with the Boltzmann distribution of E at temperature T ; the result is (Gamow and Teller, 1938; Thompson, 1957)

$$R_G = \frac{16S_{ij}(T)_G r_{ij}^* \tau_{ij}^2}{3^{5/2} \pi (1 + \delta_{ij}) \hbar} n_i n_j \exp(-\tau_{ij}), \quad (2.12)$$

where

$$\tau_{ij} = 3 \left[\frac{\pi}{2} \right]^{2/3} \left[\frac{E_G}{k_B T} \right]^{1/3} \quad (2.13a)$$

$$= 33.81 (Z_i Z_j)^{2/3} \left[\frac{2\mu_{ij}}{m_N} \right]^{1/3} \left[\frac{T}{10^6 \text{ K}} \right]^{-1/2}, \quad (2.13b)$$

and $S_{ij}(T)_G$ is a thermal average of $S_{ij}(E)$.

In the derivation of Eq. (2.12), it has been assumed that $E_G \gg k_B T$, consistent with Eq. (2.11b), implying that $\tau_{ij} \gg 1$. In these circumstances, the integration leading to Eq. (2.12) contains in its integrand a product between a steeply rising term, $\exp(-\pi\sqrt{E_G/E})$, and a steeply decreasing Boltzmann factor, $\exp(-E/k_B T)$, as functions of E . The product thus exhibits the Gamow peak at the energy

$$E_{GP} = \frac{1}{3} \tau_{ij} k_B T. \quad (2.14)$$

The thermal average of $S_{ij}(E)$ should therefore be performed with such a distribution taken into account. The radius $r_{TP}^{(0)}$ of classical turning point for a colliding pair with the Gamow peak energy is thus given by

$$\frac{r_{TP}^{(0)}}{a_{ij}} = \frac{3}{\tau_{ij}} \Gamma_{ij}. \quad (2.15)$$

The Gamow reaction rate, Eq. (2.12), contains a factor $\exp(-\tau_{ij})$ that decreases steeply as the temperature is lowered [cf. Eq. (2.13b)]; the decrease is steeper for a pair with a larger reduced mass. These are typical features in thermonuclear reactions with bare Coulomb repulsion.

C. Few-particle processes—Screened cold fusion

The presence of electrons or other light particles such as muons may act to modify the internuclear potential

from $W_0(r)$ to

$$W_S(r) = W_0(r) S_c(r). \quad (2.16)$$

Here the function $S_c(r)$ describes the screening action of the light particles, which can follow the motion of the nuclei adiabatically. Such a screening function for the Coulomb potential between nuclei may exist, irrespective of whether the reacting nuclei are in itinerant (i.e., fluid), molecular, or cluster states.

For concreteness, we confine ourselves to the cases of screening effects of electrons, free or bound, in condensed materials in the balance of this section. As Eq. (2.16) implies, such a screening action stems from the density *variation out of uniformity*, or *polarization*, of the electrons due to the presence of distinctive nuclear charges. This should therefore be clearly distinguished from the screening potentials, to be introduced in Sec. III [cf. Eq. (3.6)], due to the internuclear many-particle correlations that can arise even when the electrons are regarded as uniform background charges, i.e., in the OCP or BIM models of dense plasmas. Salpeter's (1954) ion-sphere model, for instance, belongs to these; hence it would be a misnomer physically to call such an ion-sphere model a case of strong *electron screening*. The screening potentials in uniform background of electrons will be treated in Sec. IV.A and IV.B; interplay between the internuclear correlations and the electron screening will then be considered in Sec. IV.C.

Since $S_c(r)$ should take on unity at $r = 0$, one expands

$$S_c(r) = 1 - \frac{r}{D_s} + \dots \quad (2.17)$$

so that

$$W_S(r) = W_0(r) - E_s + \dots \quad (2.18)$$

with

$$E_s = \frac{Z_i Z_j e^2}{D_s} \quad (2.19a)$$

$$= 144.0 Z_i Z_j \left[\frac{D_s}{10^{-9} \text{ cm}} \right]^{-1} (\text{eV}). \quad (2.19b)$$

The expansion Eq. (2.17) defines the short-range screening distance D_s . Equation (2.7) may then be solved for the contact probabilities by replacing E with $E + E_s$ in Eq. (2.11) as (Salpeter, 1954)

$$|\Psi_{ij}(0)|^2 = \frac{\pi \sqrt{E_G / (E + E_s)}}{\exp[\pi \sqrt{E_G / (E + E_s)}] - 1} \quad (2.20a)$$

$$\approx \pi \left[\frac{E_G}{E + E_s} \right]^{1/2} \exp \left[-\pi \left[\frac{E_G}{E + E_s} \right]^{1/2} \right] \quad (E_G \gg E + E_s). \quad (2.20b)$$

In performing a thermal average for the "R" pairs, it is useful to introduce the *critical temperature* of screening determined from $E_{GP} = E_s$; i.e.,

$$T_{cs} = \frac{2}{\pi} \left(\frac{r_{ij}^*}{D_s} \right)^{1/2} \frac{Z_i Z_j e^2}{k_B D_s} \quad (2.21a)$$

$$= 5.7 \times 10^4 \sqrt{Z_i Z_j} \left(\frac{2\mu_{ij}}{m_N} \right)^{-1/2} \times \left(\frac{D_s}{10^{-9} \text{ cm}} \right)^{-3/2} \text{ (K).} \quad (2.21b)$$

Relative to this temperature, the strength of the electron-screening effects on nuclear reactions may be classified.

In a high-temperature regime (i.e., $E_{GP} > E_s$) such that

$$T > T_{cs}, \quad (2.22)$$

effects of the electron screening are weak; these can be treated perturbation-theoretically. Substituting Eq. (2.20) in Eq. (2.1) and averaging the result by the Boltzmann distribution yields

$$R_{ws} = \frac{16S_{ij}(T)_{ws} r_{ij}^* \tau_{ij}^2}{3^{5/2} \pi (1 + \delta_{ij}) \hbar} n_i n_j A_{ws}^{(e)} \exp(-\tau_{ij}), \quad (2.23)$$

with the classical turning point at

$$\frac{r_{TP}}{a_{ij}} = \frac{r_{TP}^{(0)}}{a_{ij}}. \quad (2.24)$$

Here $S_{ij}(T)_{ws}$ is another thermal average of $S_{ij}(E)$ appropriate to the weak screening conditions, and the enhancement factor $A_{ws}^{(e)}$ due to the electron screening is calculated as

$$A_{ws}^{(e)} = \left[1 - \frac{3E_s}{\tau_{ij} k_B T} \right] \exp \left(\frac{E_s}{k_B T} \right). \quad (2.25)$$

If, on the other hand, the condition for a strong electron screening, that is,

$$T < T_{cs}, \quad (2.26)$$

is satisfied, we find that Eq. (2.23) is replaced by (Ichimaru, Ogata, and Nakano, 1990)

$$R_{ss} = \frac{1.3S_{ij}(T)_{ss} r_{ij}^*}{(1 + \delta_{ij}) \hbar} n_i n_j \left(\frac{E_G}{E_s} \right)^{1/2} \exp \left[-\pi \left(\frac{E_G}{E_s} \right)^{1/2} \right], \quad (2.27a)$$

where $S_{ij}(T)_{ss}$ is a thermal average of $S_{ij}(E)$, different generally from either $S_{ij}(T)_G$ or $S_{ij}(T)_{ws}$, arising from the strong electron-screening conditions. The classical turning point is now at

$$r_{TP}^{(s)} = D_s \left(1 - \frac{D_s}{2\Gamma_{ij} a_{ij}} \right), \quad (2.28)$$

almost independent of the temperature in dense plasmas.

Contrary to the Gamow rates [Eq. (2.12)] or their weakly electron-screened counterparts [Eq. (2.23)], the reaction rates of Eq. (2.27a) depend weakly on temperature only through $S_{ij}(T)_{ss}$ and possibly E_s , and may increase rather steeply with the electron density via D_s . It is in this context that Cameron (1959) coined the term "pycnonuclear reactions" from the Greek *pyknos*, "compact, dense," to describe nuclear reactions under the strong electron-screening conditions that the rates depend more sensitively on density than on temperature. These analyses are applicable irrespective of whether the "R" nuclei are in a fluid, molecular, or cluster state, as long as condition (2.26) is satisfied.

It is instructive also to rewrite Eq. (2.27a) in the form of Eq. (2.23); that is,

$$R_{ss} = \frac{16S_{ij}(T)_{ss} r_{ij}^* \tau_{ij}^2}{3^{5/2} \pi (1 + \delta_{ij}) \hbar} n_i n_j A_{ss}^{(e)} \exp(-\tau_{ij}). \quad (2.27b)$$

The enhancement factor $A_{ss}^{(e)}$ due to the strong electron screening is then expressed as

$$A_{ss}^{(e)} = \frac{1.27\pi}{\tau_{ij}^2} \left(\frac{E_G}{E_s} \right)^{1/2} \exp \left[-\pi \left(\frac{E_G}{E_s} \right)^{1/2} + \tau_{ij} \right]. \quad (2.29)$$

Table I lists some of the parameters pertinent to electron-screened nuclear fusion reactions in examples of dense astrophysical and laboratory plasmas. The screening distances are estimated here through the random-phase-approximation (RPA) calculations (e.g., Pines and Nozières, 1966; Ichimaru, 1992) described in Appendix A [see Eqs. (A42) and (A74)]; the screening distances for the cases of MH and PH will be considered in Secs. V.E and V.G.

We remark that the first four astrophysical examples (WD1, WD2, BD, and GP) have turned out to be cases of weak electron screening, while the last two terrestrial examples (MH and PM) describe strong electron screening. This is somewhat ironic, since Cameron's idea of pycnonuclear processes was advanced originally for interiors of degenerate stars such as the WD. In these stars, however, the actual temperatures are usually higher than the critical temperatures of electron screening; hence the enhancement due to electron screening is relatively weak. Huge enhancement in the nuclear reaction rates expected in those degenerate stars stem principally from the screening potentials produced by internuclear many-particle processes *without* electron screening, as we shall see in subsequent sections (cf. $A_{ij}^{(0)}$ and $A_{ij}^{(e)}$ in Table IX below).

In an ultradense stellar matter, a different sort of density-sensitive, but temperature-insensitive, nuclear reaction is expected when the plasma freezes into a crystalline state. Here one usually finds $Y \gg 1$ [cf. Eq. (1.14)], so that the zero-point oscillations prevail over the thermal motion of the nuclei. We shall consider this sort of pycnonuclear reaction in Sec. IV.D.

TABLE I. Electron-screening effects in nuclear reactions. Mass densities and temperatures (T) are those assumed for the reacting nuclei. $A^{(e)}$ corresponds to either Eq. (2.25) or Eq. (2.29).

Case: Reaction:	WD1 ^{12}C - ^{12}C	WD2 ^4He - ^4He	BD p - p	GP d - p	MH d - d	PM ^7Li - p
Mass density (g/cm ³)	2×10^9	1×10^8	1×10^3	5	0.23	30
Z_1, Z_2	6,6	2,2	1,1	1,1	1,1	3,1
A_1, A_2	12,12	4,4	1,1	2,1	2,2	7,1
r_s	0.0014	0.0038	0.14	0.93	2.9	0.71
D_s (10 ⁻⁹ cm)	0.042	0.11	1.3	3.2	2.0	2.1
E_s (eV)	1.2×10^5	5.1×10^3	114	45	72	203
E_G (keV)	7.8×10^5	3.2×10^3	50	66.7	100	788
τ_{12}	229	62.8	23.4	137	636	847
$\pi\sqrt{E_G/E_s}$	250	78.5	65.7	121	117	195
T_{cs} (K)	1.1×10^7	1.5×10^6	4.0×10^4	8.6×10^3	1.4×10^4	2.4×10^4
T (K)	5×10^7	1×10^7	3×10^6	2×10^4	300	1000
$\log_{10} A^{(e)}$	12.1	2.4	0.19	11.0	222	280

Strong enhancement of nuclear reactions by electron screening is definitely in effect for dense laboratory plasmas such as MH and PH, where a term such as "electron-screened cold fusion" seems more appropriate. Huge numbers predicted on $A_{ss}^{(e)}$ are misleading, however, since these stem in part from the magnitude of τ_{ij} ; the basic thermonuclear reaction rates (2.12) are therefore extremely low.

Those elementary fusion reactions, with or without electron screening, are still binary as far as the internuclear processes are concerned. Enhancement of the reaction rates due to internuclear correlation processes is, in fact, the principal feature of dense plasmas. Effects of such many-particle effects depend in turn on the nature of binary interactions, with or without electron screening. We shall elucidate these many-particle processes in detail.

III. ENHANCEMENT BY MANY-PARTICLE PROCESSES

A. Historic remarks

In his pioneering work, Schatzman (1948) pointed out that potential barriers between reacting nuclei might be significantly lowered in dense stellar matter ($\rho_m > 10^8$ g/cm³), so that the probabilities of wave functions tunneling through the barrier would be greatly enhanced. The effects of this enhancement on supernova processes were also considered in Schatzman's work.

Cameron (1959) argued that at very high densities electron shielding would cut off nuclear Coulomb potential barriers quite close to the nuclear surface (cf. Sec. II.C). Under these circumstances the classical turning points of low-energy ions are very insensitive to the bombarding energy [cf. Eq. (2.28)]. Nuclear reaction rates thus become very insensitive to temperature but very sensitive to density. Nuclear reaction rates as functions of temperature and density were calculated by double numerical integration of the barrier penetration probability as a func-

tion of bombarding energy for a number of nuclear reactions, including the triple α reactions: $3\alpha \rightarrow ^{12}\text{C}$. Pycnonuclear reaction rates for low temperatures and high densities were calculated for reactions of heavy ions such as ^{12}C with themselves.

Salpeter (1954) originally presented an analytic treatment of the weak screening effect in a low-density, high-temperature plasma such that $\Gamma < 1$, and introduced the ion-sphere model to describe the effects of interionic correlations in the strong-coupling regime, $\Gamma > 1$. Salpeter and Van Horn (1969) then derived general expressions for nuclear reaction rates appropriate to various stellar-interior conditions. "Correction factors" or enhancement factors due to the weak or strong screening over the ordinary thermonuclear reaction rates (cf. Sec. II.A) were thereby evaluated.

From the point of view of a general statistical-mechanical theory, a significant development took place when Widom (1963) showed how certain thermodynamic functions, and also the radial distribution functions (i.e., the joint probability densities), could be expressed in terms of the potential-energy distribution in a fluid. DeWitt, Graboske, and Cooper (1973) then advanced a theory to describe the effect of weak and strong plasma screening on nuclear reactions. These authors used the Monte Carlo simulation data, pioneered by Brush, Sahlin, and Teller (1966), to analyze the effect of strong screening on nuclear reactions in dense plasmas. Graboske *et al.* (1973) used the cluster-expansion theory to treat intermediate screening on nuclear reactions.

These statistical-mechanical theories were subsequently refined by Jancovici (1977) and by Alastuey and Jancovici (1978) through careful examination of the short-range behavior of the internuclear correlation functions. The quantum pair-correlation functions appropriate to the calculation of nuclear reaction rates were formulated by treating the many-body quantum effects through a perturbation theory and by using a semiclassical approximation based on path integrals.

The physics of nuclear fusion in dense plasmas is therefore intimately related with the physics of strongly cou-

pled plasmas with $\Gamma_{ij} > 1$ (Ichimaru, 1982). The study of correlations and thermodynamic properties in such a plasma has progressed significantly in recent years through advancements in the analytic theories (Rosenfeld and Ashcroft, 1979; Iyetomi and Ichimaru, 1982; Iyetomi, Ogata, and Ichimaru, 1992) coupled with accumulation of Monte Carlo simulation data for the OCP (Brush, Sahlin, and Teller, 1966; Hansen, 1973; Slattery, Doolen, and DeWitt, 1980, 1982; Ogata and Ichimaru, 1987; Ogata, Iyetomi, and Ichimaru, 1991), for the BIM (Ichimaru, Iyetomi, and Ogata, 1988; Ogata, Iyetomi, and Ichimaru, 1990, 1991; Ogata *et al.*, 1993), for the electron-screened OCP (Ichimaru and Ogata, 1991), and for deuterons in metals (Ichimaru, Ogata, and Nakano, 1990).

The nuclear reaction rates are related to the short-range behavior of the pair-correlation functions, where the quantum-mechanical effects are essential. For those dense plasmas where the reacting pairs are in fluid states, however, the thermal de Broglie wavelengths are usually shorter than the internuclear spacings (i.e., $\Lambda_{ij} < 1$); classical treatments are applicable here. It has thus been recognized that such an interplay between short-ranged quantum correlations at nuclear distances and intermediate- to long-ranged classical correlations at internuclear distances offers a unique feature of study in a statistical-mechanical theory of nuclear reactions in dense plasmas.

B. Quantum-mechanical correlation functions

1. General approach

We consider a OCP of N particles in a volume V with Hamiltonian \mathcal{H} . Particles 1 and 2 are designated as the “R” pair; the rest, “S” nuclei. The relative coordinates and those of the center of the “R” pair are expressed as \mathbf{r} and \mathbf{R} . The joint probability density of the “R” pair at

zero separation is then given by (Alastuey and Jancovici, 1978)

$$g(0) = V^2 \frac{\langle 00 | \langle "S" | \exp(-\beta \mathcal{H}) | "S" \rangle | 00 \rangle}{\langle \mathbf{r} \mathbf{R} | \langle "S" | \exp(-\beta \mathcal{H}) | "S" \rangle | \mathbf{r} \mathbf{R} \rangle}. \quad (3.1)$$

Here $\beta = 1/k_B T$, and integrations over the respective coordinates are implied when \mathbf{r} , \mathbf{R} , or “S” is left in the bracket notation. Assuming a translational invariance of the system (i.e., fluid), we have set $\mathbf{R} = \mathbf{0}$ in the numerator of Eq. (3.1).

In the range of parameters that we study, the thermal de Broglie wavelengths are small enough for the thermodynamics of the system to be described by classical statistical mechanics (cf. Appendix A.3). This means that those configurations that contribute a non-negligible weight to the denominator of Eq. (3.1) are classical. This denominator can be replaced by $Q/(\Lambda a)^{3N}$, where $a = a_i$ and Q is the classical configuration integral

$$Q = \int d\mathbf{r}_1 \cdots d\mathbf{r}_N \exp[-\beta V(\mathbf{r}; "S")]. \quad (3.2)$$

We express the total potential energy as

$$V(\mathbf{r}; "S") = \frac{(Ze)^2}{r} + W(\mathbf{r}; "S"),$$

where $W(\mathbf{r}; "S")$ is the sum of all interactions except the one between the “R” pair.

The numerator of Eq. (3.1), however, is dominated by configurations in the neighborhood of $\mathbf{r} = \mathbf{0}$, where the potential is very steep, and thus quantum effects are essential for the relative motion between the “R” pair. Most of the motion of its center of mass, and of “S” particles, on the other hand, occurs in regions of configuration space where the potential is smooth, and these motions can be considered classical. It is therefore sufficient to keep the kinetic energy K associated with \mathbf{r} and the total potential energy explicitly in the Hamiltonian \mathcal{H} ; one thus finds

$$g(0; W) = \frac{2^{3/2} V^2 (\Lambda a)^3}{Q} \left\langle 0 \left| \left\langle "S" \right| \exp \left\{ -\beta \left[K + \frac{(Ze)^2}{r} + W(\mathbf{r}; "S") \right] \right\} \right| "S" \right\rangle | 0 \rangle. \quad (3.3)$$

In the framework of these approximations, the quantum many-body problem has been reduced to a quantum one-body problem, which, however, involves a complicated potential $W(\mathbf{r}, "S")$ depending on the coordinates of $N - 2$ “S” particles. In principle, one must first compute the matrix element in Eq. (3.3) for every value of the set of parameters “S” and afterwards perform the integration upon “S”. Alastuey and Jancovici (1978) have shown a way to accomplish this through a systematic method of successive approximations, in which the matrix elements may be evaluated through a path-integral approach (Feynman and Hibbs, 1965).

In the case of an infinitely dilute plasma, the case treat-

ed in Sec. II.B, $g(0; W)$ becomes $g(0; 0)$ and is obtained by using Eq. (3.3) with $Q = V^N$ and $W = 0$. An enhancement factor of the reaction rate due to many-nuclear processes is therefore defined and calculated as

$$A = \frac{g(0; W)}{g(0; 0)} = \frac{V^2}{Q} \left\langle "S" \right| \exp \left[-\frac{S - S_0}{\hbar} \right] \left| "S" \right\rangle. \quad (3.4)$$

Here the action S for a particle with mass $M/2$ is

$$S = \int_0^{\hbar\beta} dt \left[\frac{M}{4} \left(\frac{d\mathbf{r}}{dt} \right)^2 + \frac{(Ze)^2}{r} + W(\mathbf{r}; "S") \right] \quad (3.5)$$

along the trajectory $\mathbf{r}(t)$ that minimizes S ; the trajectories are to be taken from the origin back to the origin, in a time $\hbar\beta$, in the potential with the reversed sign. The action S_0 is a quantity analogous to Eq. (3.5), in which $W=0$ is set. If only the classical trajectories are kept, the calculation will correspond to using the WKB method (Salpeter and Van Horn, 1969; Itoh, Totsuji, and Ichimaru, 1977; Alastuey and Jancovici, 1978) to solve a Schrödinger equation at the energy of the Gamow peak, Eq. (2.14). Ogata, Iyetomi, and Ichimaru (1991) have advanced a method by which the path-integral average can be performed through an exact numerical solution to the Schrödinger equation (2.7).

2. Enhancement factors

From the complicated many-body potential $W(\mathbf{r}; "S")$, one constructs a two-body potential $H(r)$ defined by

$$\exp[\beta H(r)] = \frac{V^2}{Q} \langle "S" | \exp[-\beta W(\mathbf{r}; "S")] | "S" \rangle . \quad (3.6)$$

This function is called the *screening potential* and is related to the classical radial distribution function $g^{(c)}(r)$ via

$$g^{(c)}(r) = \exp \left\{ -\beta \left[\frac{(Ze)^2}{r} - H(r) \right] \right\} . \quad (3.7)$$

The screening potentials are analogously defined for multi-ionic and/or electron-screened plasmas, as we shall consider in Sec. IV.

In terms of the screening potentials, the *enhancement factors due to many-particle processes* are now expressed from Eq. (3.4) in a compact form as

$$A = \exp[\beta \langle H(r) \rangle_R] , \quad (3.8)$$

where $\langle \dots \rangle$ means a path-integral average with respect to the penetrating wave functions $\Psi(r)$ from $r=0$ to the classical turning point, Eq. (2.15), (2.24), or (2.28), and back. The wave functions are calculated from a solution to the Schrödinger equation (2.7) without accounting for the screening potentials. This is justifiable when the major contributions to $\langle H(r) \rangle_R$ stem from the vicinity of $\mathbf{r}=0$, since the steep nuclear potentials dominate the fluctuating many-body potentials near $\mathbf{r}=0$. Decoupling between the "S" and "R" averages is thus completed.

If the classical turning point is far shorter than the internuclear spacings, i.e.,

$$r_{TP} \ll a ,$$

then the enhancement factors are further simplified as

$$A = \exp[\beta H(0)] . \quad (3.9)$$

It is through these formulas that we establish an intimate connection between the nuclear reaction rates and the thermodynamic functions in dense plasmas.

C. Chemical potentials

The screening potentials in multi-ionic electron-screened plasmas are defined in terms of the classical radial distribution functions $g_{ij}^{(c)}(r)$ and the screened binary potentials, Eq. (2.16), as

$$H_{ij}^{(e)}(r) = W_s(r) + k_B T \ln[g_{ij}^{(c)}(r)] . \quad (3.10)$$

These are the crucial quantities in the theoretical estimates for enhancement factors of the nuclear reaction rates in dense plasmas. Explicit evaluation of such a potential calls for a careful analysis combining the Monte Carlo simulations and solutions to appropriate integral equations; these will be treated in Sec. IV.

The screening potentials have the short-range expansion in power series of r^2 , due to Widom (1963). It has been proved, in particular, that $H_{ij}(0)$ corresponds to the increment in the excess chemical potentials for the "R" pair before and after the reactions (Hoover and Poirer, 1962; Widom, 1963; DeWitt, Grabske, and Cooper, 1973; Jancovici, 1977). Let $F_{ex}^{BIM}(N_1, N_2)$ denote the excess free energy of a BIM consisting of N_1 ions with charge number Z and N_2 ions with charge number $2Z$. The OCP screening potential at $r=0$ is then given by

$$H(0) = F_{ex}^{BIM}(N, 0) - F_{ex}^{BIM}(N - 2, 1) . \quad (3.11)$$

Since in the notation of Eq. (A56)

$$\begin{aligned} \beta F_{ex}^{BIM}(N_1, N_2) &= (N_1 + N_2) f_{ex}^{BIM}(\Gamma_e, x; Z, 2Z) \\ &= N_1 f_{ex}^{OCP}(\Gamma_{11}) + N_2 f_{ex}^{OCP}(\Gamma_{22}) \\ &\quad + (N_1 + N_2) \Delta f_{ex}^{BIM}(\Gamma_e, x; Z, 2Z) , \end{aligned} \quad (3.12)$$

one finds

$$\begin{aligned} \beta H(0) &= 2f_{ex}^{OCP} - f_{ex}^{OCP}(2^{5/2}\Gamma) \\ &\quad - \frac{\partial}{\partial z} \Delta f_{ex}^{BIM}(\Gamma_e, x; Z, 2Z)|_{x=0} . \end{aligned} \quad (3.13)$$

Salpeter (1954), in his ion-sphere model (e.g., Ichimaru, 1982), set

$$f_{ex}^{OCP} = -0.9\Gamma ,$$

$$\Delta f_{ex}^{BIM}(\Gamma_e, x; Z, 2Z) = 0 ,$$

to find

$$\beta H(0)_S = 1.057\Gamma . \quad (3.14)$$

Jancovici (1977) then derived a formula,

$$\beta H(0)_J = 1.0531\Gamma + 2.2931\Gamma^{1/4} - 0.5551 \ln \Gamma - 2.35 , \quad (3.15)$$

on the basis of $f_{ex}^{OCP}(\Gamma)$ obtained from the OCP simulation data (Hansen, 1973; Hansen, Torrie, and Vieillefosse, 1977). Recent simulation results, Eqs. (A48) and (A57), may likewise be used in Eq. (3.13) for an evaluation of

$\beta H(0)$. These evaluations compare quite favorably with the direct Monte Carlo determination to be presented in Sec. IV.A; degrees of agreement increase in a latest work. This shows the importance of the departure from the linear-mixing law, the last term in Eq. (3.13), in the calculation of enhancement factors.

It is instructive further to consider the application of Eq. (3.11) to an evaluation of $\beta H(0)$ for hydrogen in metals. We first note that the short-range screening distances D_s of the metallic electrons give rise to an additional source of excess free energy (in units of $k_B T$),

$$f_{ei} = -\frac{\beta(Ze)^2}{2D_s}, \quad (3.16)$$

per an ion with electric charge Ze [cf. Eqs. (A69) and (A71)]. We also note that the electron-screened Coulomb coupling parameters of hydrogen nuclei take on reduced values [cf. Eq. (A86)],

$$\Gamma_s = \frac{\beta(Ze)^2}{a} S_c(a). \quad (3.17)$$

These result in the evaluation

$$\beta H(0) = \beta H_{ei}(0) + \beta H_{ii}^{(e)}(0), \quad (3.18)$$

with

$$\beta H_{ei}(0) = \frac{\beta(Ze)^2}{D_s}, \quad (3.19)$$

$$\begin{aligned} \beta H_{ii}^{(e)}(0) &= 2f_{ex}^{\text{OCP}}(\Gamma_s) - f_{ex}^{\text{OCP}}(2^{5/3}\Gamma_s) \\ &\quad - \frac{\partial}{\partial x} \Delta f_{ex}^{\text{BIM}}(\Gamma_s, x; 1, 2)|_{x=0}. \end{aligned} \quad (3.20)$$

Equation (3.19) is the effect that Leggett and Baym (1989) have considered as the difference in binding energies between an α particle and two deuterons in metals. These effects, in fact, belong to the few-particle processes treated in Sec. II.C and give rise to a reaction rate of Eq. (2.27) under conditions (2.26) of the electron-screened cold fusion. As we shall see numerically in Sec. V.E, the expected reaction rates stay below the exact upper bounds set by these authors.

Equation (3.20) represents the internuclear many-body processes, derived through Eq. (3.10), leading to further enhancement of the reaction rates by an approximate factor of $\exp[\beta H_{ii}^{(e)}(0)]$. Since the force fields of deuterons are screened rather strongly by metallic electrons, and effective coupling constants, Eq. (3.17), take on substantially reduced values. For calculations of possible nuclear reaction rates in metal hydrides, however, Eq. (3.20) is not applicable directly, since it has not taken into account the inhomogeneous lattice fields produced by metal atoms. Monte Carlo analyses of correlations between deuterons in such a lattice field were carried out (Ichimaru, Ogata, and Nakano, 1990) and have shown the possibility of substantial enhancement in the reaction rates due to the many-particle processes (cf. Sec. V.E).

IV. CORRELATION FUNCTIONS AND ENHANCEMENT FACTORS

A. Classical one-component-plasma

1. Monte Carlo screening potentials

Interparticle correlations in strongly coupled plasmas have been studied using Monte Carlo (MC) simulation methods (Metropolis *et al.*, 1953; James, 1980). The radial distribution function² $g(r)$ represents the probability density of finding another particle at a distance r away from a given particle, normalized so that it approaches unity as $r \rightarrow \infty$. These functions have been sampled accurately by the MC methods. Figure 1 plots the MC data of the OCP radial distribution functions at various values of Γ (Iyetomi, Ogata, and Ichimaru, 1992a). The radial distribution functions obtained in Fig. 1 clearly exhibits the effects of strong Coulombic repulsion at short distances, creating the excluded Coulomb holes around given nuclei. Physically, these Coulomb holes and the ion-sphere models (Salpeter, 1954) are similar in content and represent the consequences of internuclear correlations without participation of electron screening.

The screening potentials may then be sampled through the relation (DeWitt, Grabske, and Cooper, 1973; Itoh, Totsuji, and Ichimaru, 1977)

$$H(r) = \frac{(Ze)^2}{r} + k_B T \ln[g(r)]. \quad (4.1)$$

Examples of recent sampling (Ogata, Iyetomi, and Ichimaru, 1991) are exhibited in Figs. 2 and 3. The screening potentials cannot be derived directly from MC simulation data in the short distances, however, since the strong Coulomb repulsion makes it impossible to sample $g(r)$ at $r \approx 0$. One therefore studies the short-range values of $H(r)$ by a different method.

It has been proved (Widom, 1963) that $H(r)$ has a short-range expansion in a power series of r/a as

$$\beta H(r) = h^{(0)} - h^{(1)} \left[\frac{r}{a} \right]^2 + h^{(2)} \left[\frac{r}{a} \right]^4 + \dots \quad (4.2)$$

The coefficient $h^{(1)}$ is known to take on a value

$$h^{(1)} = \frac{\Gamma}{4} \quad (4.3)$$

in a OCP (Jancovici, 1977).

The coefficient $h^{(2)}$ is related to a mean-square value of the microscopic forces acting on a given test particle with charge $2Ze$ (Widom, 1963; Ogata, Iyetomi, and Ichimaru, 1991). Let $\Phi(r)$ be the Coulomb potential (in

²Here and hereafter, the radial distribution functions are considered only in the classical evaluations; the superscript (*c*) will thus be omitted.

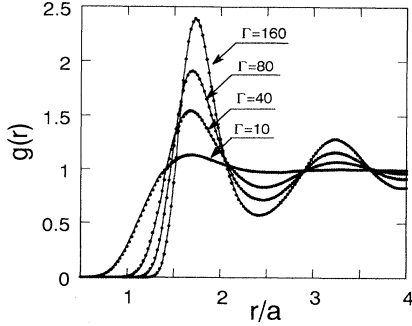


FIG. 1. Radial distribution functions of OCP fluids obtained by MC simulations with $N=1024$ at various values of Γ . The number of MC configurations generated for each run was 7×10^6 ; $g(r)$ was calculated with 200 bins in the range $0 < r < L/2$, half of the cubic MC cell with size $L = 16.2a$. From Iyetomi, Ogata, and Ichimaru (1992).

units of $k_B T$) acting on that test particle at \mathbf{r} from all other N particles forming the OCP with charge Ze . The coefficient $h^{(2)}$ is then calculated in the ensemble of MC-generated configurations as

$$h^{(2)} = \frac{a^4}{384} \left\langle \left[\left(\frac{d\Phi}{dr_1} \right)^2 - 2 \frac{d^2\Phi}{dr_1^2} \right]^2 \right\rangle - \frac{\Gamma^2}{32}, \quad (4.4)$$

where r_1 represents one of the Cartesian components of \mathbf{r} , with the statistical average $\langle \dots \rangle$ carried out over 2.5×10^5 configurations in the MC sequences. The values of $h^{(2)}$ so calculated in accordance with Eq. (4.4) are tabulated in Table II. For confirmation on the accuracy of the MC averaging, a quantity

$$I = \frac{1}{2\Gamma} \left\langle \left(\frac{d\Phi}{dr_1} \right)^2 \right\rangle,$$

which should be exactly unity for a OCP, is likewise computed and listed in Table II. Within the accuracy of the

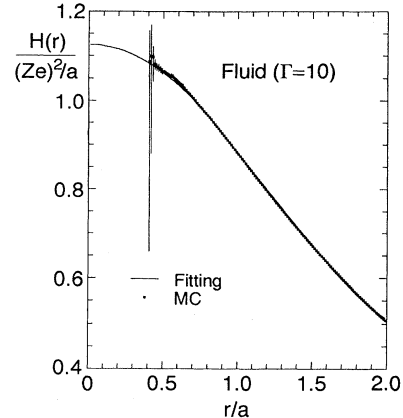


FIG. 2. Screening potential of OCP fluid at $\Gamma=10$, with the number of MC particles, $N=432$, and the number of MC configurations generated, 2.5×10^8 . The maximum extent of uncertainties in the MC sampling points is 10^{-4} unless explicitly shown by vertical bars. From Ogata, Iyetomi, and Ichimaru (1991).

MC sampling, one thus concludes that

$$h^{(2)}/\Gamma \approx 0.00 \pm 0.01; \quad (4.5)$$

the computed values, smaller in magnitude than the extent of errors, are far smaller than $h^{(1)}$. We remark that Eq. (4.5) is the result of first-principles calculations; the recent choice of $h^{(2)}/\Gamma = 0.03$ made by Rosenfeld (1992) is irrelevant.

The evaluations in Eqs. (4.3) and (4.5) enable one to extrapolate the MC data on $\beta H(r)$ accurately toward $r=0$. Combining these short-range analyses with the MC sampling of $\beta H(r)$ in the intermediate distances, Ogata, Iyetomi, and Ichimaru (1991) have derived a parametrized equation for the screening potential in a strongly coupled OCP fluid ($5 < \Gamma \leq 180$):

$$\frac{\beta H(r)}{\Gamma} = \begin{cases} A_1 - B_1^2 - \frac{1}{4}x^2, & \text{for } x \leq 2B_1, \\ A_1 - B_1 x + \frac{1}{x} \exp(C_1 \sqrt{x} - D_1), & \text{for } 2B_1 < x < 2. \end{cases} \quad (4.6)$$

Here $x = r/a$, and the fitting parameters are given by

$$\begin{aligned} A_1 &= 1.356 - 0.0213 \ln \Gamma, & B_1 &= 0.456 - 0.013 \ln \Gamma, \\ C_1 &= 9.29 + 0.79 \ln \Gamma, & D_1 &= 14.83 + 1.31 \ln \Gamma. \end{aligned} \quad (4.7)$$

In Figs. 2 and 3, comparison is made between the MC values and the fitting formula (4.6); agreement is excellent.

It should be noted that A_1 , B_1 , C_1 , and D_1 for OCP fluids contain dependence on $\ln \Gamma$. These, together with departures of Eq. (4.6) from linearity in the intermediate regime ($2B_1 < x < 2$), are the features unknown in the

earlier analyses (DeWitt, Grabske, and Cooper, 1973; Itoh, Totsuji, and Ichimaru, 1977) and constitute new findings in these elaborate MC analyses.

Finally, combining Eqs. (4.6) and (4.7), one obtains MC

TABLE II. Monte Carlo values of $h^{(2)}$ and I .

Γ	$h^{(2)}$	I
10	0.006 ± 0.088	0.989 ± 0.00098
40	-1.2 ± 1.4	0.9921 ± 0.00017
80	-5.3 ± 5.4	0.9910 ± 0.000089
160	10.1 ± 21.3	1.0077 ± 0.000069

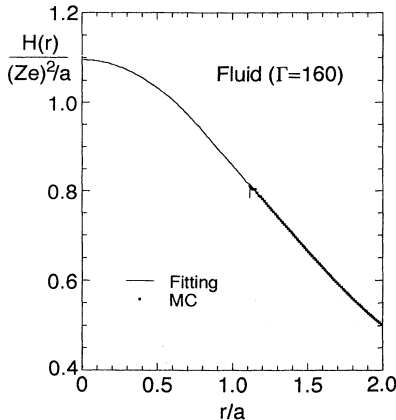


FIG. 3. Screening potential of OCP fluid at $\Gamma=160$, with the number of MC particles, $N=432$, and the number of MC configurations generated, 1.0×10^8 . The maximum extent of uncertainties in the MC sampling points is 10^{-5} unless explicitly shown by vertical bars. From Ogata, Iyetomi, and Ichimaru (1991).

values of the screening potential at zero separation as

$$\beta H(0) = 1.148\Gamma - 0.00944\Gamma \ln \Gamma - 0.000168\Gamma (\ln \Gamma)^2. \quad (4.8)$$

In light of Eq. (4.5), estimated errors in these evaluations are on the order of 0.1%.

2. Bridge functions

Correlation functions in classical fluids may be studied through the methods of integral equations (e.g., Hansen and McDonald, 1986). In a theoretical treatment of dense OCP fluids, the hypernetted-chain (HNC) scheme (van Leeuwen, Groeneveld, and De Boer, 1959; Morita, 1960) provides an accurate description of interparticle correlations and thermodynamic functions (Ichimaru, Iyetomi, and Tanaka, 1987). The HNC approximation ignores the bridge functions and the contributions arising from the bridge diagrams, in the logarithm of the radial distribution function, that is, the potential of mean force (Hansen and McDonald, 1986). The HNC scheme is good at portraying long-range correlations in a Coulombic system, while the bridge functions account for strong correlations at short distances.

Bridge functions are collections of closely connected Mayer diagrams (Hansen and McDonald, 1986). Rosenfeld and Ashcroft (1979) assumed that the bridge functions as such would not depend on details of the potential and thus should have a nearly universal functional form. The bridge functions of the OCP were thereby replaced by those of hard-sphere systems, which were short ranged and stayed negative (repulsive) over the whole range of interparticle separations. The bridge functions for the OCP, a system with a softest interparticle potential, thus provide a crucial test for such a universality hy-

pothesis. Breakdown of the universality ansatz in the vicinity of the first peak of the radial distribution function $g(r)$ was earlier demonstrated through a calculation of the lowest-order bridge diagrams in the OCP (Iyetomi and Ichimaru, 1983). Evaluation of the bridge functions therefore plays an essential part in any attempt to improve on the HNC scheme, and thereby provides an accurate description of short-range correlations essential for the rates of nuclear reactions.

The radial distribution functions of the classical OCP fluids are formulated as (Hansen and McDonald, 1986)

$$g(r) = \exp \left[-\frac{(Ze)^2}{k_B T r} + h(r) - c(r) + B(r) \right]. \quad (4.9)$$

Here $c(r)$ is the direct correlation function, related to the total correlation function

$$h(r) = g(r) - 1 \quad (4.10)$$

through the Ornstein-Zernike relation,

$$h(r) = c(r) + n \int d\mathbf{r}' c(|\mathbf{r}-\mathbf{r}'|) h(r'). \quad (4.11)$$

The $B(r)$ in Eq. (4.9) is the bridge function representing all the bridge-diagram contributions. Physical contents of $B(r)$ have been elucidated in terms of correlation formalisms based on the density-functional theory (Iyetomi and Ichimaru, 1983; Ichimaru, Iyetomi, and Tanaka, 1987).

Equation (4.9), coupled with Eq. (4.1), constitutes a basic set of equations for the correlation functions in the theory of liquid structures. One of the closure schemes for these sets of equations, the HNC approximation, adopts

$$B(r) = 0 \quad (4.12)$$

in Eq. (4.9). The HNC scheme provides an accurate description for an OCP with $\Gamma < 5$.

In a strongly coupled plasma, where the enhancement of nuclear reaction rates by many-particle processes is significant, the bridge functions need to be appropriately taken into account for the analysis of interparticle correlations. One can use the set of relations, Eqs. (4.9) and (4.11), for a rigorous determination of $B(r)$ once $g(r)$ is known by some means. To achieve this end, Iyetomi, Ogata, and Ichimaru (1992) have carried out MC simulations for $g(r)$ in the OCP fluids at four levels of Coulomb coupling: $\Gamma = 10, 40, 80$, and 160 . The number of particles confined in the cubic MC cell of size L was $N = 1024$, so that $L = 16.2a$. The long-range nature of the Coulomb potential has been accounted for through a combination of the periodic boundary conditions with the Ewald sum technique. For each run, 7×10^6 configurations were generated and $g(r)$ was sampled with 200 bins in the range of $0 < r < \frac{1}{2}L$.

The bridge functions are related to the screening potentials via

$$B(r) = \beta H(r) - h(r) + c(r). \quad (4.13)$$

The MC simulation data alone are not sufficient to determine $B(r)$ over the entire regime of interparticle separations, however, because of the finiteness in MC-cell size and strong repulsion at short distances. Issues of "extracting" the bridge functions therefore ensue (Poll, Ashcroft, and DeWitt, 1988).

Such an issue has been given a solution in a complete form by Iyetomi, Ogata, and Ichimaru (1992). Extrapolation to short ranges has been achieved by the Widom expansion, Eq. (4.2). In the long ranges, these authors noted the compressibility sum rule for the Fourier transform $\tilde{c}(k)$ of the direct correlation function (Ichimaru, Iyetomi, and Tanaka, 1987), i.e.,

$$\lim_{k \rightarrow 0} \left[\tilde{c}(k) + \frac{4\pi e^2 \beta}{k^2} \right] = \frac{1}{n} \left[1 - \frac{\kappa_0}{\kappa_T} \right]. \quad (4.14)$$

Here κ_T and κ_0 are the isothermal compressibility [cf. Eq. (A43)] and its ideal-gas value ($=\beta/n$) of the OCP.

The bridge functions so extracted have been expressed in an analytic formula as

$$\frac{B(r)}{\Gamma} = (-b_0 + c_1 x^4 + c_2 x^6 + c_3 x^8) \exp \left[-\frac{b_1}{b_0} x^2 \right], \quad (4.15)$$

with the parameters

$$\begin{aligned} b_0 &= 0.258 - 0.0612 \ln \Gamma + 0.0123 (\ln \Gamma)^2 - \frac{1}{\Gamma}, \\ b_1 &= 0.0269 + 0.0318 \ln \Gamma + 0.00814 (\ln \Gamma)^2, \\ c_1 &= 0.498 - 0.280 \ln \Gamma + 0.0294 (\ln \Gamma)^2, \\ c_2 &= -0.412 + 0.219 \ln \Gamma - 0.00251 (\ln \Gamma)^2, \\ c_3 &= 0.0988 - 0.0534 \ln \Gamma + 0.00682 (\ln \Gamma)^2. \end{aligned} \quad (4.16)$$

The accuracy of Eq. (4.15) is confined nearly within the computational errors inherent in the MC simulations over the entire regime of the interparticle separations in the parametric domain $5 < \Gamma \leq 180$.

3. Improved hypernetted-chain schemes

Once the bridge functions have been evaluated, they can be used for improvement of the HNC scheme. The analytic formula (4.15) with Eqs. (4.16), substituted for $B(r)$ in Eq. (4.9), completes the set of equations leading to such an improvement of the HNC approximation. Since all the parameters in the bridge functions have been predetermined, the numerical complexity in a solution to the improved HNC (IHNC) scheme will not exceed that in the original HNC scheme.

The validity and accuracy of the IHNC scheme have been confirmed through various points of examination: the correlation functions, the thermodynamic functions, and the compressibility sum rule (Iyetomi, Ogata, and Ichimaru, 1992). Figure 4 shows that the screening po-

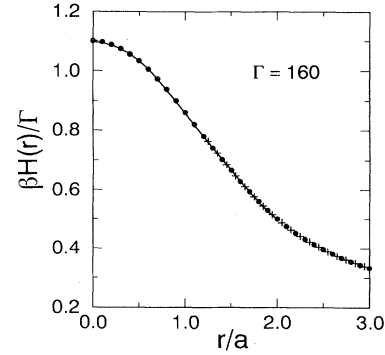


FIG. 4. Screening potential $H(r)$ for an OCP at $\Gamma=160$. The solid curve represents Eq. (4.6); the dots represent IHNC values and the crosses represent the MC values. From Iyetomi, Ogata, and Ichimaru (1992).

tential with the IHNC scheme excellently reproduces the MC and Widom-expansion values.

4. Enhancement factors

Let us proceed to consider the enhancement factor, Eq. (3.8), of thermonuclear reaction rates in a strongly coupled OCP. The path-integral average has been carried out as usual with the classical trajectories, where the WKB approximation is applicable for a solution to the Schrödinger equation (Salpeter and Van Horn, 1969; Itoh, Totsuji, and Ichimaru, 1977). Alastuey and Jancovici (1978) developed a perturbation-theoretic method by which quantum corrections beyond the WKB approximation could be evaluated.

With the screening potential given by Eq. (4.6), Ogata, Iyetomi, and Ichimaru (1991) were able to calculate the path-integral averages in Eq. (3.8) through an exact numerical solution to Eq. (2.7) with cusp condition (2.10). Over 120 parametric combinations between E and Γ , Eq. (2.7) with $W_{ij}(r)=(Ze)^2/r$ and that with

$$W_{ij}(r)=\frac{(Ze)^2}{r}-H(r), \quad (4.17)$$

have been solved numerically for the contact probabilities. The results are parametrized in an analytic formula, which is then subjected to a thermal average with respect to E over the Boltzmann distribution. The enhancement factor so calculated is expressed as

$$A = \exp(Q), \quad (4.18)$$

where

$$Q = C_0 \Gamma - \frac{5}{32} \Gamma \left[\frac{3\Gamma}{\tau} \right]^2 \left[1 + (C_1 + C_2 \ln \Gamma) \frac{3\Gamma}{\tau} + C_3 \left[\frac{3\Gamma}{\tau} \right]^2 \right] \quad (4.19)$$

with

$$\begin{aligned} C_0 &= 1.148 - 0.00944 \ln \Gamma - 0.000168 (\ln \Gamma)^2, \\ C_1 &= 1.1858, \\ C_2 &= -0.2472, \\ C_3 &= -0.07009, \end{aligned} \quad (4.20)$$

and τ given by Eq. (2.13) with $i=j$. This fit is applicable for $5 < \Gamma \leq 180$ and $3\Gamma/\tau \leq 2$. Maximum departure of the fitted values from the computed values does not exceed unity.

The first term $C_0 \Gamma$ of Eq. (4.19) corresponds to the classical contribution, Eq. (4.8). With the lowest-order quantum corrections taken into account, one finds

$$Q|_{LQ} = \beta H(0) - \frac{5}{32} \Gamma \left[\frac{3\Gamma}{\tau} \right]^2, \quad (4.21)$$

an equation first derived by Jancovici (1977).

$$\frac{\beta H_{ij}(r)}{\Gamma_{ij}} = \begin{cases} \frac{\beta H_{ij}(0)}{\Gamma_{ij}} - h_{ij}x^2, & \text{for } x \leq \frac{1}{2} \frac{B_{ij}}{h_{ij}}, \\ A_{ij} - B_{ij}x + \frac{1}{x} \exp(C_{ij}\sqrt{x} - D_{ij}), & \text{for } \frac{1}{2} \frac{B_{ij}}{h_{ij}} < x < 2. \end{cases} \quad (4.24)$$

Here $x = r/a_{ij}$, and

$$\frac{\beta H_{ij}(0)}{\Gamma_{ij}} = A_{ij} - \frac{1}{4} \frac{B_{ij}^2}{h_{ij}}, \quad (4.25)$$

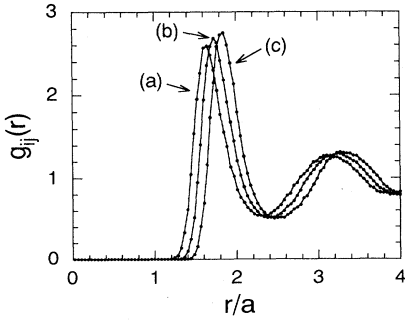


FIG. 5. Radial distribution functions $g_{ij}(r)$ in BIM with $Z_1=6$, $Z_2=8$, $x=0.5$, and $\Gamma_{11}=163.5$; $a=\langle Z \rangle^{1/3} a_e$ with $\langle Z \rangle=(1-x)Z_1+xZ_2$. The number of MC particles is $N=1024$, and the number of MC configurations generated is 7×10^6 . (a) $g_{11}(r)$, (b) $g_{12}(r)$, and (c) $g_{22}(r)$.

B. Classical binary-ionic-mixture fluids

1. Monte Carlo screening potentials

We consider a classical BIM fluid [cf. Eq. (1.12)] with

$$\Lambda_{ij} < 1, \quad (4.22)$$

characterized by the parameters of Appendix A.4. Inter-particle correlations in such a BIM fluid has been studied using MC simulation methods (Ichimaru, Iyetomi, and Ogata, 1988; Ogata, Iyetomi, and Ichimaru, 1991; Ogata *et al.*, 1993).

Figures 5 and 6 show examples of the radial distribution functions $g_{ij}(r)$ sampled in dense BIMs. The MC screening potentials defined as

$$H_{ij}(r) = \frac{Z_i Z_j e^2}{r} + k_B T \ln[g_{ij}(r)] \quad (4.23)$$

are likewise exhibited in Figs. 7 and 8.

2. Ion-sphere scaling

As in the cases of dense OCP fluids, the functional form of the screening potential can be accurately determined through a combined analysis between the MC sampling at intermediate distances ($0.4 < r/a_{ij} < 2$) and the short-range Widom (1963) expansion as (Ogata, Iyetomi, and Ichimaru, 1991)

$$h_{ij} = \frac{(Z_i^{1/3} + Z_j^{1/3})^3}{16(Z_i + Z_j)}. \quad (4.26)$$

The values of the fitting parameters are listed in Table III

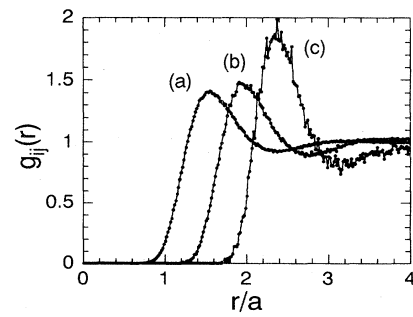


FIG. 6. Radial distribution functions $g_{ij}(r)$ in BIM with $Z_1=1$, $Z_2=3$, $x=0.1$, and $\Gamma_{11}=20$; $a=\langle Z \rangle^{1/3} a_e$ with $\langle Z \rangle=(1-x)Z_1+xZ_2$. The number of MC particles is $N=1000$, and the number of MC configurations generated is 7×10^6 . (a) $g_{11}(r)$, (b) $g_{12}(r)$, and (c) $g_{22}(r)$.

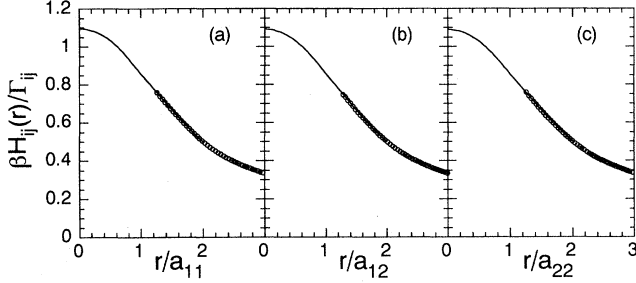


FIG. 7. Screening potentials $H_{ij}(r)$ in BIM under the same conditions as those in Fig. 5. The open circles are MC sampling values; the solid curve, fitting formula (4.24).

as the “Fluid” case.

Since the interparticle distances r in Eq. (4.24) are scaled by a_{ij} of Eq. (1.11), the dense BIM fluids are said to obey the constant electron-density, ion-sphere scaling (Salpeter, 1954; Itoh *et al.*, 1979). Parametrized values of Eq. (4.24) are also exhibited and compared with the MC values in Figs. 7 and 8. The ion-sphere scaling appears to hold reasonably well. Effects of small but non-negligible deviations from such an ion-sphere scaling on reaction rates have been considered by Ogata *et al.* (1992).

3. Enhancement factors

Enhancement factors A_{ij} for the rates of nuclear reactions between i and j are then calculated from the screening potentials, Eq. (4.24), in accordance with Eq. (3.8). Setting

$$A_{ij} = \exp(Q_{ij}), \quad (4.27)$$

$$\begin{aligned} Q_{ij} = & \beta H_{ij}(0) - \frac{5}{32} \Gamma_{ij} \left[\frac{3\Gamma_{ij}}{\tau_{ij}} \right]^2 \\ & \times \left[1 + (1.1858 - 0.2472 \ln \Gamma_{ij}) \frac{3\Gamma_{ij}}{\tau_{ij}} \right. \\ & \left. - 0.07009 \left[\frac{3\Gamma_{ij}}{\tau_{ij}} \right]^2 \right]. \quad (4.28) \end{aligned}$$

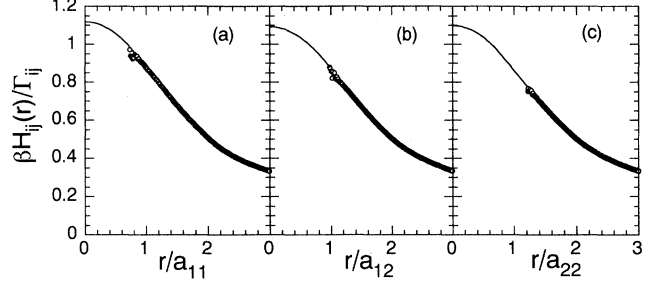


FIG. 8. Screening potentials $H_{ij}(r)$ in BIM under the same conditions as those in Fig. 6. The open circles are MC sampling values; the solid curve, fitting formula (4.24).

C. Electron-screened one-component-plasma and binary-ionic-mixture fluids

1. Screening potentials

The short-range screening effects of relativistic degenerate electrons, appropriate to WD and neutron star interiors, on Coulomb repulsion between the reacting nuclei were elucidated by Ichimaru and Utsumi (1983) with the aid of the relativistic free-electron polarizabilities (Jancovici, 1962) and the local-field corrections of the degenerate electrons (Ichimaru and Utsumi, 1981). It has been shown that the kinematic effects of relativistic degenerate electrons (e.g., Landau and Lifshitz, 1969; see also Appendix A.1) soften the electrons against compression and thus act to enhance the screening and thereby the rates of nuclear reactions. Salient results of these analyses are summarized in Appendix A.6.

To supplement such an analytic calculation, Ichimaru and Ogata (1991) conducted a MC simulation study of the screening potential for carbon matter at $\rho_m = 2 \times 10^9$ g/cm³ and $T = 10^8$ K, assuming that the interparticle potential was given by

$$W_s(r) = \frac{(Ze)^2}{r} \exp \left[-\frac{r}{D_s} \right], \quad (4.29)$$

with $Z = 6$ and $D_s/a = 3.2$, as in Eq. (A74). The screening potential $H^{(e)}(r)$ defined in Eq. (3.10) has been sampled over 5×10^6 MC configurations generated with 500 particles in the periodic boundary conditions; the result is plotted in Fig. 9.

The MC data are then fitted with analytic formulas as

TABLE III. Parameters in the BIM screening potentials.

Case	A_{ij}	B_{ij}	C_{ij}	D_{ij}
Fluid	$1.356 - 0.0213 \ln \Gamma_{ij}$	$0.456 - 0.130 \ln \Gamma_{ij}$	$9.29 + 0.79 \ln \Gamma_{ij}$	$14.83 + 1.31 \ln \Gamma_{ij}$
Solid				
(C-C)	$1.83 - 0.035\sqrt{x}$	$0.350 - 0.015\sqrt{x}$	$13.2 - 10.2\sqrt{x}$	$22.1 - 14.4\sqrt{x}$
(C-O)	1.166	0.340	13.2	22.5
(O-O)	1.183	0.350	$34.0 - 20.8\sqrt{x}$	$51.3 - 29.2\sqrt{x}$

$$\frac{H^{(e)}(r)}{(Ze)^2/a} = \begin{cases} 0.8252 - 0.2312(r/a)^2, & \text{for } r/a \leq 0.8427, \\ -1.048 + 2.071 \exp[-0.228(r/a)], & \text{for } 0.8427 < r/a < 2. \end{cases} \quad (4.30)$$

The expression for intermediate range, the second line of Eq. (4.30), stems from an actual fit of the MC data as shown in Fig. 9.

The first line, on the other hand, derives from a short-range expansion:

$$H^{(e)}(r) = H^{(e)}(0) - \frac{(Ze)^2}{12a} \left[\frac{a}{D_s} \right]^2 \times \left\langle \sum_{l \neq 1} \frac{a}{r_{1l}} \exp \left[-\frac{r_{1l}}{D_s} \right] \right\rangle \left[\frac{r}{a} \right]^2, \quad (4.31)$$

where $r_{ij} = |\mathbf{r}_i - \mathbf{r}_j|$. The statistical average in the second term can be evaluated by the MC sampling in a test-particle system in which the test particle "1" interacts with other 498 l particles via a potential $2W_s(r)$, while the 498 l particles interact with each other through the potential $W_s(r)$. The coefficient 0.2312 in the second term of Eq. (4.30) has been obtained through an evaluation of the statistical average in Eq. (4.31) over 3×10^6 MC configurations generated in such a system. With this coefficient determined, the first term of Eq. (4.31), 0.8252, stems from a smooth extrapolation towards the short-range domain. Parenthetically, the OCP value of the coefficient in the quadratic term of Eq. (4.31) has been known identically to be 0.25 [cf. Eq. (4.3)], which can be confirmed by such a MC method as well.

In the absence of electron screening, Eq. (4.8) yields $H(0)/[(Ze)^2/a] = 1.110$ for the carbon OCP under consideration. Hence one has

$$H(0) - H^{(e)}(0) = 0.285 \frac{(Ze)^2}{a}.$$

On the other hand, an application of Salpeter's ion-sphere model, Eq. (3.14), in Eq. (3.20) yields

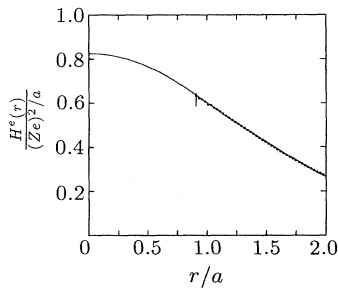


FIG. 9. Screening potential in a carbon matter with the electron-screened potential Eq. (4.29) and $D_s/a = 3.2$. The maximum extent of uncertainties in the MC sampling points is 10^{-5} , unless explicitly shown by vertical bars. From Ichimaru and Ogata (1991).

$$H(0) - H^{(e)}(0) = 1.057 \left[1 - \exp \left[-\frac{a}{D_s} \right] \right] \frac{(Ze)^2}{a} = 0.284 \frac{(Ze)^2}{a}, \quad (4.32)$$

a value in good agreement with the MC value.

2. Enhancement factors

The screening by electrons acts in two ways to influence the rates of nuclear reactions. First, as we have considered in detail in Sec. II.C and revisited briefly in Eqs. (3.16) and (3.19), the binary repulsive potentials between reacting nuclei are reduced by electrons, resulting in an enhancement of the reaction rates; these are the short-range screening effects (Ichimaru and Utsumi, 1983). The reduction in particle interactions by the screening, in turn, affects the many-body correlation processes and generally acts to lower the values of resultant enhancement factors, as compared with those in many-body processes *without* electron screening, as Eq. (4.32) illustrates. These long-range effects of electron screening (Ichimaru and Utsumi, 1984; Ichimaru and Ogata, 1991) therefore counteract the gain obtained in the short-range processes. Thus the net gain due to electron screening may not be as large as the direct-screening calculations in Sec. II.C might imply.

For generality, we present a calculation of the extra enhancement factors in dense BIM fluids arising from electron screening; transfer of the result to the electron-screened OCP cases is straightforward. In such a calculation, one can assume that the electron-screening effect, though finite and thus non-negligible, may be treated as a weak perturbation; hence the WKB approximation may be applicable in the evaluation of the enhancement factor due to the electron screening. The contact probabilities $|\Psi_{ij}(0)|^2$ are then proportional to the WKB penetration probabilities $P_{ij}(E)$ between reacting nuclei:

$$P_{ij}(E) = \exp \left[-\frac{2\sqrt{2\mu_{ij}}}{\hbar} \int_0^{r_{\text{TP}}} dr \sqrt{W_{ij}(r) - E} \right]. \quad (4.33)$$

Here the effective potential of scattering is

$$W_{ij}(r) = \frac{Z_i Z_j e^2}{r} \exp \left[-\frac{r}{D_s} \right] - H_{ij}^{(e)}(r) \quad (4.34)$$

with the screening potential

$$\frac{H_{ij}^{(e)}(r)}{Z_i Z_j e^2 / a_{ij}} = \begin{cases} 0.8252 - 0.2312 \left[\frac{r}{a_{ij}} \right]^2 & \text{for } \frac{r}{a_{ij}} \leq 0.8427 , \\ -1.048 + 2.071 \exp \left[-0.228 \frac{r}{a_{ij}} \right] & \text{for } 0.8427 < \frac{r}{a_{ij}} < 2 . \end{cases} \quad (4.35)$$

The radius of classical turning point is determined from

$$W_{ij}(r_{TP}) = E . \quad (4.36)$$

The penetration probabilities $P_{ij}^{(e)}(T)$ at temperature T with inclusion of the electron screening are consequently evaluated through thermal averages of Eq. (4.33) over the Boltzmann factor; that is,

$$P_{ij}^{(e)}(T) = \frac{2\beta^{3/2}}{\sqrt{\pi}} \int_0^\infty dE \sqrt{E} \exp(-\beta E) P_{ij}(E) . \quad (4.37)$$

Analogously, we define the penetration probabilities $P_{ij}^{(0)}(T)$ without electron screening, which may be obtained by ignoring the electron-screening effects in both

$$Q_{ij}^{(e)} = \langle Z \rangle^{1/3} \frac{a_e}{D_s} \left\{ 1 - 1.057 \frac{D_s}{a_{ij}} \left[1 - \exp \left(-\frac{a_{ij}}{D_s} \right) \right] \right\} \Gamma_{ij} + \left[0.342 - 0.354 \exp \left(-0.228 \frac{3\Gamma_{ij}}{\tau_{ij}} \right) \right] \Gamma_{ij} \frac{3\Gamma_{ij}}{\tau_{ij}} \\ - \frac{3}{8} \left[\langle Z \rangle^{1/3} \frac{a_e}{D_s} \right]^2 \Gamma_{ij} \frac{3\Gamma_{ij}}{\tau_{ij}} + 0.091 \left[\langle Z \rangle^{1/3} \frac{a_e}{D_s} \right]^{2.923} \Gamma_{ij} \left(\frac{3\Gamma_{ij}}{\tau_{ij}} \right)^{1.897} . \quad (4.40)$$

The enhancement factor (4.38) thus increases rather steeply with $\langle Z \rangle$ and the mass densities. Enhancement of nuclear reactions due to the electron screening becomes significant in high- Z materials such as carbon and oxygen at high densities near ignition.

For the nuclear reactions in plasmas with modest densities, such as those in SI, ICF, and possibly BD, one finds $\Gamma < 1$ and $\Theta > 0.1$; both correlation effects between the nuclei and screening effects by electrons may be looked upon as weak. In these circumstances, the classical turning points are located far shorter than the internuclear spacings, and thus the enhancement factors are given by Eq. (3.9).

In these weak-screening regimes, dominant effects in the enhancement of nuclear reaction rates arise from the screening of internuclear forces by electrons (Salpeter and Van Horn, 1969; Ichimaru, Tanaka, and Iyetomi, 1984); hence the enhancement factors over the Gamow rates, Eq. (2.12), are given by Eq. (2.25). A crucial problem in the evaluation of such an enhancement is the assessment of the short-range screening distance D_s which enters Eq. (2.25) via Eq. (2.19). Here it has been recognized (Tanaka, Yan, and Ichimaru, 1990) as essential to account for the effects of short-range scattering in a way that goes beyond those described by the Born approximation. The IRS, mentioned in Sec. I.D and described in

terms on the right-hand side of Eq. (4.34), i.e., unscreened BIM cases. The enhancement factors due to the electron screening are thus defined and calculated as

$$A_{ij}^{(e)} \equiv \exp(Q_{ij}^{(e)}) = \frac{P_{ij}^{(e)}(T)}{P_{ij}^{(0)}(T)} . \quad (4.38)$$

In order to derive a parametrized expression for the enhancement factors (4.38), Ichimaru and Ogata (1991) have carried out the relevant WKB integrations (4.37) for 12 cases of the combination $a_e \langle Z \rangle^{1/3} / D_s = 0.2, 0.4$, and 0.6 and $3\Gamma_{ij}/\tau_{ij} = 0.5, 1.0, 1.5$, and 2.0 , where

$$\langle Z \rangle = (1-x)Z_1 + xZ_2 . \quad (4.39)$$

The result takes the form

Appendix A.7, can account for such an effect and leads to a prediction,

$$\frac{1}{D_s} = A_1 K_s + A_2 K_b - A_3 , \quad (4.41)$$

with the aid of Eqs. (A80)–(A85).

Enhancement factors arising further from many-body correlations between electron-screened ions are then evaluated by the use of Eqs. (4.18) and (4.19) where $C_0 \Gamma$, Γ , and $3\Gamma/\tau$ are to be replaced by $1.057\Gamma \exp(-a/D_s)$, $\Gamma \exp(-a/D_s)$, and the actual radius of the classical turning point divided by a .

D. Crystalline solids

1. Monte Carlo lattice potentials

The body-centered-cubic (bcc) crystalline structures are known to have the lowest values in the Madelung energies of the Coulombic crystals (e.g., Mott and Jones, 1936); hence one usually assumes a bcc structure for a dense Coulomb solid. The lattice potential $W_{ij}^L(r)$ of such a bcc crystalline plasma is defined as the effective potential between two particles in nearest-neighbor sites, at an

interparticle separation r . The screening potential $H_{ij}^L(r)$ for a Coulomb solid is then calculated in accordance with

$$W_{ij}^L(r) = \frac{Z_i Z_j e^2}{r} - H_{ij}^L(r). \quad (4.42)$$

We remark that the major contributions to $|\Psi_{ij}(0)|^2$ arise from the s -wave scattering acts between the reacting nuclei, for which the angular-averaged lattice potential in Eq. (4.42) is valid. The factor that crucially controls such a scattering event and the resulting contact probability is then the effective potential between the nuclei in the short-range domain, where the screening potential may likewise be regarded as isotropic. The use of angular-averaged potentials therefore constitutes an accurate approximation in the treatment of nuclear reactions in solids.

These potentials can be analyzed through MC sampling methods in a way analogous to the fluid cases. Here one deals with the joint probability densities between those pairs of particles located in the nearest-neighbor sites of the bcc lattice (Ichimaru and Ogata, 1990; Ogata, Iyetomi, and Ichimaru, 1990, 1991), since only those can, in fact, constitute the reacting pairs. Figure 10 illustrates such a screening potential for an OCP solid at $\Gamma=200$. Extrapolation into the short-range domain is executed analogously with the aid of Eq. (4.2).

Salpeter and Van Horn (1969), on the other hand, advanced the following model calculation of the lattice potential: One picks a pair of nearest-neighbor particles in a bcc crystal (with the lattice constant b and the nearest-neighbor distance d), and then calculates the electrostatic energy as a function of the interparticle separation r with the center of mass fixed. In their fully relaxed approximation, these authors subsequently adjusted the resultant screening potential near $r=0$ in accordance with the ion-sphere model of Salpeter (1954). The screening potential for a OCP solid obtained in such a relaxed lattice

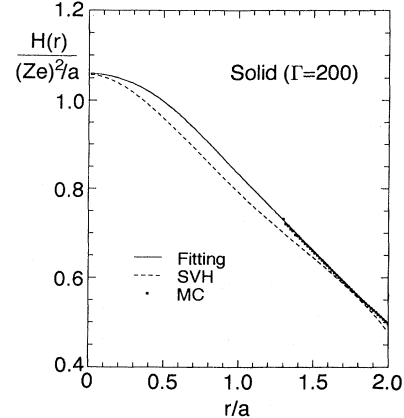


FIG. 10. Screening potential between pairs of the first nearest-neighbor particles for a OCP solid at $\Gamma=200$. The maximum extent of uncertainties in the MC sampling points is 10^{-4} , unless explicitly shown by vertical bars. SVH refers to Eq. (4.43); Fitting, Eq. (4.44). From Ogata, Iyetomi, and Ichimaru (1991).

model was expressed as

$$\begin{aligned} \frac{H^{SVH}(r)}{(Ze)^2/b} = & 1.1547 + 1.1602(1-y) - 1.0394(1-y)^2 \\ & + 2.5690(1-y)^3 - 1.6971(1-y)^4, \end{aligned} \quad (4.43)$$

where $y=r/d$. This potential is also exhibited in Fig. 10 for comparison with the MC values; a reasonable similarity is observed between the two potentials.

The carbon-oxygen (C-O) BIM screening potentials, an important case for the supernova study and determined through those MC and extrapolation procedures, are expressed in parametrized forms as (Ogata, Iyetomi, and Ichimaru, 1991)

$$\frac{\beta H_{ij}^L(r)}{\Gamma_{ij}} = \begin{cases} \frac{\beta H_{ij}(0)}{\Gamma_{ij}} - h_{ij}x^2 & \text{for } x \leq \frac{1}{2} \frac{B_{ij}}{h_{ij}}, \\ A_{ij} - B_{ij}x + \frac{1}{x} \exp(C_{ij}\sqrt{x} - D_{ij}) & \text{for } \frac{1}{2} \frac{B_{ij}}{h_{ij}} < x < 2. \end{cases} \quad (4.44)$$

Here $x=r/a_{ij}$, and

$$\frac{\beta H_{ij}(0)}{\Gamma_{ij}} = A_{ij} - \frac{1}{4} \frac{B_{ij}^2}{h_{ij}}, \quad (4.44a)$$

$$h_{ij} = \frac{(Z_i^{1/3} + Z_j^{1/3})^3}{16(Z_i + Z_j)}. \quad (4.44b)$$

The values of A_{ij} , B_{ij} , C_{ij} , and D_{ij} are listed in Table III for C-O bcc crystals. The cases of an OCP solid can be recovered with these formulas in the OCP limit of either $x=0$ or $x=1$.

It should be remarked that the short-range screening potentials, Eq. (4.44), between C-C are here found to depend on x , the molar fraction of oxygen. As x increases, the screening potential is therefore predicted to decrease in the short ranges, implying a blocking effect of oxygen against the pycnonuclear reactions of carbon, to be treated in the next section. Analogous composition-dependent effects in the short-range screening potentials between C-O and between O-O, however, have not been found, to the extent and accuracy of the simulation study thus far carried out (Ogata *et al.*, 1993).

2. Pycnonuclear reaction rates in C-O solids

For nuclear reactions in C-O BIM solids, one can show (Ogata, Iyetomi, and Ichimaru, 1991) that a condition for pycnonuclear reactions,

$$Y \gg 1 ,$$

is satisfied either for carbon or for oxygen. The nuclei forming quantum solids are thus in the ground state at their equilibrium lattice sites, performing zero-point vibrations. The principal problem then is the evaluation of contact probabilities $|\Psi_{ij}(0)|^2$ for the reaction rates in such a quantum solid.

This problem is approached through a solution to Eq. (2.7) in which Eq. (4.42) is substituted for $W_{ij}(r)$ (Ogata, Iyetomi, and Ichimaru, 1991). Thus E in Eq. (2.7) corresponds to the ground-state energy of a particle trapped around the potential minimum of $W_{ij}^L(r)$ at $r_m = 1.76a_{ij}$. Equation (2.7) has been solved by numerical integration starting from $r \approx 0$ to $r = 2a_{ij}$, with the boundary conditions (a) “cusp” Eq. (2.10), and (b) a self-consistent ground state, where $\Psi_{ij}(r)$ take on maxima at r_m with the values E equal to the expectation values of $-(\hbar^2/2\mu_{ij})d^2/dr^2 + W_{ij}^L(r)$ over the volume Ω . The solution is therefore exact without resorting to the conventional WKB approximation.

The contact probabilities $|\Psi_{ij}(0)|^2$ are thus computed in 45 cases for the combinations of C-C, C-O, and O-O in BIM solids over the range of mass densities, $(2 \times 10^6) - 10^{11}$ g/cm³. The results are then parametrized in analytic formulas as functions of the molar fraction x of oxygen with fitting errors in $\ln[\Psi_{ij}(0)]$ less than 6%. Finally, the pycnonuclear reaction rates in the C-O BIM solids are obtained from Eq. (2.1) as

$$R_{ij}^{\text{PYC}} (\text{s}^{-1}) = \frac{K\rho_8^\alpha}{1+\delta_{ij}} \exp \left[-\frac{K_1 + K_2 \sqrt{x}}{\rho_8^{1/6}} \right. \\ \left. - K_3 - K_4 \sqrt{x} \right]. \quad (4.45a)$$

Here ρ_8 means the mass density in units of 10^8 g/cm³; the parameters α , K , K_1 , K_2 , K_3 , and K_4 are listed in Table IV. In the determination of K , the values of the cross-section parameters (Fowler, Caughlan, and Zimmerman, 1967, 1975) $S_{\text{CC}} = 8.83 \times 10^{16}$, $S_{\text{CO}} = 1.15 \times 10^{21}$, and

$S_{\text{OO}} = 2.31 \times 10^{27}$, in units of MeV b, have been used. The blocking effects of oxygen on the pycnonuclear reactions enter through the x dependence represented by the coefficients K_2 and K_4 ; these do not vanish with C-C reactions. The reaction rates (4.45a), independent of temperatures, increase steeply with the mass density.

The pycnonuclear reaction rates in OCP solids were calculated by Salpeter and Van Horn (1969) in the WKB approximation. With the relaxed-lattice model potential of Eq. (4.43), their carbon-reaction rates read

$$R^{\text{SVH}} (\text{s}^{-1}) = 1.11 \times 10^{38} \rho_8^{7/12} \exp \left[-\frac{263.3}{\rho_8^{1/6}} \right]. \quad (4.45b)$$

Numerical agreement between Eqs. (4.45a) and (4.45b) appears almost perfect, despite differences in the screening potentials (cf. Fig. 10) and in the ways the Schrödinger equation was solved.

Recently, Schramm and Koonin (1990) revisited the Salpeter–Van Horn calculations of pycnonuclear fusion rates and attempted to improve these calculations by taking additional account of what they called the dynamic polarization effects of the surrounding lattice. For the reason mentioned in the last paragraph of Sec. II.A, it is irrelevant to evoke an additional account of such a dynamic process in the calculation of the reaction rates.

3. Pycnonuclear reaction rates in binary-ionic-mixture solids

In a BIM solid, the distance between two neighboring nuclei—which are the only ones capable of participating in pycnonuclear reactions—is approximately equal to the sum of the ion-sphere radii of the two nuclei, $r_m \approx a_i + a_j$.

To examine the accuracy of this ion-sphere scaling, Ogata *et al.* (1993) have performed a series of MC samplings for the joint probabilities $g_{ij}(r)$ between i and j nuclei in ground-state BIM solids for 20 different cases, with combinations of the parameter values $x = \frac{5}{432}, \frac{1}{4}, \frac{1}{2}, \frac{3}{4}$ and $Z_j/Z_i \equiv R_Z = \frac{4}{3}, \frac{5}{3}, 2, 3, 4$. Generally, in BIM solids, the ground-state configurations deviate significantly from the simple periodic bcc lattice structure, mainly because $a_i \neq a_j$ for $Z_i \neq Z_j$. In fact, for $R_Z \geq \frac{5}{3}$, it has been observed that ground states are characterized more appropriately as aperiodic glassy solids. Under these cir-

TABLE IV. Parameters in Eq. (4.45a) for the pycnonuclear reaction rates.

Parameter	C-C	C-O	O-O
K	$1.30 \times 10^{31} \frac{1-x}{3+x}$	$1.11 \times 10^{35} \frac{\sqrt{x(1-x)}}{3+x}$	$1.42 \times 10^{41} \frac{x}{3+x}$
α	0.397	0.421	0.455
K_1	257.486	327.132	414.706
K_2	2.636		
K_3	-15.114	-15.940	-16.192
K_4	-0.560		

cumstances, the exact MC nearest-neighbor separation $r_{m,ij}$ may be determined from the observed peak position of $g_{ij}(r)$; the results are then expressed as the sum of the ion-sphere-scaling contribution and a deviation therefrom:

$$r_{m,ij} = 1.76a_{ij} + \Delta r_{m,ij}. \quad (4.46)$$

The deviations $\Delta r_{m,ij}$, characterizing the extra distortions in the particle configurations due to the charge disparities in the BIM solids, have been measured in the MC data; the results can be summarized in the following parametrized forms as functions of molar fraction of x of the j species for $0 \leq x \leq 1$ and $1 \leq R_Z < 4.5$:

$$\frac{\Delta r_{m,11}}{a_{11}} = 0.44 \frac{(R_Z - 1)(2.3 - R_Z)}{R_Z^2} x^{1.3}, \quad (4.47a)$$

$$\frac{\Delta r_{m,12}}{a_{12}} = -0.043 \frac{\sqrt{R_Z - 1}}{1 + 100x^{1.3}}, \quad (4.47b)$$

$$\frac{\Delta r_{m,22}}{a_{22}} = -0.17 \frac{(R_Z - 1)(2.3 - R_Z)}{R_Z^2} (1-x)^{1.3}. \quad (4.47c)$$

A number of observations are in order concerning these results: (1) The corrections to the ion-sphere scaling are small but non-negligible. (2) For the relative magnitudes of the deviations, one has $|\Delta r_{m,11}| > |\Delta r_{m,22}| \gg |\Delta r_{m,12}|$. (3) $\Delta r_{m,11}$ and $\Delta r_{m,22}$ are opposite in sign. (4) $\Delta r_{m,11}$ is positive for $R_Z < 2.3$, corresponding to the “blocking effect” of nuclear reactions discovered for C-O solids. When R_Z is not excessively large, the phase-space reduction effect of the heavier (i.e., higher- Z) nuclei is likewise small; these heavier nuclei simply act as obstacles for reactions between the lighter (i.e., lower- Z) nuclei. (5) For $R_Z > 2.3$, on the other hand, $\Delta r_{m,11}$ takes on negative values, implying enhancement in the pycnonuclear rates for the lighter species. This enhancement stems from a “catalyzing action” of the heavier elements, which reduces the effective volume available to the lower- Z nuclei, thus reducing the internuclear separations. This catalyzing action is a new feature discovered in these MC simulation studies of BIM solids.

The pycnonuclear rates of the previous section are now generalized to cover various combinations of nuclear species in BIM solids (Ichimaru, Ogata, and Van Horn, 1992); the reaction rates per cm^3 per second are expressed as

$$R_{ij} = \frac{1.34 \times 10^{32}}{1 + \delta_{ij}} \frac{X_i X_j (A_i + A_j)}{Z_i Z_j (A_i A_j)^2} S_{ij} \rho_m \times \lambda_{ij}^{-1.809} \exp(-2.460 \lambda_{ij}^{-1/2}), \quad (4.48)$$

where

$$\lambda_{ij} = (\frac{3}{4})^{1/2} \frac{r_{ij}^*}{r_{m,ij}}, \quad (4.49)$$

S_{ij} are the cross-section factors (in MeV barns) for the

BIM, ρ_m is the mass density, and A_i and X_i are the mass number and mass fraction of the i species.

E. Hydrogen in metal hydrides

1. Monte Carlo simulations in metallic lattices

Observation of nuclear fusion reactions between itinerant hydrogen in metal hydrides (MH_x) claimed in recent experiments (e.g., Jones *et al.*, 1989) has created a challenge to condensed-matter physics, calling for a theoretical account of how two hydrogen nuclei can come to fuse by overcoming the Coulombic repulsive forces in such a metallic environment. Other experiments (e.g., Gai *et al.*, 1989; Ziegler *et al.*, 1989) conducted under analogous settings, however, have not shown any significant observation of nuclear reactions. One therefore speculates that the rates of nuclear reactions should depend extremely delicately on the states of reacting pairs at short distances.

The itinerant hydrogen in metal differs from that in either stellar interiors or the ICF plasmas in two important aspects: Hydrogen nuclei are strongly screened by valence electrons and by nearly localized electrons in hybridized states (Alefeld and Völk, 1978; Ichimaru, Nakano, Ogata, Tanaka, Iyetomi, and Tajima, 1990). The metal atoms situated at periodic or aperiodic (due to defects) lattice sites create inhomogeneous fields which act to trap (or to localize) the hydrogen nuclei and thereby to alter microscopic features of the short-range correlations. Owing to these influences of the screening electrons and the inhomogeneous lattice fields, the hydrogen in a metal hydride bears a dual character of itinerant and trapped particles (Ichimaru, Ogata, and Nakano, 1990).

The lattice fields of metal atoms in which hydrogen nuclei “move” are constructed so that the following observed features may be taken into account: In densely hydrated phases, both Pd and Ti assume a face-centered-cubic (fcc) structure with lattice constants $d = 4$ and 4.4 \AA , respectively. In a Pd lattice (Drexel *et al.*, 1976; Alefeld and Völk, 1978), hydrogen sits around the octahedral (O) sites, where the potential assumes local minima with curvature $\Phi'' \approx 1.1 \text{ eV \AA}^{-2}$. Barrier height between the minima, $\Delta\Phi \approx 0.23 \text{ eV}$, is inferred from diffusivity. The separation between nearest-neighbor O sites is 2.8 \AA . In a Ti lattice (Pan and Webb, 1965; Korn and Zamir, 1970; Alefeld and Völk, 1978), the tetrahedral (T) sites are the local minima with curvature $\Phi'' \approx 5.1 \text{ eV \AA}^{-2}$, barrier height $\Delta\Phi \approx 0.51 \text{ eV}$, and the nearest-neighbor separation 2.2 \AA .

Since the heights of the potential barriers substantially exceed the room temperatures, the bulk of the hydrogen nuclei would be in trapped states around O or T sites. As finiteness of diffusivity implies, a small fraction of the hydrogen remains in itinerant states. In a nonequilibrium situation, this fraction may take on a larger value, approaching unity.

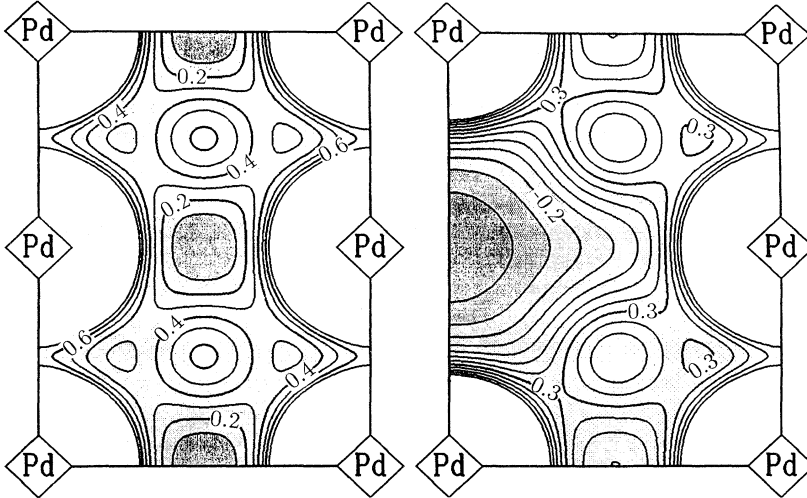


FIG. 11. Equipotential contours for deuterons in eV on the $\{110\}$ plane of fcc Pd lattices. The zero level is taken at the octahedral sites (with dark shadow) in a periodic lattice (left); potential in a lattice with defect is on the right. From Ichimaru, Ogata, and Nakano (1990).

For a construction of Pd and Ti fields with the features mentioned above, model potentials of the following equations between metal and hydrogen were proposed (Ichimaru, Ogata, and Nakano, 1990):

$$V_{\text{Pd-H}}(r) = \frac{22.2 \text{ eV } \text{\AA}}{r} \exp \left[-\frac{r}{0.42 \text{ \AA}} \right], \quad (4.50\text{a})$$

$$\begin{aligned} V_{\text{Ti-H}}(r) = & \frac{31.8 \text{ eV } \text{\AA}}{r} \left[\exp \left[-\frac{r}{0.51 \text{ \AA}} \right] \right. \\ & + \left[\frac{r}{1.095 \text{ \AA}} \right]^{10.57} \\ & \times \exp \left[-\frac{r}{0.23 \text{ \AA}} \right] \Big]. \end{aligned} \quad (4.50\text{b})$$

The equipotential contours on the $\{110\}$ planes of the fcc lattices so calculated for Pd and Ti with and without missing atoms (defects) are portrayed in Figs. 11 and 12. As expected, a broad potential minimum appears around

a defect, which may further trap one or more hydrogen atoms.

The model potentials $V_{\text{H-H}}(r)$ of binary interaction between hydrogen in PdH and TiH_2 were calculated in terms of the charge form factors derived for the $s-d$ hybridized electrons and by taking account of dielectric screening due to the valence electrons (Ichimaru, Nakano, Ogata, Tanaka, Iyetomi, and Tajima, 1990). The result was expressed as a summation between the repulsive and attractive parts,

$$V_{\text{H-H}}(r) = V_R(r) + V_A(r), \quad (4.51)$$

which were parametrized as

$$V_R(r) = \frac{e^2}{\epsilon_c r} \left[\exp \left[-\frac{r}{D_s} \right] + \left(\frac{r}{r_R} \right)^p \exp \left[-\frac{r}{D_i} \right] \right], \quad (4.52)$$

$$V_A(r) = -\frac{e^2}{\epsilon_c r} \left(\frac{r}{r_A} \right)^q \exp \left[-\frac{r}{D_A} \right]. \quad (4.53)$$

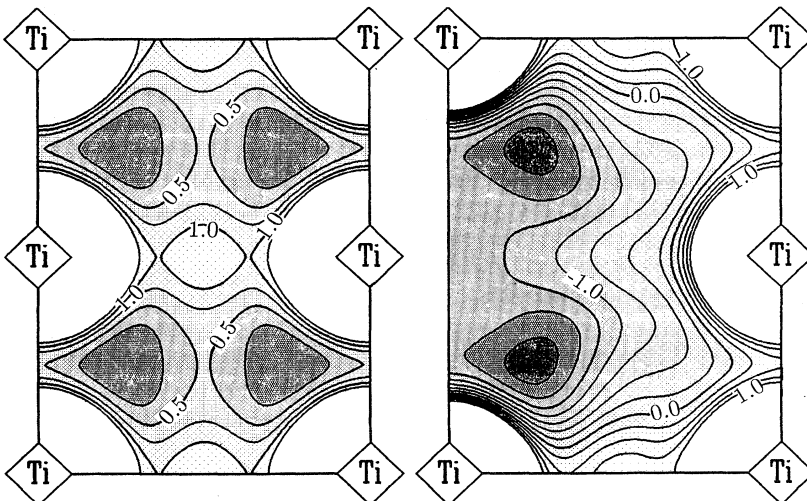


FIG. 12. Same as Fig. 11, but for fcc Ti lattices. The zero level is taken at the tetrahedral sites. From Ichimaru, Ogata, and Nakano (1990).

TABLE V. Parameters in Eqs. (4.52) and (4.53) for the model potentials describing electron-screened hydrogen-hydrogen interaction in metal hydrides.

Parameter	PdH	TiH ₂
ϵ_c	1.25	1.36
D_s (Å)	0.19	0.28
r_R (Å)	1.04	1.00
D_R (Å)	0.18	0.17
r_A (Å)	0.74	0.61
D_A (Å)	0.23	0.25
p	8.9	10.0
q	2.7	2.9

The adopted values (Ichimaru, Ogata, and Nakano, 1990) for the core-electron dielectric constant ϵ_c , the short-range screening length D_s , and other parameters in these formulas for PdH and TiH₂ are listed in Table V.

Between Eqs. (4.52) and (4.53), the repulsive part $V_R(r)$ represents the major contribution in short ranges, where the nuclear reactions are most effectively influenced by interparticle correlations. The screening potential associated with such a repulsive part may then be defined as

$$H_R(r) = V_R(r) + k_B T \ln[g_R(r)]. \quad (4.54)$$

Here $g_R(r)$ refers to a joint probability density for a (fictitious) system of hydrogenic nuclei interacting via $V_R(r)$ in the inhomogeneous lattice fields of Fig. 11 or 12.

Such a correlation function can likewise be sampled through a MC simulation method designed appropriately for the hydrogen-in-metal cases (Ichimaru, Ogata, and Nakano, 1990). Periodic lattice fields for the MC simulation were determined by placing 500 metal atoms at fcc sites in a MC cell with periodic boundary conditions. Fields with defects were produced by removing eight metal atoms randomly so that no pairs of defects occupied nearest-neighbor sites. The corresponding numbers

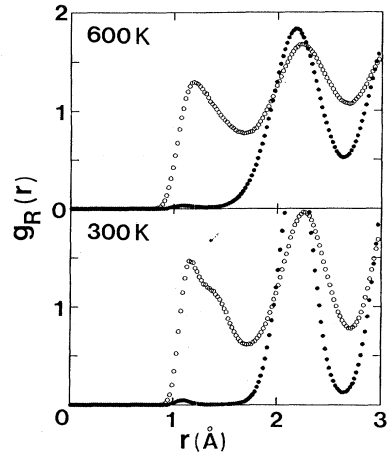


FIG. 14. Same as Fig. 13, but in Ti. From Ichimaru, Ogata, and Nakano (1990).

of hydrogen atoms, 500 for PdH and 1000 for TiH₂, were placed in the cell at random. A sequence of MC configurations was then generated through the random displacements of hydrogen positions, in the Metropolis algorithm (Metropolis *et al.*, 1953) with the canonical distribution for the sum of interaction energies between metal and hydrogen and between hydrogen atoms. Several runs of such simulations were performed to cover various cases of metal hydrides at temperatures of 300, 600, and 1200 K. Each run consisted typically of $(1-3) \times 10^4$ configurations per hydrogen atom to ensure an equilibrated metastable state in the system.

The joint probability densities $g_R(r)$ were sampled in the statistical ensemble of particle configurations generated by such a simulation. As Figs. 13 and 14 illustrate, the lattice fields act to develop humps in $g_R(r)$ at short distances inside the major humps corresponding to the nearest-neighbor O or T sites. Those short-distance

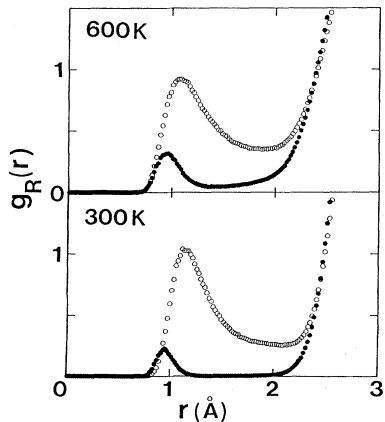


FIG. 13. Joint probability densities between deuterons in Pd for the repulsive potential, Eq. (4.52). Solid circles are for the case of the periodic lattice; open circles, a lattice with defects. From Ichimaru, Ogata, and Nakano (1990).

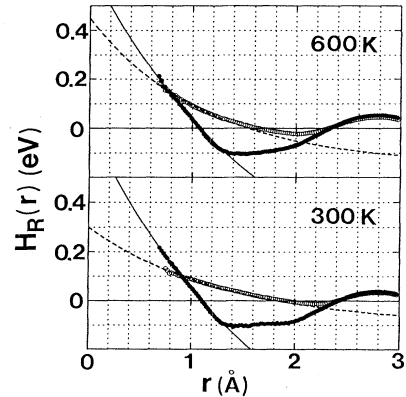


FIG. 15. Repulsive screening potentials between deuterons in Pd and their short-range fitting by the formula $A + B \exp(-Cr)$. Solid circles and lines are for the periodic lattice; open circles and dashed lines are for lattice with defects. From Ichimaru, Ogata, and Nakano (1990).

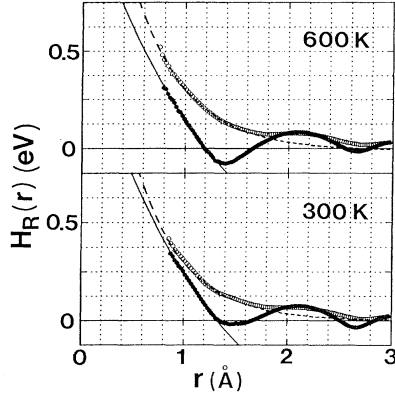


FIG. 16. Same as Fig. 15, but in Ti. From Ichimaru, Ogata, and Nakano (1990).

humps are the consequences of the potential “dimples” in the lattice fields, which induce effective attraction between hydrogen atoms in trapping sites.

Figures 15 and 16 show the values of $H_R(r)$ resulting from Figs. 13 and 14 via Eq. (4.54). The “visible” short-range parts can be fitted quite accurately by a functional form, $H_R(r) = A + B \exp(-Cr)$, so that extrapolation of such a fit to $r = 0$ would yield $H_R(0) = A + B$. Table VI lists the values of $\beta H_R(0)$ so determined.

2. Enhancement factors

Hydrogen nuclei (protons, deuterons, or tritons) in metals are strongly screened by metallic electrons, so that the fundamental reaction rates are given by R_{ss} in Eq. (2.27). Enhancement factors $A_{ij}^{(M)}$ ($i, j = p, d, t$) over these fundamental rates are then calculated with the screening potentials $H_R(r)$ and the short-range screening distances

TABLE VI. Values of $\beta H_R(0)$ determined by the Monte Carlo sampling method for hydrogen atoms in metals. [L] means a case with periodic lattice fields; [D] means a case with defects.

Metal hydride	T (K)	$\beta H_R(0)$
PdH [L]	1200	5.8
	600	12.6
	300	27.1
PdH [D]	1200	4.4
	600	8.7
	300	11.6
TiH ₂ [L]	1200	9.6
	600	21.6
	300	48.2
TiH ₂ [D]	1200	16.6
	600	38.1
	300	81.5

D_s in the manner elucidated in Secs. IV.B and IV.C.

Writing thus

$$A_{ij}^{(M)} = \exp(Q_{ij}^{(M)}) , \quad (4.55)$$

Ichimaru, Ogata, and Nakano (1990) find

$$\begin{aligned} Q_{ij}^{(M)} = & \beta H_R(0) - \frac{5}{32} \Gamma_{ij}^{(M)} \left[\frac{3\Gamma_{ij}^{(M)}}{\tau_{ij}^{(M)}} \right]^2 \\ & \times \left[1 + (1.1858 - 0.2472 \ln \Gamma_{ij}^{(M)}) \frac{3\Gamma_{ij}^{(M)}}{\tau_{ij}^{(M)}} \right. \\ & \left. - 0.07009 \left[\frac{3\Gamma_{ij}^{(M)}}{\tau_{ij}^{(M)}} \right]^2 \right] \end{aligned} \quad (4.56)$$

with

$$\Gamma_{ij}^{(M)} \approx 0.94 \beta H_R(0) , \quad (4.57)$$

$$\tau_{ij}^{(M)} \approx \pi (D_s / r_{ij}^*)^{1/2} - \ln [\pi (D_s / r_{ij}^*)^{1/2}] . \quad (4.58)$$

Equation (4.56) stems from Eq. (4.28), in which Eq. (4.57) is set by the use of Salpeter’s ion-sphere model (3.14) in Eq. (3.20); and Eq. (4.58) is derived from comparison between Eqs. (2.15) and (2.28). Equations (4.57) and (4.58) are therefore approximate evaluations for hydrogen in metal, affecting the quantum correction terms in Eq. (4.56).

V. RATES OF NUCLEAR FUSION REACTIONS

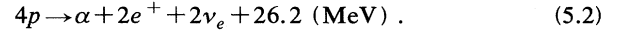
The analyses for the many-body enhancement factors on reaction rates, presented in the previous sections, are applied to an estimation of the nuclear reaction rates in specific examples of dense astrophysical and laboratory plasmas in this section: Astrophysical condensed plasmas under consideration include the solar interior (SI), the interior of a brown dwarf (BD), the interior of a giant planet (GP), a white-dwarf (WD) progenitor of a supernova, and surfaces of accreting white dwarfs and neutron stars. Examples of the condensed plasmas in the laboratories are those found in the inertial confinement fusion (ICF) experiments, in metal hydrides (MH) such as PdD and TiD₂, in cluster-impact fusion experiments, and in ultrahigh-pressure liquid metals (PM).

A. Solar interior and inertial confinement fusion plasmas

One of the proton-proton ($p-p$) chains consists in



which altogether yields



The cross-section parameters S_{ij} and the Q values, the nuclear energy released by the reaction, are (Bahcall and Ulrich, 1988)

$$S_{pp} = 4.07 \times 10^{-22} \text{ (keV b)}, \quad (5.3a)$$

$$Q(p-p) = 1.442 \text{ (MeV)},$$

$$S_{dp} = 2.5 \times 10^{-4} \text{ (keV b)}, \quad (5.3b)$$

$$Q(d-p) = 5.494 \text{ (MeV)},$$

$$S_{^3\text{He}^3\text{He}} = 5.15 \times 10^3 \text{ (keV b)}, \quad (5.3c)$$

$$Q(^3\text{He}-^3\text{He}) = 12.860 \text{ (MeV)}.$$

The chain (5.1), starting with ${}^1\text{H}(p, e^+ \nu_e){}^2\text{D}$, involves a β process and thus is extremely slow; the rate is controlled by these slow processes.

In Table VII, two cases of fusion rates and enhancement factors associated with $p-p$ reactions in the central parts of the SI are treated; case SI1 corresponds to conditions near the center, and SI2, those at $r \approx 0.2R_s$. The mass densities and temperatures are the values appropriate to hydrogen. The enhancement factors $A_{ws}^{(e)}$ and $A_{ws}^{(i)}$ are calculated with Eq. (2.25) and as described in the last paragraph of Sec. IV.C.2. The net reaction rates are thus given by

$$R = A_{ws}^{(e)} A_{ws}^{(i)} R_G. \quad (5.4)$$

The enhancement $A_{ws}^{(e)}$ due to weak electron screening near the center is approximately 2.2%, and that $A_{ws}^{(i)}$ due to many-body correlations in electron-screened protons amounts to 4.8%.

In the calculation of the local densities P of fusion power generated by $p-p$ reactions per unit mass (including other elements as well) in Table VII, we have taken the effective Q value at 13.1 MeV on account of (5.2). Those values in the central parts exceed naturally the average value $1.93 \times 10^{-7} \text{ W/g}$ of the solar luminosity per mass cited earlier.

In Table VII we also list examples of calculations for ICF plasmas. Here, reactions $t(d, n){}^4\text{He}$ with parameters (Jackson, 1957)

$$S_{td} = 1.7 \times 10^4 \text{ (keV b)}, \quad (5.5)$$

$$Q(t-d) = 17.6 \text{ (MeV)}$$

are considered in a mixture of deuterium and tritium with equal molar concentrations. Enhancement due to electron screening and ion-ion correlations is negligible in such a relatively dilute and high-temperature plasma.

B. Interiors of giant planets and brown dwarfs

For examination of the rates of $p-p$ reactions and of possible deuteron burning, we consider a hydrogen plasma with an admixture of deuterons at a molar fraction of 3×10^{-5} . In addition to $p-p$ and $d-p$ reactions, two branches, $d(d, n){}^3\text{He}$ and $d(d, p)t$, of the $d-d$ reactions are analyzed with a total-cross-section parameter and an average Q value (Krauss *et al.*, 1987):

$$S_{dd} = 103 \text{ (keV barns)}, \quad Q(d-d) = 3.6 \text{ (MeV)}. \quad (5.6)$$

The cases of BD and GP satisfy the conditions for weak electron screening (2.22) (cf. Table I); calculations of enhancement factors and reaction rates are analogous to those in the cases of SI and ICF. Table VIII lists the results of such calculations for examples of BD and GP plasmas.

We note that enhancement factors arising from combined effects between electron screening and ion-ion correlations in the assumed BD conditions take on a fairly large magnitude of 2.4; such an enhancement should be properly taken into account in the estimation of critical masses for hydrogen burning in the very low-mass stars and BDs. Deuteron burning is quite efficient in such stellar objects, with characteristic times of reaction on the order of a few minutes; hence deuterons should have burned away in the initial stages of stellar evolution.

Despite a substantial enhancement by 10 to 11 orders of magnitude due to electron screening, rates of deuteron burning in Jovian planets remain minuscule. The estimat-

TABLE VII. Reaction rates and enhancement factors in SI and ICF plasmas. Mass densities (ρ_m) and temperatures (T) are those assumed for the reacting nuclei.

Case: Reaction:	SI1 $p-p$	SI2 $p-p$	ICF1 $t-d$	ICF2 $t-d$
ρ_m (g/cm ³)	56.2	24.9	30.0	2.0
T (K)	1.5×10^7	9.3×10^6	5.0×10^7	1.0×10^8
τ_{ij}	13.7	16.1	12.3	9.75
$\log_{10} R_G$ (s ⁻¹)	-17.69	-18.93	7.40	7.13
Γ_{ij}	0.072	0.076	0.010	0.002
Λ_{ij}	0.023	0.023	0.0049	0.0014
Θ	2.23	3.21	31.8	387
D_s (10 ⁻⁹ cm)	3.97	5.48	11.9	20.0
Γ_s	0.044	0.047	0.0079	0.0014
$\log_{10} A_{ws}^{(e)}$	0.010	0.012	0.000	0.000
$\log_{10} A_{ws}^{(i)}$	0.020	0.022	0.004	0.000
$\log_{10} P$ (s ⁻¹)	-17.66	-18.90	7.41	7.33
$\log_{10} P$ (W/g)	-5.56	-6.80	19.23	18.96

TABLE VIII. Reaction rates and enhancement factors for hydrogen plasmas in BD and GP. Mass densities and temperatures assumed for BD cases are 10^3 g/cm^3 and $3 \times 10^6 \text{ K}$; those for GP cases, 5 g/cm^3 and $2 \times 10^4 \text{ K}$. In both cases the molar fraction of deuterons is assumed to be 3×10^{-5} .

Case: Reaction:	BD1 <i>p-p</i>	BD2 <i>d-p</i>	BD3 <i>d-d</i>	GP1 <i>d-p</i>	GP2 <i>d-d</i>
τ_{ij}	23.4	25.8	29.5	137	157
$\log_{10} R_G (\text{s}^{-1})$	-20.20	-3.18	-4.07	-52.36	-60.25
Γ_{ij}	0.76	0.76	0.76	19.4	19.4
Λ_{ij}	0.14	0.12	0.003	0.25	0.006
Θ	0.010	0.010	0.010	0.023	0.023
$D_s (10^{-9} \text{ cm})$	1.30	1.30	1.30	3.21	3.21
Γ_s	0.43	0.43	0.00	5.07	0.00
$\log_{10} A_{ws}^{(e)}$	0.162	0.164	0.167	10.94	11.01
$\log_{10} A_{ws}^{(i)}$	0.197	0.197	0.000	2.32	0.000
$\log_{10} R (\text{s}^{-1})$	-19.84	-2.82	-3.90	-39.10	-49.24
$\log_{10} P (\text{W/g})$	-7.75	4.38	3.11	-31.91	-42.23

ed power production rates are far smaller than average Jovian luminosity per unit mass, $2.4 \times 10^{-13} \text{ W/g}$ (Hubbard, 1980), and thus cannot take part in accounting for the excess infrared luminosity.

C. White-dwarf progenitors of supernovae

1. Dense C-O mixtures

Nuclear reaction rates in dense BIMs of carbon (C) and oxygen (O) are essential quantities governing the evolution and ignition in white-dwarf progenitors of type-I supernovae (Barkat, Wheeler, and Buchler, 1972; Graboske, 1973; Couch and Arnett, 1975). Phase diagrams associated with freezing transitions in such BIMs have been elucidated (Barrat, Hansen, and Mochkovitch, 1988; Ichimaru, Iyetomi, and Ogata, 1988; Ogata *et al.*, 1993). The short-range correlations responsible for nuclear reactions in dense matter are influenced strongly by such phase properties as well as by the quantum and classical many-body effects.

First-principles calculations of nuclear reaction rates in dense C-O BIMs were performed by Ogata, Iyetomi,

and Ichimaru (1991) in the fluid phases as well as in bcc crystalline phases. In so doing, we extended the quantum statistical treatment, developed originally by Jancovici (1977) for OCP, to the BIM situations. Salient features of the theory were described in Secs. IV.B and IV.D. In Table IX, results of calculations for reaction rates and enhancement factors are presented. The fundamental reaction rates are given by the Gamow rates of Eq. (2.12). The enhancement factors $A_{ij}^{(0)}$ of 23 to 39 orders of magnitude are obtained by the use of Eqs. (4.27) and (4.28).

Let us note that these high enhancement rates have been obtained under the condition that the density distributions of the electrons remain *uniform* and *constant*. The enhancement stems solely from the many-particle correlation effects between ionic nuclei elucidated in Sec. III; electrons do *not* participate in the act of screening in the derivation of $A_{ij}^{(0)}$. It is therefore physically a misnomer to call those the cases of strong *electron* screening, as in some of the astrophysical literature.

2. Screening by relativistic electrons

The short- and intermediate-range screening effects of relativistic degenerate electrons on enhancement of nu-

TABLE IX. Reaction rates and enhancement factors for dense carbon-oxygen matter in WD. Mass density and temperature are assumed to be $4 \times 10^9 \text{ g/cm}^3$ and 10^8 K ; the molar fraction of oxygen, at 50%. The degeneracy parameter of the electrons is $\Theta = 2.1 \times 10^{-4}$; their screening distance $D_s = 3.4 \times 10^{-11} \text{ cm}$.

Reaction	C-C	C-O	O-O
S_{ij} (MeV b)	8.83×10^{16}	1.15×10^{21}	2.31×10^{27}
$Q(i-j)$ (MeV)	13.931	16.754	16.541
τ_{ij}	181.827	230.294	293.691
$\log_{10} R_G (\text{s}^{-1})$	-43.35	-59.96	-81.47
Γ_{ij}	56.6	71.9	91.5
Λ_{ij}	0.47	0.42	0.37
Γ_s	41.4	51.7	64.7
$\log_{10} A_{ij}^{(0)}$	23.49	29.95	38.34
$\log_{10} A_{ij}^{(e)}$	1.18	1.57	2.08
$\log_{10} R (\text{s}^{-1})$	-18.69	-28.44	-40.96
$\log_{10} P (\text{W/g})$	-8.01	-17.68	-30.31

clear reactions have been elucidated in Sec. IV.C. Effects of electron screening are weak. It has nonetheless been pointed out that enhancement of nuclear reactions due to the electron screening becomes significant in high-Z materials such as carbon and oxygen at high densities near ignition (Ichimaru and Ogata, 1991).

The extra enhancement factors resulting from the electron screening, applicable to the WD cases, have been formulated in Eqs. (4.38)–(4.40). The electronic enhancement factors $A_{ij}^{(e)}$ computed for the WD cases of Table IX amount to 1.2 to 2.1 orders of magnitude. The net reaction rate is thus calculated as

$$R = A_{ij}^{(0)} A_{ij}^{(e)} R_G . \quad (5.7)$$

As an example of application for the reaction rates and enhancement factors, we exhibit in Fig. 17 the carbon ignition curves, that is, the loci of the points on the density-temperature plane for which the ^{12}C - ^{12}C energy release equals the neutrino loss, for the cases with and without consideration of the electronic screening effects. Following the conventional treatments (Arnett and Truran, 1969; Nomoto, 1982a), we have assumed the rate of such an energy release to be approximately 3×10^{17} erg/g, and have used the neutrino-loss rates compiled by Itoh *et al.* (1989). It is found that the WD1 case corresponds to near the ignition conditions, due mainly to the huge enhancement factors $A_{ij}^{(0)}$ stemming from the many-particle processes.

D. Helium burning—Triple α reactions

Helium burning is one of the major processes of nuclear reactions in stellar evolution. The triple α reactions (Salpeter, 1952b; Hoyle, 1954) take place in three steps:

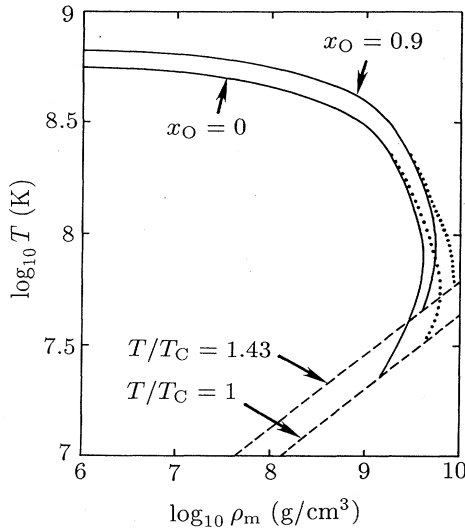
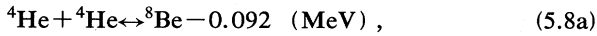
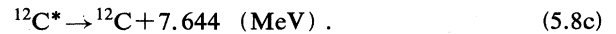
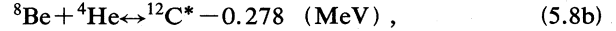


FIG. 17. Carbon ignition curves in C-O BIM fluids with electron screening (solid curves) and without (dashed curves). T_C is the freezing temperature of a carbon OCP, and x_O is the molar fraction of oxygen. From Ichimaru and Ogata (1991).



Here $^{12}\text{C}^*$ denotes a ^{12}C nucleus in its second excited state, and the energy differences are taken from Ajzenberg-Selove and Busch (1980) and Ajzenberg-Selove (1984). Since the first two reactions in (5.8) are endoergic, it is essential that these processes take place as resonant reactions; the 3α rate becomes exponentially small for temperatures less than about 10^8 K, at densities typical of normal stellar interiors (e.g., Clayton, 1968).

Helium burning is expected to be one of the major reaction processes also in white dwarfs and on neutron stars accreting in close binary systems (Nomoto, Thielemann, and Miyaji, 1985). The density and temperature conditions in which helium burning would occur in compact stars may differ widely from those in normal stars. In some cases, helium burning is so explosive as to give rise to x-ray bursters in neutron stars (Lewin and Joss, 1983) and to type-I supernovae in white dwarfs (Nomoto, 1982a, 1982b).

Accumulation of helium thus eventually leads to ignition of helium. The ignition conditions depend mainly on the accretion rate (e.g., Sugimoto and Miyaji, 1981; Nomoto, Thielemann, and Miyaji, 1985). For slower accretion, the temperature in the accreted matter is lower because of slower compressional heating relative to radiative cooling; as a result the ignition is delayed to higher density. Cameron (1959) pointed out that the 3α reaction at temperatures as low as $T \ll 10^8$ K is no longer a resonant but rather a nonresonant reaction; the Gamow peak energy [e.g., Eq. (2.14)] falls far below the threshold energy of resonance.

The rates of resonant 3α reactions have been given in Fowler, Caughlan, and Zimmerman (1975) and in Harris *et al.* (1983), which made use of the latest experimental information. Nomoto (1982a) and, subsequently, Nomoto, Thielemann, and Miyaji (1985) presented approximate analytic formulas for the rates of $\alpha+\alpha$ and $^{8}\text{Be}+\alpha$ using updated nuclear data. Denoting

$$\langle ij \rangle = \langle \sigma_{ij} \sqrt{2E/\mu_{ij}} \rangle_R \quad (5.9)$$

in the notation of Sec. II.A, one thus obtains for the nonresonant $\alpha+\alpha$ and $^{8}\text{Be}+\alpha$ rates as (Nomoto, Thielemann, and Miyaji, 1985)

$$\begin{aligned} \langle \alpha\alpha \rangle^* = & 6.914 \times 10^{-15} T_9^{-2/3} \exp(-13.489 T_9^{-1/3}) \\ & \times (1 + 0.031 T_9^{1/3} + 8.009 T_9^{2/3} + 1.732 T_9 \\ & + 49.883 T_9^{4/3} + 27.426 T_9^{5/3}) \text{ (cm}^3/\text{s}), \end{aligned} \quad (5.10)$$

$$\begin{aligned} \langle \alpha^8\text{Be} \rangle = & 4.167 \times 10^{-17} T_9^{-2/3} \exp(-23.567 T_9^{-1/3}) \\ & \times (1 + 0.018 T_9^{1/3} + 5.249 T_9^{2/3} + 0.650 T_9 \\ & + 19.176 T_9^{4/3} + 6.034 T_9^{5/3}) \text{ (cm}^3/\text{s}). \end{aligned} \quad (5.11)$$

Here T_9 denotes the temperature in units of 10^9 K, and the asterisk in Eq. (5.10) means that the rate $\langle \alpha\alpha \rangle$ has been calculated by including the E -dependent part of the α width for ${}^8\text{Be}$.

Another significant advancement in the treatment of 3α reactions was hastened by Fushiki and Lamb (1987), who presented an S -matrix calculation of the reaction rates with approximate inclusion of the screening potentials. These authors likewise used experimental values for the widths of the nuclear states and obtained reaction rates in good agreement with those of Nomoto, Thielemann, and Miyaji (1985) in those cases where the effects of screening were neglected. They presented a treatment of the pycnonuclear regime where in their definition the screening potential was greater than the Gamow peak energy. A physical distinction between electron screening and nuclear many-body effects, however, has remained unclear in their treatment.

The enhancement factors $A(3\alpha)$ in 3α reactions have been formulated by Ogata, Ichimaru, and Van Horn (1992) through the following argument: The lifetime

$$\tau_{\text{Be}} \approx \frac{\hbar}{\gamma_{\text{Be}}} \approx 10^{-16} \text{ (s)}, \quad (5.12)$$

with the half-width of Be, $\gamma_{\text{Be}} = 6.8$ eV (Ajzenberg-Selove and Busch, 1980). Relaxation times for reacting ${}^4\text{He}$ and ${}^8\text{Be}$ may be estimated through the ion-sphere cross sections, $\approx \pi a_{ij}^2$, as

$$\tau_{\text{rel}} \approx 10^{-18} \rho_8^{-1/3} T_7^{-1/2} \text{ (s)}. \quad (5.13)$$

One thus finds $\tau_{\text{rel}} \ll \tau_{\text{Be}}$ in the density-temperature regime of interest. Correlations between ${}^4\text{He}$ and ${}^8\text{Be}$ nuclei may thus be treated as those in equilibrated ${}^4\text{He}$ - ${}^8\text{Be}$ BIMs. The 3α reaction rates are proportional to the product of the ${}^4\text{He}$ - ${}^4\text{He}$ and ${}^4\text{He}$ - ${}^8\text{Be}$ contact probabilities, i.e., $g_{{}^4\text{He}{}^4\text{He}}(0)g_{{}^4\text{He}{}^8\text{Be}}(0)$; it is *not* necessary to consider the triple correlations under these circumstances. The enhancement factors are therefore calculated as

$$A(3\alpha) = \exp(Q_{{}^4\text{He}{}^4\text{He}} + Q_{{}^4\text{He}{}^8\text{Be}} + Q_{{}^4\text{He}{}^4\text{He}}^{(e)} + Q_{{}^4\text{He}{}^8\text{Be}}^{(e)}), \quad (5.14)$$

where Q_{ij} and $Q_{ij}^{(e)}$ have been given by Eqs. (4.28) and (4.40).

E. Metal hydrides—PdD and TiD₂

The analyses presented in Sec. IV.E have shown that the Coulomb fields around deuterons in PdD and TiD₂ are heavily screened by the metallic electrons within a screening distance D_s (cf. Table V). The critical temperature Eq. (2.21) of electron screening for d - d reactions is far greater than ambient temperatures, so that the basis reaction rates are given by R_{ss} in Eq. (2.27). The enhancement factors $A_{ij}^{(M)}$ over these basic rates due to the many-particle processes of the screened deuterons have been formulated as in Eqs. (4.55)–(4.58).

In thermodynamic equilibrium, only a fraction of deuterons are in itinerant fluid states in metal deuterides (Ichimaru, Ogata, and Nakano, 1990). The fraction f_{itin} of such itinerant deuterons is estimated as

$$f_{\text{itin}} \approx \exp\{-\beta[\Delta\Phi - \frac{3}{2}\hbar\sqrt{(\Phi''/m_d)}]\}, \quad (5.15)$$

where m_d refers to the mass of a deuteron; $\Delta\Phi$ and Φ'' are inhomogeneous lattice-field parameters given in Sec. IV.E.1.

Table X lists the values of the reaction rates, the enhancement factors, and the fractions of itinerant deuterons, computed for lattice cases of PdD and TiD₂ at two different temperatures. A number of observations are in order: (1) The electron-screened cold-fusion rates R_{ss} are independent of temperature; the values are well below the upper bounds set forth by Leggett and Baym (1989). (2) The electron screening is more efficient and consequently R_{ss} takes on a magnitude larger in Pd than in Ti. (3) This efficient electronic screening, in turn, shaves off the

TABLE X. Reaction rates and enhancement factors for deuterons in metal deuterides. Mass densities (ρ_m) and temperatures (T) are assumed parameters; n_d is the number density of deuterons; f_{itin} is the fraction of itinerant deuterons in equilibrium.

Case: Material:	MH1 PdD	MH2	MH3	MH4 TiD ₂
ρ_m (g/cm ³)	11.3			4.1
n_d (cm ⁻³)	6.25×10^{22}			9.4×10^{22}
T (K)	300	600	300	600
Λ_{ij}	0.45	0.32	0.52	0.37
E_s (eV)	75.79		51.43	
$\log_{10} R_{ss}$ (s ⁻¹)	−37.04		−51.38	
Γ_{ij}	356.3	178.2	408.3	204.1
Γ_s	0.09	0.05	3.1	1.6
$\log_{10} A_{ij}^{(M)}$	10.90	5.39	17.71	9.09
$\log_{10} R$ (s ⁻¹)	−30.14	−35.65	−33.67	−42.29
$\log_{10} P$ (W/g)	−20.63	−26.14	−23.54	−32.17
$\log_{10} f_{\text{itin}}$	−3.76	−2.43	−7.08	−4.09

Coulomb fields around deuterons more effectively and thereby results in a smaller value of the many-body enhancement factor $A_{ij}^{(M)}$ in Pd than in Ti. (4) Being a statistical-correlation effect, the enhancement factor decreases steeply as the temperature increases. (5) The microscopic lattice fields act to trap deuterons more effectively in Ti than in Pd. (6) The largest reaction rate in the table is $R \approx 7.2 \times 10^{-31} (\text{s}^{-1})$ in PdD at $T = 300 \text{ K}$ with an assumption that $f_{\text{itin}} \approx 1$ (meaning in a nonequilibrium state). This rate implies approximately one to two d - d reactions per year per unit volume (cm^3) of PdD.

F. Cluster-impact fusion

The analyses presented in the foregoing sections can be applied to an estimation of the reaction rates expected in the cluster-impact fusion experiments [Beuhler, Friedlander, and Friedman, 1989, 1992(E); Bae, Lorents, and Young, 1991; Vandenbosch *et al.*, 1991]. Let us suppose that N -molecule clusters $(\text{D}_2\text{O})_N$ impinge on a titanium-deuteride target with a kinetic energy E_{cluster} per cluster, break up into deuterons and oxygen ions, and thermalize with atoms in the target. The resultant effective temperature of the deuterons may be estimated as

$$T_{\text{eff}} \approx \frac{E_{\text{cluster}}}{30Nk_B}. \quad (5.16)$$

Deuterons with such a temperature can approach each other classically against the mutual Coulomb repulsion to a distance

$$D_{\text{cl}} \approx \frac{e^2}{k_B T_{\text{eff}}}. \quad (5.17)$$

The Coulomb fields around deuterons in Ti, however, are screened by the metallic electrons within a distance D_s , which has been estimated as $2.8 \times 10^{-9} \text{ cm}$ in Table V. Hence the estimated maximum density that those thermalized deuterons may attain is given by

$$n_{\text{max}} \approx \frac{3}{4\pi D_{\text{min}}^3}, \quad (5.18)$$

where D_{min} takes on the smaller value between D_{cl} and D_s .

One can substitute these density-temperature estimates to calculations of the reaction rates and possible enhancement factors using the formulations described in Secs. II–IV. In the ranges of parameters used in the experiments, the weak electron-screening condition of (2.22) applies; the d - d reactions here can be treated in a way analogous to the BD3 and GP2 cases of Table VII. For example, at $E_{\text{cluster}} = 250 \text{ keV}$, the Gamow reaction rate $R_G (\text{s}^{-1})$ and the total enhancement factor $A = A_{\text{ws}}^{(e)} A_{\text{ws}}^{(i)}$ as functions of N take on the values $R_G = 1.1 \times 10^{-2}$, $A = 3.0$ ($N = 50$); $R_G = 3.1 \times 10^{-7}$, $A = 3.2$ ($N = 100$); $R_G = 1.1 \times 10^{-20}$, $A = 63$ ($N = 500$). It does not appear that these values can account for the “cluster” effects im-

plied in the earlier experiments. The recent finding of the traces of high-velocity beam contaminants [artifacts; Beuhler, Friedlander, and Friedman, 1992(E)] should be the cause of the apparent enhancement.

G. Ultrahigh-pressure liquid metals

The nuclear reactions in PM cases differ in an essential way from those in the MH cases in that the reacting nuclei are in *metallized, fluid states* where a substantial enhancement of the reaction rate due to the many-particle processes is expected, as in the SN cases (Ichimaru, 1991). In the metallized d - p mixtures, the electron-screened internuclear potential is expressed as

$$V_{dp}(r) = \frac{e^2}{r} S_c(r), \quad (5.19)$$

where $S_c(r)$ is the screening function given by Eq. (A84).

At an ambient temperature and below, the metallic hydrogen forms a quantum solid rather than a semiclassical fluid. Protons and deuterons perform zero-point vibrations around their lattice sites, and their nuclear reaction rates are determined as in Eq. (4.48) from the contact probabilities between adjacent nuclei. A calculation along these lines has shown (Ichimaru, 1991) that the pycnonuclear reaction rate in D-H matter with $\rho_m \approx 5 \text{ g/cm}^3$ takes on a minuscule magnitude of 10^{-57} s^{-1} .

For exploitation of the enhancement factors arising from the many-particle processes of Sec. III, at least one of the reacting nuclear species needs to be in a fluid state. A melting temperature derived from a criterion of Lindemann type (e.g., Pines, 1963) for hydrogen may be written as

$$T_m \approx \frac{e^2}{180a_{ij}k_B} \frac{k_m^2}{k_m^2 + K_{s0}^2}, \quad (5.20)$$

with

$$k_m^2 = \frac{3}{5}(6\pi^2 n_H)^{2/3} \quad (5.21)$$

the mean-square value of phonon wave numbers in hydrogen. Here K_{s0} is a screening parameter calculated as Eq. (A80) in which n_f is replaced by n_e (i.e., $X = 0$), the total number density of the free electrons; n_H in Eq. (5.21) denotes the number density of hydrogen.

As we choose the temperature in the vicinity of Eq. (5.20), Λ_{ij} parameters in the PM cases of Table XI take on values near unity. Quantum effects in the “S” nuclei should begin to play a role here. These are problems that remain to be investigated.

The critical temperatures, Eq. (2.21), of electron screening for PM1 and PM2 cases of d - p BIM fluids in Table XI exceed 10^4 K , so that the basic reaction rates before the enhancement by many-particle processes are given by R_{ss} of Eq. (2.27). Since E_G/D_s in the exponential decay factor of R_{ss} is proportional to μ_{ij} , the reduced mass of the pair of reacting nuclei, it is advantageous

TABLE XI. Reaction rates and enhancement factors for ultrahigh-pressure liquid metals. Mass densities (ρ_m) and temperatures (T) are assumed parameters; P_e is the total pressure of the conduction electrons. In each case, the molar fraction of the BIM is assumed to be 50%.

Case: Reaction:	PM1 $d-p$	PM2 $d-p$	PM3 ${}^7\text{Li}-p$	PM4 ${}^7\text{Li}-p$
ρ_m (g/cm ³)	2.5	8.5	16.0	140
T (K)	650	1200	700	2000
P_e (Mbar)	17.2	148	80.9	3375
Λ_{ij}	0.95	1.05	0.88	1.07
r_s	1.17	0.78	0.87	0.43
D_s (10 ⁻⁹ cm)	3.85	3.21	2.24	1.75
$\log_{10} R_{ss}$ (s ⁻¹)	-53.28	-49.75	-77.53	-66.58
$\Gamma_{ij}^{(s)}$	413.8	337.1	514.5	371.1
$\log_{10} A_{ij}^{(i)}$	68.19	87.30	118.5	133.5
$\log_{10} R$ (s ⁻¹)	29.41	36.44	52.55	56.15
$\log_{10} P$ (W/g)	-23.87	-11.32	-24.97	-10.43
	-12.63	-0.07	-13.66	0.89

from the point of view of nuclear fusion to choose one of the species as proton and thereby to minimize such a decay. For metallic hydrogen, the combination of d and p may thus be preferred.

The enhancement factors due to many-body correlations in the electron-screened nuclei are then expressed as

$$A_{ij}^{(i)} = \exp(Q_{ij}^{(i)}) , \quad (5.22)$$

where

$$\begin{aligned} Q_{ij}^{(i)} = & 1.057 \Gamma_{ij}^{(s)} - \frac{5}{32} \Gamma_{ij}^{(s)} \left[\frac{r_{\text{TP}}^{(s)}}{a_{ij}} \right]^2 \\ & \times \left[1 + (1.1858 - 0.2472 \ln \Gamma_{ij}^{(s)}) \left[\frac{r_{\text{TP}}^{(s)}}{a_{ij}} \right] \right. \\ & \left. - 0.07009 \left[\frac{r_{\text{TP}}^{(s)}}{a_{ij}} \right]^2 \right] , \end{aligned} \quad (5.23)$$

$$\Gamma_{ij}^{(s)} = \Gamma_{ij} S_c(a_{ij}) ; \quad (5.24)$$

$r_{\text{TP}}^{(s)}$ and D_s have been given by Eqs. (2.28) and (4.41).

PM1 exemplifies a case in which a detectable level of reactions is predicted, while a power production is expected in PM2. Significant levels of reaction rates are obtained in both cases owing to enhancement by approximately 30 to 37 orders of magnitude arising from many-particle processes. The values of electronic pressures (calculated with the electronic equations of state in Appendix A.2) and temperatures in the table may suggest a possible experiment for $d-p$ reactions by shock compression of liquid metallic hydrogen.

As far as the fusion study is concerned, lithium hydride under ultrahigh pressure appears to offer another system of interest, though the ranges of temperatures and pressures required for significant reactions are substantially greater than those in the cases of liquid metallic hydrogen.

Here one considers reactions,



with parameters (Bahcall and Ulrich, 1988),

$$\begin{aligned} S_{\text{Li}-p} &= 52 \text{ (keV b)} , \\ Q({}^7\text{Li}-p) &= 17.347 \text{ (MeV)} . \end{aligned} \quad (5.25b)$$

It is an interesting system because lithium hydrides are stable compounds under laboratory conditions, and because the reaction products in (5.25a) are α particles, which are easier to handle. The reduced mass between Li and H is about the same as that between D and H. The nuclear charge $Z_{\text{Li}} = 3$, however, acts to reduce the reaction rate considerably; consequently, higher mass densities, temperatures, and pressures are required.

A lithium atom has the ionization potentials of 5.39 eV (first) and 75.64 eV (second, denoted as E_{2b} ; see, e.g., Allen, 1973). Cases PM3 and PM4 of ultrahigh-pressure LiH in Table XI may be looked upon as BIMs consisting of Li^+ , p , and the corresponding number of free electrons. Taking into account the two 1s electrons bound in Li^+ as well as of the screening parameter K_{s0} of the free electrons, we write the electron-screened internuclear potential between lithium and proton as (Ichimaru, 1991)

$$V_{\text{Li}-p}(r) = \frac{3e^2}{r} S_{\text{Li}-p}(r) \quad (5.26)$$

with

$$S_{\text{Li}-p}(r) = A_s \exp(-K_{s0}r) + (A_b + A_x r) \exp(-K_{b0}r) , \quad (5.27)$$

where

$$A_s = 1 - \frac{2}{3} \frac{K_{b0}^4}{(K_{b0}^2 - K_{s0}^2)^2} , \quad (5.28a)$$

$$A_b = \frac{2K_{b0}^4}{3(K_{b0}^2 - K_{s0}^2)^2} , \quad (5.28b)$$

$$A_x = \frac{K_{b0}^3}{3(K_{b0}^2 - K_{s0}^2)^2} , \quad (5.28c)$$

and

$$K_{b0} = \frac{\sqrt{8mE_{b2}}}{\hbar}. \quad (5.29)$$

The *electron-screened* Coulomb-coupling parameter for the ions is given by

$$\Gamma_{ij}^{(s)} = \Gamma_{ij} \exp(-K_{s0}a_{ij}), \quad (5.30)$$

and

$$\frac{1}{D_s} = A_s K_{s0} + A_b K_{b0} - A_x. \quad (5.31)$$

PM3 represents a case in which a detectable level of reactions is expected, while fusion power may be generated in PM4. Here again, these significant levels of reaction rates are obtained owing to enhancement by approximately 52 to 57 orders of magnitude due to many-body correlations in the systems of electron-screened nuclei. The values of electronic pressures and temperatures implied in the table are high. It is hoped that an extension of current high-pressure experimental techniques may make such an experiment possible in the near future. A detection of such a nuclear reaction in ultrahigh-pressure liquid metal will then make the first laboratory demonstration of the nuclear processes in supernovae and may lead to an examination of the validity of extrapolating cross sections, such as Eq. (2.4), into regimes of extremely low energies on the order of 0.1 eV.

VI. EPILOGUE

We have thus far reviewed theories and applications of the rates of nuclear reactions and the factors of enhancement arising from electron screening and/or internuclear many-body correlations in dense plasmas. The physical origins of the latter two mechanisms of enhancement are clearly distinguished. It has been shown that the reaction rates are intimately related to the thermodynamic functions of dense plasmas through the screening properties and the Coulombic chemical potentials. Nuclear reactions in supernovae and those projected in ultrahigh-pressure liquid metals share a feature in common in that both depend on huge enhancement factors resulting from strong internuclear correlations.

ACKNOWLEDGMENTS

The work leading to this review was carried out as a part of research activities through the Japan-U.S. Cooperative Science Program: Phase Transitions in Dense Astrophysical Plasmas, supported jointly by the Japan Society for the Promotion of Science and by the U.S. National Science Foundation. The author is extremely grateful to H. M. Van Horn of the University of Rochester, the principal investigator on the U.S. side, and to H. Iyetomi and S. Ogata, collaborators on the Japanese side, for cooperation and pertinent discussions

on these and related subjects through the Program. Thanks are due to D. Baldwin, M. Date, H. E. DeWitt, W. Horton, W. B. Hubbard, K. Husimi, N. Itoh, B. Jancovici, W. Kohn, J. Meyer-ter-Vehn, K. Nomoto, M. N. Rosenbluth, T. Tajima, F.-T. Thielemann, H. Totsuji, J. P. Vary, and P. Vashishta for useful discussions. The research was supported in part also by the Ministry of Education, Science, and Culture of Japan through Research Grants No. 01460246 and No. 04455010.

APPENDIX A: THERMODYNAMIC FUNCTIONS FOR DENSE PLASMAS

Rates of nuclear reactions in dense plasmas depend in a number of crucial ways on their thermodynamic functions. Enhancement due to internuclear many-particle processes is described in terms of increments in the excess chemical potentials before and after nuclear reactions. Screening distances of internuclear potentials are likewise described by the compressibilities of electron gases. In this appendix, we summarize thermodynamic properties in various realization of dense plasmas. Basic parameters characterizing those plasmas have been defined in Sec. I.D.

1. Relativistic electron gases in the ground state

The electron gas under consideration is a kind of OCP in which the average charge densities are fixed at values specified by the densities of the uniform neutralizing charges. The Helmholtz free energy is therefore an appropriate thermodynamic potential under these circumstances (e.g., Landau and Lifshitz, 1969). Let the Helmholtz free energy per unit volume be expressed as a sum of the noninteracting and exchange-correlation parts:

$$F = F_0 + F_{xc} \quad (A1a)$$

$$= F_0 + F_x + F_c. \quad (A1b)$$

The ground-state energy is the value of the free energy at $T=0$ (Salpeter, 1961).

For $\Theta < 0.1$, which amounts to consideration of the ground state, one finds

$$F_0 = \frac{m^4 c^5}{\pi^2 \hbar^3} \left[\frac{1}{8} x_F (2x_F^2 + 1) \sqrt{x_F^2 + 1} - \frac{1}{3} x_F^3 - \frac{1}{8} \sinh^{-1} x_F \right]. \quad (A2)$$

In the nonrelativistic case $x_F \ll 1$,

$$F_0 = \frac{3n_e \hbar^2}{10m} (3\pi^2 n_e)^{2/3}. \quad (A3a)$$

In the extreme relativistic case $x_F \gg 1$,

$$F_0 = \frac{3n_e \hbar c}{4} (3\pi^2 n_e)^{1/3}. \quad (A3b)$$

The exchange and correlation energies in the ground

state are evaluated in the dielectric formulation. Jancović (1962) has derived a relativistic (longitudinal) dielectric function $\epsilon^1(k, \omega)$ in the random-phase approximation (RPA) (e.g., Pines and Nozières, 1966; Ichimaru, 1992), relative to the dielectric function $\epsilon_0(k, \omega)$ of the vacuum, with which

$$F_{xc} = \sum_{k \neq 0} \left[\frac{1}{4\pi} \int_{-\infty}^{\infty} dz \ln \frac{\epsilon^1(k, iz)}{\epsilon_0(k, iz)} - \frac{2\pi e^2 n_e}{k^2} \right]. \quad (\text{A4})$$

In the high-density r_s expansion, one thus finds

$$\begin{aligned} F_x &= \frac{e^2 m^4 c^4}{(2\pi)^3 \hbar^4} [(\sinh^{-1} x_F - x_F \sqrt{1+x_F^2})^2 \\ &\quad - \frac{4}{3} x_F^3 \sqrt{1+x_F^2} \sinh^{-1} x_F \\ &\quad + \frac{2}{3} (1+x_F^2)^2 \ln(1+x_F^2) - \frac{5}{3} x_F^4 - \frac{2}{3} x_F^2] , \end{aligned} \quad (\text{A5})$$

$$F_c = \frac{e^2 m^4 c^3}{3\pi^4 \hbar^5} (1 - \ln 2) x_F^3 \sqrt{1+x_F^2} \ln r_s . \quad (\text{A6})$$

In the nonrelativistic case $x_F \ll 1$, these expressions take on values,

$$F_x = -\frac{3}{4} \left[\frac{3}{2\pi} \right]^{2/3} \frac{n_e e^2}{a_e} \approx -0.4582 \frac{n_e e^2}{a_e} , \quad (\text{A7})$$

$$F_c = \frac{n_e e^4 m}{\pi^2 \hbar^2} (1 - \ln 2) \ln r_s . \quad (\text{A8})$$

The most accurate evaluations for the ground-state energy in nonrelativistic electron gases thus far have been those due to Ceperley and Alder (1980) using the Green's-function Monte Carlo (GFMC) method (e.g., Ceperley and Kalos, 1979). The values of the correlation energy so calculated at $r_s = 1, 2, 5, 10, 20, 50$, and 100 are listed in Table XII.

These values have then been interpolated by Vosko, Wilk, and Nusair (1980) through a Padé approximant technique in a formula,

$$r_s \frac{dE_c(r_s)}{dr_s} = y_0 \frac{1+y_1 x}{1+y_1 x + y_2 x^2 + y_3 x^3} . \quad (\text{A9a})$$

Here

$$E_c(r_s) = \frac{2\hbar^2}{n_e e^4 m} F_c \quad (\text{A10})$$

TABLE XII. Correlation energies (mRy) of electron gases at $T=0$ in the GFMC, STLS, and RPA schemes.

r_s	GFMC	STLS	RPA
1	-119.6	-124	-157
2	-90.2	-92	-124
5	-56.33	-56	-85
10	-37.22	-36	
20	-23.00	-22	
50	-11.40		
100	-6.379		

is the correlation energy per electron in rydbergs.

$$\text{Ry} = \frac{e^4 m}{2\hbar^2} = 13.6058 \text{ eV} ; \quad (\text{A11})$$

$x = \sqrt{r_s}$, and

$$y_0 = 0.0621814, \quad y_1 = 9.81379 ,$$

$$y_2 = 2.82214, \quad y_3 = 0.736411 .$$

Integration of the differential Eq. (A9a) is performed with the small- r_s (i.e., high-density) boundary condition (Gell-Mann and Brueckner, 1957; Onsager, Mittag, and Stephen, 1966),

$$E_c^{\text{GB}}(r_s) = y_0 \ln r_s - 0.09329 . \quad (\text{A12})$$

The result takes the form

$$\begin{aligned} E_c(r_s) &= y_0 \left\{ \ln \frac{x^2}{X(x)} + \frac{2b}{Q} \tan^{-1} \frac{Q}{2x+b} \right. \\ &\quad - \frac{bx_0}{X(x_0)} \left[\ln \frac{(x-x_0)^2}{X(x)} \right. \\ &\quad \left. \left. + \frac{2(b+2x_0)}{Q} \tan^{-1} \frac{Q}{2x+b} \right] \right\} , \end{aligned} \quad (\text{A9b})$$

where

$$X(x) = x^2 + bx + c, \quad Q = \sqrt{4c - b^2} . \quad (\text{A13})$$

The best-fitting parameters x_0, b, c were found to be -0.409286, 13.0270, and 42.7198 for the paramagnetic case, and -0.743294, 20.1231, and 101.578 for the ferromagnetic case, respectively (Vosko, Wilk, and Nusair, 1980).

2. Electron liquids at finite temperatures

The electron is a fermion with spin quantum number $\frac{1}{2}$. The quantum states, designated by the momentum $\mathbf{p} = \hbar \mathbf{k}$ and spin σ , are occupied by the electrons according to the Fermi distribution (e.g., Landau and Lifshitz, 1969)

$$f_\sigma(\mathbf{p}) = \frac{1}{\exp \left[\frac{(\hbar k)^2 / 2m - \mu_0}{k_B T} \right] + 1} . \quad (\text{A14})$$

Here μ_0 is the chemical potential of the noninteracting electron gas, which is determined from the normalization

$$\int \frac{d\mathbf{p}}{(2\pi\hbar)^3} f_\sigma(\mathbf{p}) = n_\sigma , \quad (\text{A15})$$

where n_σ denotes the number density of the electrons with spin σ . For the electrons in a paramagnetic state, $n_\sigma = n_e/2$, half of the total number density of the electrons.

In the treatment of a free-electron gas at finite temperatures, it is useful to define the Fermi integrals

$$I_\nu(\alpha) \equiv \int_0^\infty dt \frac{t^\nu}{\exp(t-\alpha)+1} . \quad (\text{A16})$$

The normalization condition (A15) is then expressed as

$$I_{1/2}(\alpha) = \frac{2}{3} \Theta^{-3/2} , \quad (\text{A17})$$

where

$$\alpha = \frac{\mu_0}{k_B T} . \quad (\text{A18})$$

The Fermi pressure P_F of the free-electron gas is likewise expressed as

$$\frac{P_F}{n_e k_B T} = \Theta^{3/2} I_{3/2}(\alpha) . \quad (\text{A19})$$

The Helmholtz free energy per unit volume F_0 of the ideal-gas part is then calculated as

$$\frac{F_0}{n_e k_B T} = \alpha - \frac{P_F}{n_e k_B T} . \quad (\text{A20})$$

Useful fitting formulas for the chemical potential and the Fermi pressure are

$$\begin{aligned} \frac{\mu_0}{k_B T} &= -\frac{3}{2} \ln \Theta + \ln \frac{4}{3\sqrt{\pi}} \\ &+ \frac{A \Theta^{-(b+1)} + B \Theta^{-(b+1)/2}}{1 + A \Theta^{-b}} , \end{aligned} \quad (\text{A21})$$

with $A = 0.25954$, $B = 0.072$, and $b = 0.858$; and

$$\frac{P_F}{n_e k_B T} = 1 + \frac{2}{5} \frac{X \Theta^{-(y+1)} + Y \Theta^{-(y+1)/2}}{1 + X \Theta^{-y}} , \quad (\text{A22})$$

with $X = 0.27232$, $Y = 0.145$, and $y = 1.044$. Maximum deviations of Eq. (A21) from the exact values determined from Eq. (A17) are about 0.19% at $\Theta \approx 0.05$; those of Eq. (A22) from the exact values determined from Eq. (A19) are about 0.26% at $\Theta \approx 5$.

In the classical limit, i.e., when $\Theta \gg 1$, the Fermi integrals may be expanded as (e.g., Pathria, 1972)

$$I_\nu(\alpha) = \Gamma(\nu+1) \sum_{s=1}^{\infty} (-1)^{s+1} \exp(s\alpha) s^{-(\nu+1)} , \quad (\text{A23})$$

where

$$\Gamma(\xi) = \int_0^\infty dt t^{\xi-1} \exp(-t) \quad (\text{A24})$$

is the gamma function. In this limit one thus has

$$\frac{\mu_0}{k_B T} = -\frac{3}{2} \ln \Theta + \ln \frac{4}{3\sqrt{\pi}} , \quad (\text{A25a})$$

$$\frac{P_F}{n_e k_B T} = 1 . \quad (\text{A25b})$$

In the quantum limit of strong degeneracy, i.e., when $\Theta \ll 1$,

$$\begin{aligned} I_\nu(\alpha) &= \frac{\alpha^{\nu+1}}{\nu+1} \left[1 + \sum_{s=1}^{\infty} 2(1-2^{1-2s})\zeta(2s) \right. \\ &\quad \times \left. \frac{(\nu+1)!}{(\nu+1-2s)!} \alpha^{-2s} \right] , \end{aligned} \quad (\text{A26})$$

where

$$\zeta(\xi) = \sum_{\nu=1}^{\infty} \frac{1}{\nu^\xi} \quad (\xi > 1) \quad (\text{A27})$$

is Riemann's zeta function. Hence

$$\mu_0 = E_F , \quad (\text{A28a})$$

$$P_F = \frac{2}{5} n_e E_F . \quad (\text{A28b})$$

The exchange and correlation parts of the thermodynamic functions for interacting electron gases, which may more appropriately be called the *electron liquids*, are calculated in the dielectric formulation, where the strong-coupling effects beyond the RPA are described by the local-field corrections (e.g., Ichimaru, 1992). The interaction energy u_{xc} per unit volume in units of $k_B T$, calculated as the statistical average of the interaction part of the Hamiltonian, is expressed as a function of Γ_e and Θ . The exchange-correlation free energy per electron in the same units is then calculated through the coupling-constant integrations (e.g., Fetter and Walecka, 1971) as

$$f_{xc}(\Gamma_e, \Theta) \equiv \frac{F_{xc}}{n_e k_B T} = \int_0^{\Gamma_e} dx \frac{u_{xc}(x, \Theta)}{x} . \quad (\text{A29})$$

The excess part of pressure is thus given (e.g., Ichimaru, Iyetomi, and Tanaka, 1987) by

$$p_{ex}(\Gamma_e, \Theta) \equiv \frac{P_{ex}}{n_e k_B T} = \frac{u_{xc}(\Gamma_e, \Theta)}{3} - \frac{2\Theta}{3} \frac{\partial f_{xc}}{\partial \Theta} \Big|_{\Gamma_e} . \quad (\text{A30})$$

The Hartree-Fock energy, representing the first-order exchange effects, has been accurately evaluated and parametrized by Perrot and Dharma-wardana (1984) as

$$u_{xc}^{\text{HF}}(\Gamma_e, \Theta) = -a_{\text{HF}}(\Theta) \Gamma_e , \quad (\text{A31})$$

with

$$a_{\text{HF}}(\Theta) = \frac{(9\pi/4)^{1/3}}{\pi} \frac{a_0}{a_1} \tanh \frac{1}{\Theta} , \quad (\text{A32})$$

$$a_0 = 0.75 + 3.04363\Theta^2 - 0.09227\Theta^3 + 1.7035\Theta^4 , \quad (\text{A33a})$$

$$a_1 = 1 + 8.31051\Theta^2 + 5.1105\Theta^4 . \quad (\text{A33b})$$

The interaction energy in the RPA has been evaluated at finite temperatures by a number of investigators (Montroll and Ward, 1958; Englert and Brout, 1960; Gupta and Rajagopal, 1980; Dharma-wardana and Taylor, 1981). The RPA may not be valid for those strongly coupled electron liquids at metallic densities, for example,

with $2 \leq r_s \leq 6$. Here we employ a static local-field correction (e.g., Ichimaru, 1992) due to Singwi, Tosi, Land, and Sjölander (STLS) (1968), and derive explicit expressions for the thermodynamic functions applicable to such an electron liquid at finite temperatures (Tanaka and Ichimaru, 1986; Ichimaru, Iyetomi, and Tanaka, 1987).

The exchange-correlation energies calculated in the STLS scheme have been parametrized in analytic formulas as

$$u_{\text{xc}}^{\text{STLS}}(\Gamma_e, \Theta) = -\Gamma_e \frac{u_0}{u_1}, \quad (\text{A34})$$

$$u_0 = a(\Theta) + b(\Theta)\sqrt{\Gamma_e} + c(\Theta)\Gamma_e, \quad (\text{A35a})$$

$$u_1 = 1 + d(\Theta)\sqrt{\Gamma_e} + e(\Theta)\Gamma_e, \quad (\text{A35b})$$

with

$$a(\Theta) = a_{\text{HF}}(\Theta), \quad (\text{A36})$$

$$b(\Theta) = \sqrt{\Theta} \tanh \left[\frac{1}{\sqrt{\Theta}} \right] \frac{b_0}{b_1}, \quad (\text{A37})$$

$$b_0 = 0.341 308 + 12.070 873 \Theta^2 + 1.148 889 \Theta^4,$$

$$b_1 = 1 + 10.495 346 \Theta^2 + 1.326 623 \Theta^4,$$

$$c(\Theta) = \left[0.872 496 + 0.025 248 \exp \left(-\frac{1}{\Theta} \right) \right] e(\Theta), \quad (\text{A38})$$

$$d(\Theta) = \sqrt{\Theta} \tanh \left[\frac{1}{\sqrt{\Theta}} \right] \frac{d_0}{d_1}, \quad (\text{A39})$$

$$d_0 = 0.614 925 + 16.996 055 \Theta^2 + 1.489 056 \Theta^4,$$

$$d_1 = 1 + 10.109 35 \Theta^2 + 1.221 84 \Theta^4,$$

$$e(\Theta) = \Theta \tanh \left[\frac{1}{\Theta} \right] \frac{e_0}{e_1}, \quad (\text{A40})$$

$$e_0 = 0.539 409 + 2.522 206 \Theta^2 + 0.178 484 \Theta^4,$$

$$e_1 = 1 + 2.555 501 \Theta^2 + 0.146 319 \Theta^4.$$

The coupling-constant integration of Eq. (A29) is performed with Eq. (A34) to yield

$$\begin{aligned} f_{\text{ex}}^{\text{STLS}}(\Gamma_e, \Theta) = & -\frac{c}{e} \Gamma_e - \frac{2}{e} \left[b - \frac{cd}{e} \right] \sqrt{\Gamma_e} - \frac{1}{e} \left[\left[a - \frac{c}{e} \right] - \frac{d}{e} \left[b - \frac{cd}{e} \right] \right] \\ & \times \ln |e\Gamma_e + d\sqrt{\Gamma_e} + 1| + \frac{2}{e\sqrt{4e-d^2}} \left[d \left[a - \frac{c}{e} \right] + \left[2 - \frac{d^2}{e} \right] \left[b - \frac{cd}{e} \right] \right] \\ & \times \left[\tan^{-1} \left[\frac{2e\sqrt{\Gamma_e} + d}{\sqrt{4e-d^2}} \right] - \tan^{-1} \left[\frac{d}{\sqrt{4e-d^2}} \right] \right]. \end{aligned} \quad (\text{A41})$$

The condition that $4e - d^2 > 0$ is satisfied for any Θ .

Spin-dependent correlations and thermodynamic functions for electron liquids at arbitrary degeneracy and spin polarization have been investigated through a solution to another self-consistent set of integral equations in the modified-convolution approximation (MCA; see Tago, Utsumi, and Ichimaru, 1981). Analytic expressions for the thermodynamic functions, analogous to Eqs. (A34) and (A41), have been derived; phase boundary curves, arising from divergence of the isothermal compressibility and of the spin susceptibility, have been thereby obtained (Tanaka and Ichimaru, 1989).

These thermodynamic functions for electron liquids play the central part in the estimates of the screening distances D_s considered in Sec. II.C. In a treatment based on a generalization of the Thomas-Fermi approximation (e.g., Pines, 1963), the screening parameter, i.e., the reciprocal of D_s , in the electron liquid is given by

$$K_s \equiv \frac{1}{D_s} = \sqrt{4\pi(n_e e)^2 \kappa_T}, \quad (\text{A42})$$

where

$$\kappa_T = \frac{1}{n_e} \frac{\partial n_e}{\partial P} \Big|_{T,V} = \frac{1}{n_e^2 \frac{\partial^2 F}{\partial n_e \partial n_e}} \Big|_{T,V} \quad (\text{A43})$$

is the isothermal compressibility of the electron liquid. If the ideal-gas contributions, such as Eq. (A2), (A20), or (A22), are used, Eq. (A42) will yield the Thomas-Fermi parameter for $\Theta \ll 1$ and the Debye-Hückel parameter for $\Theta \gg 1$.

3. Dense semiclassical one-component-plasma fluids of ions

The thermodynamic functions for a weakly coupled OCP ($\Gamma \ll 1$) have been calculated rigorously by the giant-cluster expansion method (Abe, 1959). Thus, expressing the internal energy per ion (in units of $k_B T$) as a sum of an ideal-gas part ($= \frac{3}{2}$) and the excess,

$$u = \frac{3}{2} + u_{\text{ex}}^{\text{ABE}}(\Gamma), \quad (\text{A44})$$

one finds

$$u_{\text{ex}}^{\text{ABE}}(\Gamma) = -\frac{\sqrt{3}}{2}\Gamma^{3/2} - 3\Gamma^3 \left[\frac{3}{8}\ln(3\Gamma) + (\gamma/2) - \frac{1}{3} \right], \quad (\text{A45a})$$

where $\gamma = 0.57721\dots$ is Euler's constant. The first term on the right-hand side of Eq. (A45a) is the Debye-Hückel (1923) contribution. Equation (A45a) accurately represents the excess internal energy for $\Gamma < 0.1$.

In the strong-coupling regime $1 \leq \Gamma < 180$ the excess internal energy has been evaluated by computer simulations (Slattery, Doolen, and DeWitt, 1982; Ogata and Ichimaru, 1987), with the result

$$\begin{aligned} u_{\text{ex}}^{\text{OI}}(\Gamma) = & -0.898004\Gamma + 0.96786\Gamma^{1/4} \\ & + 0.220703\Gamma^{-1/4} - 0.86097. \end{aligned} \quad (\text{A45b})$$

In the intermediate-coupling regime $0.1 \leq \Gamma < 1$ the excess internal energy has been calculated (Slattery, Doolen, and DeWitt, 1980) through a solution to the hypernetted-chain integral equations (e.g., Hansen and McDonald, 1986). Using these HNC values, one finds a formula connecting Eqs. (A45a) and (A45b),

$$u_{\text{ex}}(\Gamma) = \frac{u_{\text{ex}}^{\text{ABE}}(\Gamma) + (3 \times 10^3)\Gamma^{5.7}u_{\text{ex}}^{\text{OL}}(\Gamma)}{1 + (3 \times 10^3)\Gamma^{5.7}}. \quad (\text{A46})$$

This formula is therefore applicable for a classical OCP with $\Gamma < 180$.

The Helmholtz free energy per ion in units of $k_B T$ is again expressed as the sum of the ideal part [Eq. (A20) with Eqs. (A25a) and (A25b)] and the excess, the latter of which may be obtained by a coupling-constant integration of Eq. (A45) or (A46), as in Eq. (A29); in the weak-coupling regime, one thus has

$$\begin{aligned} f = & f_0 + f_{\text{ex}}^{\text{ABE}} \\ = & \ln \frac{\Lambda^3}{e} - \frac{\Gamma^{3/2}}{\sqrt{3}} - \frac{\Gamma^3}{2} \left[\frac{3}{4}\ln(3\Gamma) + \gamma - \frac{11}{12} \right]. \end{aligned} \quad (\text{A47})$$

In the strong-coupling regime $1 \leq \Gamma < 180$ one likewise obtains from Eq. (A46)

$$\begin{aligned} f_{\text{ex}}(\Gamma) = & -0.898004\Gamma + 3.87144\Gamma^{1/4} \\ & - 0.882812\Gamma^{-1/4} - 0.86097\ln\Gamma \\ & - 2.52692. \end{aligned} \quad (\text{A48})$$

As Λ increases in a OCP with higher densities and lower temperatures, quantum corrections in free energies arise from Wigner-Kirkwood expansions (e.g., Landau and Lifshitz, 1969; Hansen and McDonald, 1986) in powers of \hbar^2 as

$$f = f^{(0)} + f^{(1)} + f^{(2)} + \dots \quad (\text{A49})$$

Here

$$f^{(0)} = f_0 + f_{\text{ex}}(\Gamma) \quad (\text{A50})$$

is the classical term as given by Eqs. (A47) and (A48),

$$f^{(1)} = \Gamma \frac{\Lambda^2}{16\pi}, \quad (\text{A51})$$

$$f^{(2)} = -[12J(\Gamma) + 9K(\Gamma) + 1]\Gamma^2 \frac{\Lambda^4}{3840\pi^2}, \quad (\text{A52})$$

with

$$J(\Gamma) = \frac{a^6}{3N} \left\langle \sum_{i \neq j}^N \frac{1}{r_{ij}^6} \right\rangle, \quad (\text{A53a})$$

$$K(\Gamma) = \frac{a^6}{9N} \left\langle \sum_{i \neq j \neq k}^N \left[3 \frac{(\mathbf{r}_{ij} \cdot \mathbf{r}_{ik})^2}{r_{ij}^5 r_{ik}^5} - \frac{1}{r_{ij}^3 r_{ik}^3} \right] \right\rangle; \quad (\text{A53b})$$

$r_{ij} = |\mathbf{r}_{ij}| = |\mathbf{r}_i - \mathbf{r}_j|$, N represents the total number of ions, and $\langle \dots \rangle$ refers to a statistical average. These quantities have been evaluated as

$$\begin{aligned} J(\Gamma) = & 0.13573 + 0.17362/\Gamma^{1/2} + 0.92707/\Gamma \\ & - 0.09740/\Gamma^{3/2} + 1.7824/\Gamma^2 + 1.9878/\Gamma^3 \end{aligned} \quad (\text{A53c})$$

and $K(\Gamma) \approx -0.091964$ (Hansen and Vieillefosse, 1975; Iyetomi, Ogata, and Ichimaru, 1992b).

4. Classical binary-ionic-mixture fluids

The thermodynamic functions for dense BIM fluids have been investigated extensively for construction of the phase-separation diagrams (Stevenson, 1980; Barrat, Hansen, and Mochkovitch, 1988; Ichimaru, Iyetomi, and Ogata, 1988) associated with freezing transitions in the interiors of white dwarfs. Substantial progress has been achieved since then, due primarily to advancements in MC simulations (Ogata, Iyetomi, and Ichimaru, 1991; Ogata *et al.*, 1993) and the analytic theories (Iyetomi, Ogata, and Ichimaru, 1992). Here we summarize the principal results on the thermodynamic functions, which enter Eq. (3.13) for an estimate on enhancement of nuclear reaction rates.

We consider a BIM fluid in a volume V containing N_1 and N_2 particles of species "1" and "2" with charge numbers Z_1 and Z_2 ($= R_Z Z_1$; $R_Z > 1$), respectively. The number density of electrons is then given by

$$n_e = \frac{N_1 Z_1 + N_2 Z_2}{V}, \quad (\text{A54})$$

and Eqs. (1.9) and (1.13a) define various plasma coupling parameters, which we assume to be greater than unity.

Let x denote the atomic fraction of "2" species, so that

$$x = \frac{N_2}{N_1 + N_2}. \quad (\text{A55})$$

The excess Helmholtz free energy per ion (in units of $k_B T$) for the BIM fluid is expressed as

$$\begin{aligned} f_{\text{ex}}^{\text{BIM}}(\Gamma_e, x; Z_1, Z_2) = & (1-x)f_{\text{ex}}^{\text{OCP}}(\Gamma_{11}) + x f_{\text{ex}}^{\text{OCP}}(\Gamma_{22}) \\ & + \Delta f_{\text{ex}}^{\text{BIM}}(\Gamma_e, x; Z_1, Z_2). \end{aligned} \quad (\text{A56})$$

Here $f_{ex}^{OCP}(\Gamma)$ is the excess Helmholtz free energy for the OCP given by Eq. (A48).

If $\Delta f_{ex}^{BIM}(\Gamma_e, x; Z_1, Z_2) = 0$, then Eq. (A56) is said to satisfy a linear-mixing law for the BIM free energies based on the constant electron-density, ion-sphere scaling (Salpeter, 1954), characterized by Eq. (1.11). Though small in magnitude, deviations from the linear-mixing

law do exist (Ichimaru, Iyetomi, and Ogata, 1988) and have been analyzed quantitatively through a series of MC simulation studies (Ogata *et al.*, 1993). The simulations were performed for 37 cases with $0.01 \leq x \leq 0.5$, $5 \leq \Gamma \leq 200$, and $Z_2/Z_1 = \frac{4}{3}, 3$, and 5; over these parametric domains, the simulation data are expressed in an analytic formula as

$$\begin{aligned} \Delta f_{ex}^{BIM}(\Gamma_e, x; Z_1, Z_2) = & 0.32 \frac{\sqrt{R_Z - 1}(xR_Z - 0.11)(x^{0.5} + 2 \times 10^{-3})}{(R_Z - 0.22)(x^{1.7} + 5 \times 10^{-5})} x(1-x) \left[1 - \frac{1}{\Gamma_{11}} \right] \\ & + 0.0551 \frac{(R_Z - 1)^{1.8}x(1-x)}{1 + 1.12(R_Z - 1)x} \quad (\Gamma_{11} > 1). \end{aligned} \quad (A57)$$

It is notable that the first term on the right-hand side, the principal term in $\Delta f_{ex}^{BIM}(\Gamma_e, x; Z_1, Z_2)$, changes its sign near $x = 0$ (i.e., for $x < 0.11/R_Z$) as a function of x . The deviations are quantities essential for analyses of the possibilities of phase separation as well as for estimates of the enhancement in nuclear reactions.

5. Quantum-mechanical one-component-plasma solids of ions

In a quantum-mechanical Coulomb solid, the Helmholtz free energy per ion in units of $k_B T$ is expressed as the sum of the bcc Madelung-energy term and the harmonic and anharmonic contributions:

$$f = -0.895 929\Gamma + f_{HM} + f_{AH}. \quad (A58)$$

In the semiclassical regime $Y \ll 1$, the harmonic and anharmonic contributions have been evaluated with inclusion of the quantum corrections up to \hbar^4 terms by Hansen and Vieillefosse (1975):

$$f_{HM}^{CL} = -0.845 88 + 3 \ln Y + \frac{Y^2}{8} - (1.9038 \times 10^{-3})Y^4, \quad (A59)$$

$$\begin{aligned} f_{AH}^{CL} = & - \left[\frac{10.84}{\Gamma} + \frac{176.4}{\Gamma^2} + \frac{5.980 \times 10^4}{\Gamma^3} \right] \\ & - \frac{Y^2}{80} \left[\frac{1.2993}{\Gamma} + \frac{61.252}{\Gamma^2} \right]. \end{aligned} \quad (A60)$$

The first term on the right-hand side of Eq. (A60) was due to Dubin (1990).

The ground-state energy ($T \rightarrow 0$) of a bcc Coulomb solid has been obtained by Carr, Coldwell-Horsfall, and Fein (1961):

$$f_{HM}^{QM} = 1.3286 \frac{\Gamma}{\sqrt{R_s}}, \quad (A61a)$$

$$f_{AH}^{QM} = -0.365 \frac{\Gamma}{R_s}, \quad (A61b)$$

where

$$R_s = \left[\frac{3}{4\pi n_i} \right]^{1/3} \frac{M(Ze)^2}{\hbar^2}. \quad (A62)$$

The free energies of bcc Coulomb solids at arbitrary values of Y have been calculated by Iyetomi, Ogata, and Ichimaru (1993) using a path-integral Monte Carlo method (e.g., Creutz and Freedman, 1981). The harmonic term takes the form

$$f_{HM} = 3 \ln \{ 2 \sinh[(Y/2)g(Y)] \}, \quad (A63)$$

with

$$g(Y) = \frac{0.7543 + 0.092 45 Y^2 + 0.003 386 Y^4}{1 + 0.1046 Y^2 + 0.003 823 Y^4}. \quad (A64)$$

The computed values of f for 48 combinations of Y and R_s are then used in a derivation of a parametrized equation for f_{AH} ; we find

$$\begin{aligned} f_{AH} = & - \frac{9\Gamma Y}{4} \frac{P(\xi) - 0.081 67 P(\xi) Y^2 + Q(\xi) Y^4}{1 + 0.085 Y^2 + R(\xi) Y^6} \\ & \times \coth^2 \left[\frac{Y}{2} \right]. \end{aligned} \quad (A65)$$

Here

$$\xi \equiv \Gamma \tanh \frac{8.5}{Y}, \quad (A66)$$

$$P(\xi) = \frac{1.204}{\xi^2} + \frac{19.60}{\xi^3} + \frac{6.644 \times 10^3}{\xi^4}, \quad (A67a)$$

$$Q(\xi) = \frac{0.001 805}{\xi^2} + \frac{0.085 07}{\xi^3} + 0.009 444 P(\xi), \quad (A67b)$$

$$R(\xi) = 0.085 32 \xi^2 Q(\xi). \quad (A67c)$$

Note that

$$\lim_{Y \rightarrow 0} \xi = \Gamma \quad \text{and} \quad \lim_{Y \rightarrow \infty} \xi = 8\sqrt{R_s}. \quad (A68)$$

The formulas (A63) and (A65) reproduce both the semi-

classical and ground-state results, Eqs. (A59)–(A61), in the respective limits.

6. Screening by relativistic electrons

Thus far we have investigated the thermodynamic properties for the individual constituents, electrons and ions, of a plasma. In an ultradense plasma with $r_s \leq 0.01$, appropriate to the interiors of degenerate stars, the Fermi energy of electrons is relativistically high [cf. Eq. (1.7)], so that their coupling with ions is indeed weak. The kinematic effects of relativistic degenerate electrons (e.g., Landau and Lifshitz, 1969) soften the electrons against compression and thus act to enhance their polarizations. A standard method for treating these polarization effects has been the Thomas-Fermi approximation [e.g., Eq. (A42)].

The dielectric formulation (e.g., Pines and Nozières, 1966; Ichimaru, 1992) offers an alternative method for deriving the excess interaction energy due to the polarization. Let the wave-number- (k -) and frequency- (ω -) dependent, longitudinal dielectric function of the electrons be $\epsilon(k, \omega)$. The energy increment per ion in units of

$$\epsilon(k, 0) = 1 + \left[\frac{k_{TF}}{k} \right]^2 \left[\frac{2}{3} \sqrt{1+x_F^2} - \frac{2x_F x^2}{3} \sinh^{-1} x_F + \sqrt{1+x_F^2} \frac{1+x_F^2 - 3x_F^2 x^2}{6x_F^2 x} \ln \left| \frac{1+x}{1-x} \right| - \frac{1-2x_F^2 x^2}{6x_F^2 x} \sqrt{1+x_F^2 x^2} \ln \left| \frac{\sqrt{1+x_F^2 x^2} + x \sqrt{1+x_F^2}}{\sqrt{1+x_F^2 x^2} - x \sqrt{1+x_F^2}} \right| \right]. \quad (\text{A72})$$

Here $x = k/2k_F$ and

$$k_{TF} = \frac{e \sqrt{12\pi m n_e}}{\hbar k_F} \quad (\text{A73})$$

is the (nonrelativistic) Thomas-Fermi wave number. In the nonrelativistic limit $x_F \rightarrow 0$, Eq. (A72) reduces to the static ($\omega=0$) values of the Lindhard dielectric function (Lindhard, 1954).

The screening length, Eq. (A71), has been evaluated by Ichimaru and Utsumi (1983) with the Jancovici screening function (A72); the result has been parametrized as

$$\frac{a_e}{D_s} = 0.1718 + 0.09283R + 1.591R^2 - 3.800R^3 + 3.706R^4 - 1.311R^5, \quad (\text{A74})$$

where $R = 10r_s$. This formula reproduces the computed values over the domain $0 \leq r_s \leq 0.1$ with digressions of less than 0.7%.

It is noteworthy that the screening length (in units of a_e) takes on a finite value 5.8 in the limit of high densities ($r_s \rightarrow 0$), while the nonrelativistic Thomas-Fermi length ($k_{TF} a_e$) diverges in the same limit. This finiteness is obviously a consequence of relativistic effects. For a

$k_B T$ due to polarization of electrons is then given by

$$u_{\text{pol}} = \frac{(Ze)^2}{2\pi^2 k_B T} \int d\mathbf{k} \frac{1}{k^2} \left[\frac{1}{\epsilon(k, 0)} - 1 \right]. \quad (\text{A69a})$$

Setting

$$u_{\text{pol}} = - \frac{(Ze)^2}{D_s k_B T}, \quad (\text{A69b})$$

we define and calculate an effective distance D_s of screening as

$$\frac{a_e}{D_s} = \left[\frac{18}{\pi^2} \right]^{1/3} \int_0^\infty dt \left[1 - \frac{1}{\epsilon(k_F t, 0)} \right]. \quad (\text{A70})$$

A free energy corresponding to Eq. (A69) can be obtained through a charge-strength integration as

$$f_{\text{pol}} = - \frac{(Ze)^2}{2D_s k_B T}. \quad (\text{A71})$$

The RPA static dielectric function for the relativistic electrons in the ground state has been obtained by Jancovici (1962),

comparison, one notes that the relativistic Thomas-Fermi length, $(4/9\pi)^{1/3} \sqrt{\pi \hbar c / 4e^2}$, takes on 5.4, a similar magnitude. Effects of the electron screening may thus remain considerable in dense stellar materials.

7. Dense electron-ion two-component plasma: The incipient-Rydberg-state model

We now summarize salient features in the thermodynamic and correlation functions for nonrelativistic electron-ion two-component plasmas (TCPs) with emphasis on the effects of strong coupling between electrons and ions. The results are relevant for a description of microscopic states in liquid metallic plasmas.

The binding energy of an electron in a 1s state of an atom with a nuclear charge Ze is given by

$$E_b = \frac{Ze^2}{2R_B} \quad (\text{A75})$$

with the Bohr radius,

$$R_B = \frac{\hbar^2}{mZe^2}. \quad (\text{A76})$$

A ratio between E_b and a relevant kinetic energy mea-

sures the degree to which the strong electron-ion coupling affects the properties of a dense TCP. The strong Coulomb coupling beyond the RPA in the plasma may be accounted for by the local-field corrections in the dielectric formulation (e.g., Ichimaru, 1992).

Strong interparticle correlations in dense plasmas near metal-insulator transitions have been analyzed using an integral equation approach, which adopts the HNC approximation for the classical ion-ion correlation and the MCA for the quantum-mechanical electron-electron and electron-ion correlations (Tanaka, Yan, and Ichimaru, 1990). The results have clearly revealed the emergence of "incipient Rydberg state (IRS)" for the electron-ion correlations in the *metallic* (plasma) phase near the metal-insulator boundaries. The IRS is a way of accounting for those effects of strong ion-electron correlations beyond the RPA and of mutual scattering beyond the Born approximation; the true bound states of electrons are *not* considered in the IRS model. The IRS acts significantly to modify the equation of state and to enhance the rates of electron scattering for a TCP in the metallic state.

We proceed to construct an IRS model (Ichimaru, 1993) for describing the thermodynamic properties of an electron-ion TCP. We shall formulate the model for general cases of the TCP with $Z \geq 1$. An explicit comparison of the model predictions with the results of microscopic calculations (Tanaka, Yan, and Ichimaru, 1990) is presently possible only for a hydrogen plasma ($Z=1$). The IRS description of the TCP with $Z > 1$ appears physically plausible, but is proposed here as a working hypothesis.

The IRS may be characterized by the parameter

$$x_b = \left\{ Zr_s \tanh \left[\frac{\hbar}{m} \left(\frac{2\pi}{mk_B T} \right)^{1/2} n_e^{1/3} \right] \right\}^{1/2}. \quad (\text{A77})$$

When the electrons are in a state of complete Fermi degeneracy $\Theta \ll 1$, one finds

$$x_b^4 = \left(\frac{9\pi}{4} \right)^{2/3} \frac{E_b}{E_F}, \quad (\text{A78a})$$

where E_F is Eq. (1.7) in a nonrelativistic case. In the classical limit $\Theta \gg 1$, one has

$$x_b^4 = (36\pi)^{1/3} \frac{E_b}{k_B T}. \quad (\text{A78b})$$

In the sense stated above, x_b^4 thus characterizes the strength of Coulomb coupling between electrons and ions in the TCP.

Let us introduce a parameter,

$$X = \frac{x_b}{1+x_b}, \quad (\text{A79})$$

meaning a fraction of the electrons in the IRS; $n_f = (1-X)n_e$ designates the number density of electrons in ordinary "free" states, while $n_b = Xn_e$ denotes that in

the IRS corresponding to those parts of free-electron behavior in the strong coupling. The latter thus describes the effects beyond the Born approximation in scattering between electrons and ions (Tanaka, Yan, and Ichimaru, 1990).

We define characteristic screening parameters associated with those free and IRS electrons:

$$K_s = \left[\frac{6\pi n_f e^2}{E_f} \right]^{1/2}, \quad (\text{A80})$$

$$K_b = \frac{2}{r_B} \frac{8 + 12R_B K_s}{(2 + R_B K_s)^3}, \quad (\text{A81})$$

where

$$E_f = E_{f0} U(\Theta_f) \quad (\text{A82})$$

with

$$E_{f0} = \frac{(\hbar k_f)^2}{2m}, \quad (\text{A83a})$$

$$k_f = (3\pi n_f)^{1/3}, \quad (\text{A83b})$$

$$\Theta_f = \frac{k_B T}{E_{f0}}, \quad (\text{A83c})$$

$$U(z) = \frac{3z}{2} \left[1 + \frac{13}{15} \frac{C}{z^{1.75} + Cz} - \frac{1}{5} z \left(\frac{C}{z^{1.75} + Cz} \right)^2 \right], \quad (\text{A83d})$$

and $C = 0.488$. The function $U(z)$ stems from the isothermal compressibility for the ideal-gas electrons. Consequently, K_s turns into the Thomas-Fermi screening parameter when $\Theta_f \ll 1$ and into the Debye-Hückel screening parameter when $\Theta_f \gg 1$.

The electrons, in both free states combined, then contribute a screening function to the ion fields as

$$S_c(r) = A_1 \exp(-K_s r) + (A_2 + A_3 r) \exp(-K_b r), \quad (\text{A84})$$

where

$$A_1 = 1 - X \frac{K_b^4}{(K_b^2 - K_s^2)^2}, \quad (\text{A85a})$$

$$A_2 = X \frac{K_b^4}{(K_b^2 - K_s^2)^2}, \quad (\text{A85b})$$

$$A_3 = \frac{X}{2} \frac{K_b^3}{K_b^2 - K_s^2}. \quad (\text{A85c})$$

The electron-screened Coulomb coupling parameter for the ions is given by

$$\Gamma_s = \Gamma S_c(a) \simeq \Gamma \exp \left[-\frac{a}{D_s} \right], \quad (\text{A86})$$

where D_s is given by Eq. (4.41). The validity of such a reduced coupling parameter has been verified by Monte Carlo simulations (Ichimaru and Ogata, 1991) and by solutions to liquid integral equations (Ichimaru, Nakano,

Ogata, Tanaka, Iyetomi, and Tajima, 1990).

In the IRS model, the normalized interaction energy may be defined and decomposed as follows:

$$\begin{aligned} u_{\text{ex}}(\Gamma, \Theta; Z) &\equiv \frac{U_{\text{int}}}{\sqrt{n_i n_e k_B T}} \\ &= \sqrt{n_e / n_i} u_{ee} \\ &\quad + \sqrt{n_i / n_e} (u_{ii} + u_{ei} + \delta u_{ei}). \end{aligned} \quad (\text{A87})$$

Here U_{int} is the total interaction energy in a unit volume; u_{ee} , u_{ii} , and u_{ei} are appropriately normalized interaction energies between electron-electron, ion-ion, and electron-ion; and δu_{ei} is a classical, weak-coupling correction to u_{ei} . The normalized excess free energy and pressure are then calculated in accordance with Eqs. (A29) and (A30). In reference to Eqs. (A34) and (A46), these interaction energies are calculated as

$$u_{ee} = u_{\text{xc}}^{\text{STLS}}(\Gamma_{ee}, \Theta), \quad (\text{A88})$$

$$u_{ii} = u_{\text{ex}}(\Gamma_s), \quad (\text{A89})$$

$$u_{ei} = (1 - X) u_{ei}^F + X u_{ei}^B, \quad (\text{A90})$$

$$\begin{aligned} \delta u_{ei} &= [(\sqrt{2} - 1) u_{\text{ex}}^{\text{ABE}}(\Gamma_s) - (1 - X) u_{ei}^F + (\sqrt{3}/2) \Gamma_e^{3/2}] \\ &\quad \times \exp(-\Gamma_e^{3/2} - 30\Theta^{-1/2}), \end{aligned} \quad (\text{A91})$$

with

$$u_{ei}^F = -0.94 [1 + 0.16 \exp(-\Theta^{-1/2})] \frac{(Ze)^2 K_s}{k_B T}, \quad (\text{A92})$$

$$u_{ei}^B = -\tanh \left[\frac{2\pi}{mk_B T} \right]^{1/2} n_e^{1/3} \frac{(Ze)^2 K_b}{2k_B T}. \quad (\text{A93})$$

Table XIII compares the theoretical (Tanaka, Yan, and Ichimaru, 1990) and the IRS model values for the normalized interaction energy u_{ex} in liquid metallic hydrogen ($Z=1$) at 34 selected combinations of Γ and Θ . Except for the extremely degenerate case with $\Gamma=43.441$

TABLE XIII. Normalized interaction energy $u_{\text{ex}} = U_{\text{int}} / n_i k_B T$ for hydrogen plasmas at selected combinations of Γ and Θ . $u_{\text{ex}}^{\text{TYI}}$ is that due to Tanaka, Yan, and Ichimaru (1990); $u_{\text{ex}}^{\text{IRS}}$ is from Eq. (A87); and $\Delta u_{\text{ex}} = u_{\text{ex}}^{\text{TYI}} - u_{\text{ex}}^{\text{IRS}}$.

Γ	Θ	$u_{\text{ex}}^{\text{TYI}}$	$u_{\text{ex}}^{\text{IRS}}$	Δu_{ex}
0.05	10	-0.0272	-0.0251	-0.0021
0.1	10	-0.0756	-0.0724	-0.0032
0.2	10	-0.2184	-0.2371	0.0187
0.3	10	-0.4588	-0.5001	0.0413
0.35	10	-0.6919	-0.6694	-0.0225
0.1	5	-0.0750	-0.6969	-0.0053
0.2	5	-0.2077	-0.2007	-0.0070
0.3	5	-0.3907	-0.3963	0.0056
0.4	5	-0.6519	-0.6593	0.0074
0.5	5	-1.0950	-0.9909	-0.1041
0.1	1	-0.0757	-0.0807	0.0050
0.3	1	-0.3320	-0.3320	0.0000
0.5	1	-0.6690	-0.6580	-0.0110
0.7	1	-1.0809	-1.0597	-0.0212
0.9	1	-1.5843	-1.5454	-0.0389
1.0	1	-1.8822	-1.8218	-0.0604
1.1	1	-2.2299	-2.1213	-0.1086
0.2	0.27151	-0.1802	-0.1917	0.0115
1.0	0.27151	-1.3345	-1.3178	-0.0167
1.6	0.27151	-2.4290	-2.3864	-0.0426
2.0	0.27151	-3.2654	-3.2083	-0.0571
2.5	0.27151	-4.4818	-4.3713	-0.1105
0.5	0.1	-0.5119	-0.5344	0.0225
1.0	0.1	-1.1662	-1.1805	0.0143
2.0	0.1	-2.6454	-2.6263	-0.0191
3.0	0.1	-4.2885	-4.2498	-0.0387
4.0	0.1	-6.0860	-6.0553	-0.0307
5.0	0.1	-8.0595	-8.0561	-0.0034
5.3401	0.1	-8.9749	-8.9808	0.0059
5.3401	0.01	-6.8544	-6.9012	0.0467
10.0	0.01	-13.2900	-13.2739	-0.0161
16.29	0.01	-22.5731	-22.5054	-0.0677
30.0	0.01	-44.2590	-44.6475	0.3885
43.441	0.01	-67.5204	-69.4036	1.8833

and $\Theta=0.01$, digressions remain negligibly small so that $|\Delta u_{\text{ex}}| \ll 1$, far below the level of thermal energy $k_B T$. In the extremely degenerate cases, one has $|u_{\text{ex}}| \gg 1$, so that digressions $|\Delta u_{\text{ex}}| \approx 1$ are likewise acceptable.

The strong electron-ion coupling in the liquid metallic hydrogen affects in a number of ways the degrees of ionization for the “impurity” atoms immersed in it (Ichimaru, 1993). The effects include (a) modification in the equation of state for the hydrogen plasma; (b) shifts (shallowing) of the impurity atomic levels by screening; and (c) interaction between impurity atoms and hydrogen plasma. Solutions to these problems bear important consequences for opacities and for internal structures and evolution in various stellar objects, including giant planets, brown dwarfs, and the Sun.

The IRS descriptions on strong electron-ion coupling can be extended straightforwardly to the cases of electron-screened BIMs. Such an analysis leads to modified predictions of the rates of electron-screened cold fusion (cf. Sec. II.C) and the enhancement due to many-particle processes (cf. Sec. III) for nuclear reactions in metallic substances, through screening functions such as Eqs. (A84) and (A86).

APPENDIX B: DERIVATION OF EQUATION (2.1)

We consider scattering between nuclei 1 and 2 with relative velocity v and reduced mass μ via the Coulomb potential $Z_1 Z_2 e^2 / r$; we define $\kappa \equiv \mu v / \hbar$ and $\eta \equiv Z_1 Z_2 e^2 / \hbar v$.

The usual boundary condition in the treatment of scattering problems assumes an incident plane wave in the z direction. The asymptotic ($r \rightarrow \infty$) form of the Coulomb wave function is then calculated (e.g., Schiff, 1968) as

$$\Psi(\mathbf{r}) \rightarrow \exp[i\kappa z + i\eta \ln(r-z)] \left[1 + \frac{\eta^2}{i\kappa(r-z)} \right] + \frac{f_c(\theta)}{r} \exp[i(\kappa r - \eta \ln 2\kappa r)], \quad (\text{B1})$$

where $f_c(\theta)$ is the angular function of the scattered wave and r represents the radial coordinate with respect to the scattering center.

With the normalization, such as Eq. (2.3), the wave function takes on the value at the origin,

$$|\Psi(0)|^2 = \frac{2\pi\eta}{\exp(2\pi\eta)-1}, \quad (\text{B2})$$

and the incident flux ($z \rightarrow -\infty$) is

$$\frac{\hbar}{2i\mu} [\Psi^*(\nabla\Psi) - \Psi(\nabla\Psi)^*] = v. \quad (\text{B3})$$

With the aid of the Coulomb cross section, Eq. (2.4), expressed for OCP, the reaction rate is calculated as

$$R_{12} = \sigma(E)v = 2S(E)r^*|\Psi(0)|^2/\pi\hbar. \quad (\text{B4})$$

This equation leads to Eq. (2.1).

If, on the other hand, the boundary condition of scattering is such that only the s waves are considered, the wave function is expressed as a superposition of incident and outgoing contributions:

$$\Psi(\mathbf{r}) = \frac{1}{2i} (\Psi^{(+)} e^{i\eta_0} - \Psi^{(-)} e^{-i\eta_0}), \quad (\text{B5})$$

where

$$\eta_0 = \arg \Gamma(1+i\eta) \quad (\text{B6})$$

and asymptotically ($r \rightarrow \infty$)

$$\Psi^{(\pm)}(r) = \frac{1}{r} \exp[\pm(i\kappa r - i\eta \ln 2\kappa r)]. \quad (\text{B7})$$

The normalization (2.3) and the Coulomb relation (B2) hold in this case as well, and the incident and outgoing fluxes are calculated in accordance with Eq. (B3) as $4\pi v$ and $-4\pi v$, respectively. With these s -wave boundary conditions, one then finds

$$R_{12} = \sigma(E)4\pi v = 8S(E)r^*|\Psi(0)|^2/\hbar. \quad (\text{B8})$$

This evaluation therefore is larger by a factor of 4π than Eq. (B4) and leads to the reaction rate cited in Salpeter and Van Horn (1969) and in Ogata, Iyetomi, and Ichimaru (1991).

Since the cross section is measured experimentally with the plane-wave boundary conditions, and since the Coulomb scattering in plasmas involves partial wave contributions other than $l=0$ as well, we regard Eq. (2.1), derived from Eq. (B4), as a fundamental formula for the rate of nuclear fusion.

REFERENCES

- Abe, R., 1959, Prog. Theor. Phys. **21**, 475.
- Ajzenberg-Selove, F., 1984, Nucl. Phys. A **413**, 1.
- Ajzenberg-Selove, F., and C. L. Busch, 1980, Nucl. Phys. A **336**, 1.
- Alastuey, A., and B. Jancovici, 1978, Astrophys. J. **226**, 1034.
- Alefeld, G., and J. Völk, 1978, Eds., *Hydrogen in Metals* (Springer, Berlin), Vols. I and II.
- Allen, C. W., 1973, *Astrophysical Quantities*, 3rd ed. (Athlone, London).
- Anders, E., and N. Grevesse, 1989, Geochim. Cosmochim. Acta **53**, 197.
- Armstrong, K. R., D. A. Harper, Jr., and F. J. Low, 1972, Astrophys. J. Lett. **178**, L89.
- Arnett, W. D., and J. W. Truran, 1969, Astrophys. J. **157**, 339.
- Ashcroft, N. W., and D. Stroud, 1978, in *Solid State Physics*, edited by H. Ehrenreich, F. Seitz, and D. Turnbull (Academic, New York), Vol. 33, p. 1.
- Bae, Y. K., D. C. Lorents, and S. E. Young, 1991, Phys. Rev. A **44**, R4091.
- Bahcall, J. N., W. F. Huebner, S. H. Lubow, P. D. Parker, and R. K. Ulrich, 1982, Rev. Mod. Phys. **54**, 767.
- Bahcall, J. N., and R. K. Ulrich, 1988, Rev. Mod. Phys. **60**, 297.
- Barkat, Z., J. C. Wheeler, and J.-R. Buchler, 1972, Astrophys. J. **171**, 651.

- Barrat, J. L., J. P. Hansen, and R. Mochkovitch, 1988, *Astron. Astrophys.* **199**, L15.
- Baym, G., and C. J. Pethick, 1975, *Annu. Rev. Nucl. Sci.* **25**, 27.
- Baym, G., C. J. Pethick, and P. Sutherland, 1971, *Astrophys. J.* **170**, 299.
- Bethe, H. A., 1990, *Rev. Mod. Phys.* **62**, 801.
- Beuhler, R. J., Y. Y. Chu, G. Friedlander, and L. Friedman, 1991, *Phys. Rev. Lett.* **67**, 473.
- Beuhler, R. J., G. Friedlander, and L. Friedman, 1989, *Phys. Rev. Lett.* **63**, 1292.
- Beuhler, R. J., G. Friedlander, and L. Friedman, 1992, *Phys. Rev. Lett.* **68**, 2108(E).
- Brush, S. G., H. L. Sahlin, and E. Teller, 1966, *J. Chem. Phys.* **45**, 2102.
- Burrows, A., W. B. Hubbard, and J. I. Lumine, 1989, *Astrophys. J.* **345**, 939.
- Cameron, A. G. W., 1959, *Astrophys. J.* **130**, 916.
- Canal, R., J. Isern, and J. Labay, 1982, *Nature (London)* **296**, 225.
- Canal, R., and E. Schatzman, 1976, *Astron. Astrophys.* **46**, 229.
- Carr, W. J., 1961, *Phys. Rev.* **122**, 1437.
- Carr, W. J., R. A. Coldwell-Horsfall, and A. E. Fein, 1961, *Phys. Rev.* **124**, 747.
- Carraro, C., B. Q. Chen, S. Schramm, and S. E. Koonin, 1990, *Phys. Rev. A* **42**, 1349.
- Carraro, C., A. Schäfer, and S. E. Koonin, 1988, *Astrophys. J.* **331**, 565.
- Ceperley, D. M., and B. J. Alder, 1980, *Phys. Rev. Lett.* **45**, 566.
- Ceperley, D. M., and M. H. Kalos, 1979, in *Monte Carlo Methods in Statistical Physics*, edited by K. Binder (Springer, Berlin).
- Clayton, D. D., 1968, *Principles of Stellar Evolution and Nucleosynthesis* (McGraw-Hill, New York).
- Couch, R. G., and W. D. Arnett, 1975, *Astrophys. J.* **196**, 791.
- Creutz, M., and B. Freedman, 1981, *Ann. Phys. (N.Y.)* **132**, 427.
- D'Antona, F., 1987, *Astrophys. J.* **320**, 653.
- D'Antona, F., and I. Mazzitelli, 1985, *Astrophys. J.* **296**, 502.
- Day, C. S., and Y. Tawara, 1990, *Mon. Not. R. Astron. Soc.* **245**, 31.
- Debye, P., and E. Hückel, 1923, *Phys. Z.* **24**, 185.
- DeWitt, H. E., H. C. Grboske, and M. C. Cooper, 1973, *Astrophys. J.* **181**, 439.
- Dharma-wardana, M. W. C., and R. Taylor, 1981, *J. Phys. C* **14**, 629.
- Drexel, W., A. Murani, D. Tocchetti, W. Kley, I. Sosnowska, and D. K. Ross, 1976, *J. Phys. Chem. Solids* **37**, 1135.
- Dubin, D. H. E., 1990, *Phys. Rev. A* **42**, 4972.
- Echenique, P. M., J. R. Manson, and R. H. Ritchie, 1990, *Phys. Rev. Lett.* **64**, 1413.
- Endo, H., 1990, Ed., *Liquid and Amorphous Metals VII* (North-Holland, Amsterdam).
- Englert, F., and R. Brout, 1960, *Phys. Rev.* **120**, 1085.
- Fetter, A. L., and J. D. Walecka, 1971, *Quantum Theory of Many-Particle Systems* (McGraw-Hill, New York).
- Feynman, R. P., and A. R. Hibbs, 1965, *Quantum Mechanics and Path Integrals* (McGraw-Hill, New York).
- Fienberg, R. T., 1990, *Sky Telesc.* **80**, 370.
- Forrest, W. J., M. F. Skrutskie, and M. A. Shure, 1988, *Astrophys. J. Lett.* **330**, L119.
- Fortov, V. E., 1982, *Usp. Fiz. Nauk* **138**, 361 [Sov. Phys. Usp. **25**, 781 (1983)].
- Fortov, V. E., V. E. Bespalov, M. I. Kulish, and S. I. Kuz, 1990, in *Strongly Coupled Plasma Physics*, edited by S. Ichimaru (North-Holland/Yamada Science Foundation, Amsterdam), p. 571.
- Fowler, W. A., G. R. Caughlan, and B. A. Zimmerman, 1967, *Annu. Rev. Astron. Astrophys.* **5**, 523.
- Fowler, W. A., G. R. Caughlan, and B. A. Zimmerman, 1975, *Annu. Rev. Astron. Astrophys.* **13**, 69.
- Fushiki, I., and D. Q. Lamb, 1987, *Astrophys. J.* **317**, 368.
- Gai, M., S. L. Rugari, R. H. France, B. J. Lund, Z. Zhao, A. J. Davenport, H. S. Isaacs, and K. G. Lynn, 1989, *Nature (London)* **340**, 29.
- Gamow, G., 1928, *Z. Phys.* **51**, 204.
- Gamow, G., and E. Teller, 1938, *Phys. Rev.* **53**, 608.
- Gell-Mann, M., and K. A. Brueckner, 1957, *Phys. Rev.* **106**, 354.
- Graboske, H. C., 1973, *Astrophys. J.* **183**, 177.
- Graboske, H. C., H. E. DeWitt, A. S. Grossman, and M. S. Cooper, 1973, *Astrophys. J.* **181**, 457.
- Graboske, H. C., J. B. Pollack, A. S. Grossman, and R. J. Ollness, 1975, *Astrophys. J.* **199**, 265.
- Gupta, U., and A. K. Rajagopal, 1980, *Phys. Rev. A* **21**, 2064.
- Gurney, R. W., and E. U. Condon, 1929, *Phys. Rev.* **33**, 127.
- Hafner, J., 1987, *From Hamiltonians to Phase Diagrams* (Springer, Berlin).
- Hansen, J.-P., 1973, *Phys. Rev. A* **8**, 3096.
- Hansen, J.-P., and I. R. McDonald, 1986, *Theory of Simple Liquids*, 2nd ed. (Academic, London).
- Hansen, J.-P., G. M. Torrie, and P. Vieillefosse, 1977, *Phys. Rev. A* **16**, 2153.
- Hansen, J.-P., and P. Vieillefosse, 1975, *Phys. Lett. A* **53**, 187.
- Harris, M. J., W. A. Fowler, G. R. Caughlan, and B. A. Zimmerman, 1983, *Annu. Rev. Astron. Astrophys.* **21**, 165.
- Hemley, R. J., and H. K. Mao, 1991, in *Proceedings of the APS 1991 Topical Conference on Shock Compression of Condensed Matter*, Williamsburg, VA, June 17–20, 1991, edited by S. C. Schmidt, R. D. Dick, J. W. Forbes, and D. J. Tasker (North-Holland, Amsterdam), p. 27.
- Hoover, W. G., and J. C. Poirier, 1962, *J. Chem. Phys.* **37**, 1041.
- Hora, H., 1991, *Plasmas at High Temperature and Density* (Springer, Berlin).
- Hoyle, F., 1954, *Astrophys. J. Suppl. Ser.* **1**, 121.
- Hubbard, W. B., 1968, *Astrophys. J.* **152**, 745.
- Hubbard, W. B., 1980, *Rev. Geophys. Space Sci.* **18**, 1.
- Hubbard, W. B., 1984, *Planetary Interiors* (Van Nostrand Reinhold, New York).
- Hubbard, W. B., and M. S. Marley, 1989, *Icarus* **78**, 102.
- Ichimaru, S., 1982, *Rev. Mod. Phys.* **54**, 1017.
- Ichimaru, S., 1990, Ed., *Strongly Coupled Plasma Physics* (North-Holland/Yamada Science Foundation, Amsterdam).
- Ichimaru, S., 1991, *J. Phys. Soc. Jpn.* **60**, 1437.
- Ichimaru, S., 1992, *Statistical Plasma Physics: Basic Principles* (Addison-Wesley, Reading, MA).
- Ichimaru, S., 1993, in *Physics of Strongly Coupled Plasmas*, edited by H. M. Van Horn and S. Ichimaru (Univ. of Rochester, New York, in press).
- Ichimaru, S., H. Iyetomi, and S. Ogata, 1988, *Astrophys. J. Lett.* **334**, L17.
- Ichimaru, S., H. Iyetomi, and S. Tanaka, 1987, *Phys. Rep.* **149**, 92.
- Ichimaru, S., A. Nakano, S. Ogata, S. Tanaka, H. Iyetomi, and T. Tajima, 1990, *J. Phys. Soc. Jpn.* **59**, 1333.
- Ichimaru, S., and S. Ogata, 1990, in *Strongly Coupled Plasma Physics*, edited by S. Ichimaru (North-Holland/Yamada Science Foundation, Amsterdam), p. 101.
- Ichimaru, S., and S. Ogata, 1991, *Astrophys. J.* **374**, 647.
- Ichimaru, S., S. Ogata, and A. Nakano, 1990, *J. Phys. Soc. Jpn.*

- 59**, 3904.
 Ichimaru, S., S. Ogata, and H. M. Van Horn, 1992, *Astrophys. J. Lett.* **401**, L35.
 Ichimaru, S., S. Tanaka, and H. Iyetomi, 1984, *Phys. Rev. A* **29**, 2033.
 Ichimaru, S., and K. Utsumi, 1981, *Phys. Rev. B* **24**, 7385.
 Ichimaru, S., and K. Utsumi, 1983, *Astrophys. J. Lett.* **269**, L51.
 Ichimaru, S., and K. Utsumi, 1984, *Astrophys. J.* **286**, 363.
 Ingersoll, A. P., G. Münch, G. Neugebauer, and G. S. Orton, 1976, in *Jupiter*, edited by T. Gehrels (University of Arizona, Tucson), p. 85.
 Itoh, N., T. Adachi, M. Nakagawa, Y. Kohyama, and H. Munakata, 1989, *Astrophys. J.* **339**, 354.
 Itoh, N., H. Totsuji, and S. Ichimaru, 1977, *Astrophys. J.* **218**, 477; **220**, 742(E).
 Itoh, N., H. Totsuji, S. Ichimaru, and H. E. DeWitt, 1979, *Astrophys. J.* **239**, 1079; **239**, 414(E).
 Iyetomi, H., and S. Ichimaru, 1982, *Phys. Rev. A* **25**, 2434.
 Iyetomi, H., and S. Ichimaru, 1983, *Phys. Rev. A* **27**, 3241.
 Iyetomi, H., S. Ogata, and S. Ichimaru, 1992, *Phys. Rev. A* **46**, 1051.
 Iyetomi, H., S. Ogata, and S. Ichimaru, 1993, *Phys. Rev. B* (in press).
 Jackson, J. D., 1957, *Phys. Rev.* **106**, 330.
 James, F., 1980, *Rep. Prog. Phys.* **43**, 73.
 Jancovici, B., 1962, *Nuovo Cimento* **25**, 428.
 Jancovici, B., 1977, *J. Stat. Phys.* **17**, 357.
 Jones, E. S., E. P. Palmer, J. B. Czirr, D. L. Decker, G. L. Jensen, J. M. Thorne, S. F. Taylor, and J. Rafelski, 1989, *Nature (London)* **338**, 737.
 Kafatos, M. C., R. S. Harrington, and S. P. Maran, 1986, Eds., *Astrophysics of Brown Dwarfs* (Cambridge University, Cambridge, England).
 Kim, Y. E., J.-H. Yoon, R. A. Rice, and M. Rabinowitz, 1992, *Phys. Rev. Lett.* **68**, 373.
 Korn, C., and D. Zamir, 1970, *J. Phys. Chem. Solids* **31**, 489.
 Krauss, A., H. W. Becker, H. P. Tautvatter, and C. Rolfs, 1987, *Nucl. Phys. A* **465**, 150.
 Kumar, S. S., 1963, *Astrophys. J.* **137**, 1121.
 Landau, L. D., and E. M. Lifshitz, 1969, *Statistical Physics*, 2nd ed., translated by J. B. Sykes and M. J. Kearsley (Addison-Wesley, Reading, MA).
 Leggett, A. J., and G. Baym, 1989, *Phys. Rev. Lett.* **63**, 191.
 Lewin, W. H. G., and P. C. Joss, 1983, in *Accretion Driven Stellar X-Ray Sources*, edited by W. H. G. Lewin and E. P. J. Van den Heuvel (Cambridge University, Cambridge, England), p. 115.
 Liebert, J., 1980, *Annu. Rev. Astron. Astrophys.* **18**, 363.
 Liebert, J., and R. G. Probst, 1987, *Annu. Rev. Astron. Astrophys.* **25**, 473.
 Lindhard, J., 1954, *K. Dan. Vidensk. Selsk. Mat. Fys. Medd.* **28**, No. 8.
 Low, F. J., 1966, *Astron. J.* **71**, 391.
 Lumine, J. I., W. B. Hubbard, and M. S. Marley, 1986, *Astrophys. J.* **310**, 238.
 Mao, H. K., R. J. Hemley, and M. Hanfland, 1990, *Phys. Rev. Lett.* **65**, 484.
 Menzel, D. H., W. W. Coblenz, and C. O. Lampland, 1926, *Astrophys. J.* **63**, 177.
 Metropolis, N., A. W. Rosenbluth, M. N. Rosenbluth, A. H. Teller, and E. Teller, 1953, *J. Chem. Phys.* **21**, 1087.
 Mitler, H. E., 1977, *Astrophys. J.* **212**, 513.
 Mochkovitch, R., 1983, *Astron. Astrophys.* **122**, 212.
 Montroll, E. W., and J. C. Ward, 1958, *Phys. Fluids* **1**, 55.
 Morita, T., 1960, *Prog. Theor. Phys.* **23**, 829.
 Mostovych, A. N., K. J. Kearney, J. A. Stamper, and A. J. Schmitt, 1991, *Phys. Rev. Lett.* **66**, 612.
 Mott, N. F., and H. Jones, 1936, *The Theory of the Properties of Metals and Alloys* (Clarendon, Oxford).
 Motz, H., 1979, *The Physics of Laser Fusion* (Academic, London).
 Nellis, W. J., J. A. Moriarty, A. C. Mitchell, M. Ross, R. G. Dandrea, N. W. Ashcroft, N. C. Holmes, and G. R. Gathers, 1988, *Phys. Rev. Lett.* **60**, 1414.
 Nelson, L. A., S. A. Rappaport, and P. C. Joss, 1986, in *Astrophysics of Brown Dwarfs*, edited by M. C. Kafatos, R. S. Harrington, and S. P. Maran (Cambridge University, Cambridge, England), p. 177.
 Nomoto, K., 1982a, *Astrophys. J.* **253**, 798.
 Nomoto, K., 1982b, *Astrophys. J.* **257**, 780.
 Nomoto, K., and Y. Kondo, 1991, *Astrophys. J. Lett.* **367**, L19.
 Nomoto, K., F.-K. Thielemann, and S. Miyaji, 1985, *Astron. Astrophys.* **149**, 239.
 Ogata, S., 1992, *Phys. Rev. A* **44**, 1122.
 Ogata, S., and S. Ichimaru, 1987, *Phys. Rev. A* **36**, 5451.
 Ogata, S., and S. Ichimaru, 1989, *Phys. Rev. Lett.* **62**, 2293.
 Ogata, S., S. Ichimaru, and H. M. Van Horn, 1992, unpublished.
 Ogata, S., H. Iyetomi, and S. Ichimaru, 1990, in *Strongly Coupled Plasma Physics*, edited by S. Ichimaru (North-Holland/Yamada Science Foundation, Amsterdam), p. 59.
 Ogata, S., H. Iyetomi, and S. Ichimaru, 1991, *Astrophys. J.* **372**, 259.
 Ogata, S., H. Iyetomi, S. Ichimaru, and H. M. Van Horn, 1993, in *Physics of Strongly Coupled Plasmas*, edited by H. M. Van Horn and S. Ichimaru (Univ. of Rochester, New York, in press).
 Onsager, L., L. Mittag, and M. J. Stephen, 1966, *Ann. Phys. (Leipzig)* **18**, 71.
 Pan, S. S., and F. J. Webb, 1965, *J. Nucl. Sci. Eng.* **23**, 194.
 Pathria, R. K., 1972, *Statistical Mechanics* (Pergamon, Oxford).
 Pereira, N. R., J. Davis, and N. Rostoker, 1989, Eds., *Dense Z-Pinches*, AIP Conf. Proc. No. 195 (AIP, New York).
 Perrot, F., and M. W. C. Dharma-wardana, 1984, *Phys. Rev. A* **30**, 2619.
 Pines, D., 1963, *Elementary Excitations in Solids* (Benjamin, New York).
 Pines, D., and P. Nozières, 1966, *The Theory of Quantum Liquids* (Benjamin, New York).
 Poll, P. D., N. W. Ashcroft, and H. E. DeWitt, 1988, *Phys. Rev. A* **37**, 1672.
 Rosenfeld, Y., 1992, *Phys. Rev. A* **46**, 1059.
 Rosenfeld, Y., and N. W. Ashcroft, 1979, *Phys. Rev. A* **20**, 1208.
 Ruoff, A. L., H. Xia, H. Luo, and Y. K. Vohra, 1990, *Rev. Sci. Instrum.* **61**, 3830.
 Salpeter, E. E., 1952a, *Phys. Rev.* **88**, 547.
 Salpeter, E. E., 1952b, *Astrophys. J.* **115**, 326.
 Salpeter, E. E., 1954, *Aust. J. Phys.* **7**, 373.
 Salpeter, E. E., 1961, *Astrophys. J.* **134**, 669.
 Salpeter, E. E., and H. M. Van Horn, 1969, *Astrophys. J.* **155**, 183.
 Saumon, D., W. B. Hubbard, G. Chabrier, and H. M. Van Horn, 1992, *Astrophys. J.* **391**, 827.
 Schatzman, E., 1948, *J. Phys. Rad.* **9**, 46.
 Schatzman, E., 1958, *White Dwarfs* (North-Holland, Amsterdam).

- Schiff, L. I., 1968, *Quantum Mechanics*, 3rd ed. (McGraw-Hill, New York).
- Schramm, S., and S. E. Koonin, 1990, *Astrophys. J.* **365**, 296.
- Shapiro, S. L., and S. A. Teukolsky, 1983, *Black Holes, White Dwarfs, and Neutron Stars* (Wiley, New York).
- Singwi, K. S., and M. P. Tosi, 1981, in *Solid State Physics*, edited by H. Ehrenreich, F. Seitz, and D. Turnbull (Academic, New York), Vol. 36, p. 177.
- Singwi, K. S., M. P. Tosi, R. H. Land, and A. Sjölander, 1968, *Phys. Rev.* **48**, 589.
- Slattery, W. L., G. D. Doolen, and H. E. DeWitt, 1980, *Phys. Rev. A* **21**, 2087.
- Slattery, W. L., G. D. Doolen, and H. E. DeWitt, 1982, *Phys. Rev. A* **26**, 2255.
- Smoluchowski, R., 1967, *Nature (London)* **215**, 691.
- Starrfield, S., J. W. Truran, W. M. Sparks, and G. S. Kutter, 1972, *Astrophys. J.* **176**, 169.
- Stevenson, D. J., 1980, *J. Phys. (Paris)* **41**, C2-61.
- Stevenson, D. J., 1982, *Annu. Rev. Earth Planet. Sci.* **10**, 257.
- Stevenson, D. J., 1991, *Annu. Rev. Astron. Astrophys.* **29**, 163.
- Stevenson, D. J., and E. E. Salpeter, 1976, in *Jupiter*, edited by T. Gehrels (University of Arizona, Tucson), p. 85.
- Stevenson, D. J., and E. E. Salpeter, 1977, *Astrophys. J. Suppl. Ser.* **35**, 239.
- Sugimoto, D., and S. Miyaji, 1981, in *Fundamental Problems in the Theory of Stellar Evolution*, IAU Symp. Vol. 93, edited by D. Sugimoto, D. Q. Lamb, and D. N. Schramm (Reidel, Dordrecht), p. 191.
- Tago, K., K. Utsumi, and S. Ichimaru, 1981, *Prog. Theor. Phys.* **65**, 54.
- Tanaka, S., and S. Ichimaru, 1986, *J. Phys. Soc. Jpn.* **55**, 2278.
- Tanaka, S., and S. Ichimaru, 1989, *Phys. Rev. B* **39**, 1036.
- Tanaka, S., X.-Z. Yan, and S. Ichimaru, 1990, *Phys. Rev. A* **41**, 5616.
- Thompson, W. B., 1957, *Proc. Phys. Soc. London Sect. B* **70**, 1.
- Vandenbosch, R., T. A. Trainor, D. I. Will, J. Neubauer, and I. Brown, 1991, *Phys. Rev. Lett.* **67**, 3567.
- Van Horn, H. M., 1971, in *White Dwarfs*, edited by W. J. Luyten (Reidel, Dordrecht), p. 136.
- Van Horn, H. M., 1990, in *Strongly Coupled Plasma Physics*, edited by S. Ichimaru (North-Holland/Yamada Science Foundation, Amsterdam), p. 3.
- Van Horn, H. M., 1991, *Science* **252**, 384.
- van Leeuwen, J. M. J., J. Groeneveld, and J. De Boer, 1959, *Physica* **25**, 792.
- Vosko, S. H., L. Wilk, and M. Nusair, 1980, *Can. J. Phys.* **58**, 1200.
- Whelen, J., and I. Iben, 1973, *Astrophys. J.* **186**, 1007.
- Widom, B., 1963, *J. Chem. Phys.* **39**, 2808.
- Wigner, E. P., 1934, *Phys. Rev.* **46**, 1002.
- Wigner, E. P., 1938, *Trans. Faraday Soc.* **34**, 678.
- Wigner, E. P., and H. B. Huntington, 1935, *J. Chem. Phys.* **3**, 764.
- Winget, D. E., C. J. Hansen, J. Liebert, H. M. Van Horn, G. Fontaine, R. E. Nather, S. O. Kepler, and D. Q. Lamb, 1987, *Astrophys. J. Lett.* **315**, L77.
- Ziegler, J. F., T. H. Zabel, J. J. Cuomo, V. A. Brusic, G. S. Carrill III, E. J. O'Sullivan, and A. D. Marwick, 1989, *Phys. Rev. Lett.* **62**, 2929.